Study of stimuli-responsive degradation using a disulfide platform in different polymeric biomaterials

Samuel Aleksanian

A Thesis
in
the Department
of
Chemistry and Biochemistry

Presented in Partial Fulfillment of the Requirements
for the Degree of Master of Science (Chemistry) at
Concordia University
Montréal, Québec, Canada

January 2014

CONCORDIA UNIVERSITY

School of Graduate Studies

This is to certify that the thesis prepared

By: **Samuel Aleksanian**

Entitled: Study of stimuli-responsive degradation using a disulfide platform in different polymeric biomaterials

and submitted in partial fulfillment of the requirements for the degree of

Master of Science (Chemistry)

complies with the regulations of the University and meets the accepted standards with respect to originality and quality.

Signed by the final examining committee:

Dr. Louis Cuccia	Chair
Dr. Christine DeWolf	Examiner
Dr. Christopher Wilds	Examiner
Dr. Jung Kwon Oh	Supervisor

Approved by_____

Chair of Department or Graduate Program Director

_____ 2014

_____

Dean of Faculty

Abstract

Study of stimuli-responsive degradation using a disulfide platform in different polymeric biomaterials

Samuel Aleksanian

Polymers have great potential as building blocks to construct biomaterials for applications in biomedicine, pharmaceutics and biotechnology. Their chemical flexibility leads to the synthesis of materials with diverse physical and mechanical properties. Specifically, stimuli-responsive polymers are engineered to undergo chemical or physical transitions in response to specific external triggers. One such response involves the cleavage or degradation of a dynamic covalent bond within the polymer structure. Particularly, the reduction of disulfide bonds has gained significant attention in the development of complex delivery systems for therapeutics. This thesis describes the development of two different reduction-responsive biomaterials.

Amphiphilic block copolymers (ABPs) self-assemble in aqueous solutions to form core/shell micelles consisting of a hydrophobic core, capable of carrying a variety of hydrophobic therapeutic agents, and a hydrophilic corona, able to improve circulation time and delay immune responses. This unique property, in addition to enhanced colloidal stability and tunable size with narrow size distribution, makes micelles promising candidates for drug delivery systems. Hence, a polyester-based reduction-responsive degradable ABP with disulfide linkages positioned repeatedly on the main chain at regular intervals is synthesized. These well-defined ABPs were synthesized by a combination of

polycondensation and atom transfer radical polymerization (ATRP). These ABPs self-assemble in aqueous solution, resulting in spherical micelles with a monomodal distribution. In the presence of a reducing agent, disulfide bonds are cleaved, leading to a destabilization of the micellar core and thus enhanced release of encapsulated model drugs. Demonstrating the potential drug delivery applications of polymeric micellar systems, functionalization with biotin (vitamin H) leads to bioconjugated micelles capable of potential cell-targeting.

Hydrogels are three-dimensional networks of hydrophilic polymers that have shown promise as tissue engineering scaffolds. Thermo-responsive hydrogels expel water above their *lower critical solution temperature* (LCST), becoming more hydrophobic, and hence lose volume. Hydrogels were synthesized by ATRP using biocompatible oligo(ethylene oxide) as a scaffolding material in the presence of a disulfide-labeled dimethacrylate cross-linker. The amount of cross-linker affects thermo-responsive and mechanical properties. Cleavage of disulfide bonds lead to an increased LCST, enhanced deswelling kinetics and a decrease in mechanical properties caused by the generation of hydrophilic dangling chains, increasing the overall hydrophilicity of hydrogels. Combined with these results, as well as enhanced release of encapsulated hydrophilic model drugs and non-toxicity, these hydrogels show promise for biomedical applications.

Acknowledgements

First, I would like to thank my supervisor, Dr. John Oh, for his help and guidance throughout my master's program. His enthusiasm and expertise in polymers encouraged me to always seek to advance my own knowledge in the field. His hands-on approach to science helped me acquire the necessary skills and knowledge at a rhythm I am still surprised of. The most valuable skill I have developed working with him is how to organize my time and work in order to be efficient, precise and fast. This thesis would have never been possible without his continuous care for me and my work.

I would also like to thank my committee members Dr. Christine DeWolf and Dr. Christopher Wilds, for their support and guidance throughout my degree. Their questions helped me understand aspects of my research I would have never thought about. Their contribution to my critical thinking and to my work cannot be stressed enough.

However, the most important people during my degree were the wonderful colleagues I shared my lab with. I would like to thank Andrew, Behnoush, Alexander, Nare, Nicky, Kaiwan, Yasaman and Soyoung for the great times we shared. Most of all, I would like to thank Behnoush Khorsand for her great friendship and support without which my experience as a master's student would not have been the same. She was the one person I could always rely on and she never hesitated to help me. I also want to thank Dr. Nicky Chan for his help with some aspects of my research and sharing his knowledge whenever needed.

Finally, I want to thank my mom Satenik, my dad Ovanes, and my brother Manouk, for supporting me these past years, which were hard on all of us. They were always there

when I needed them and were very understanding of my situation as a graduate student. They are the ones who taught me to work hard to achieve my goals and it is a lesson I will never forget. Without them, this degree would have never been possible. Words cannot express the gratitude and love I have for all of them.

Contribution of Authors

Chapters 3 and 4 of this thesis are reproduced, in part, from published manuscripts.

Chapter 3: A. Nelson-Mendez, S. Aleksanian, M. Oh, H.-S. Lim, J. K. Oh, *Soft Matter* **2011**, 7, 7441 *and* S. Aleksanian, B. Khorsand, R. Schmidt, J. K. Oh, *Polymer Chemistry* **2012**, 3, 2139.

The manuscript (*Soft Matter*) is co-authored in equal contribution with A. Nelson-Mendez, a CHEM 419 student in our lab who has worked on the synthesis and characterization of polyesters with disulfide linkages positioned repeatedly on the hydrophobic backbone. My contribution includes aqueous micellization, determination of critical micellar concentration using tensiometry, as well as loading and release of an encapsulated model drug upon the cleavage of disulfide linkages in polyester-based micellar cores. Another manuscript (*Polymer Chemistry)* is co-authored with two colleagues. B. Khorsand carried out transmission electron microscopy and cell viability measurements, while Dr. Schmidt performed atomic force microscopy analyses. The main author performed the synthesis of block copolymers, aqueous micellization, as well as loading and reduction-responsive release of an encapsulated model drug. Furthermore, the author analyzed micelle destabilization and bioconjugation of biotin on hydrophilic coronas. Acknowledgment has been given for A. Nelson-Mendez, who synthesized biotin-labeled methacrylates.

Chapter 4: S. Aleksanian, Y. Wen, N. Chan, J. Kwon Oh, *RSC Advances* **2014**, 4 (8), 3713.

This manuscript is co-authored with two colleagues in the laboratory. Y. Wen carried out cell viability studies and Dr. N. Chan determined the lower critical solution temperature of hydrogels using differential scanning calorimetry. All other experiments were performed by the author.

Table of Contents

List of Figures

List of Abbreviations

ABP	Amphiphilic block copolymer
AFM	Atomic force microscopy
AGET	Activator generated by electron transfer
ATRP	Atom transfer radical polymerization
Bpy	Bipyridine
Br-iBuBr	α-bromoisobutyryl bromide
BSA	Bovine serum albumin
BtOEOMA	Biotin-functionalized methacrylate
CMC	Critical micellar concentration
CRP	Controlled radical polymerization
DCC	N,N′-dicyclohexyl carbodiimide
DCM	Dichloromethane
DCU	Dicylcohexyl urea
D_H	Hydrodynamic diameter
DLS	Dynamic light scattering
DMAP	N,N-dimethylaminopyridine
DMSO	Dimethyl sulfoxide
DOX	Doxorubicin
DSC	Differential scanning calorimetry
DTNB	5,5'-dithiobis(2-nitrobenzoic acid) or Ellman's reagent
DTT	Dithiothreitol
EDTA	Ethylenediaminetetraacetic acid
EGFR	Epidermal growth factor receptor

EO	Ethylene oxide
EPR	Enhanced permeability and retention
FI	Fluorescence intensity
FRP	Free radical polymerization
G′	Storage (elastic) modulus
G″	Loss (viscous) modulus
GPC	Gel permeation chromatography
GSH	Glutathione
GSR	Gel swelling ratio
HABA	2-(4-hydroxyphenylazo)benzoic acid
HEK293T	Human embryonic kidney 293T
HMTETA	1,1,4,7,10,10-hexamethylaminopropyl
LCST	Lower critical solution temperature
LE	Loading efficiency
MEO_2MA	Di(ethylene glycol) methyl ether methacrylate
MePEG	Methoxy (polyethylene glycol)
M_n	Number-average molecular weight
MPS	Mononuclear phagocytic system
MTT	3-(4,5-dimethylthiazol-2-yl)-2,5-diphenyltetrazolium bromide
MTS	3-(4,5-dimethylthiazol-2-yl)-5-(3-carboxymethoxyphenyl)-2-(4-sulfophenyl)-2H-tetrazolium
MWCO	Molecular weight cut-off
M_w	Weight-average molecular weight
NMP	Nitroxide-mediated polymerization
NMR	Nuclear magnetic resonance

NR	Nile Red
N-tBAAm	N-tert-butylacrilamide
PAA	Poly(aspartic acid)
PBLA	Poly(β-benzyl L-aspartate)
PBTMC	Poly(5-benzyloxy-trimethylene carbonate)
PCL	Poly(ε-caprolactone)
PEG	Poly(ethylene glycol)
PEO	Polyethylene oxide
PEP	Poly(ethylene phthalate)
PES	Polyester
PHMssEt	Disulfide-labeled polymethacrylate
PLA	Polylactide
PMMA	Poly(methyl methacrylate)
PNIPAM	Poly(N-isopropylacrylamide)
POEOMA	Poly oligo(ethylene glycol) monomethyl ether methacrylate
PPO	Poly(p-phenylene oxide)
PS	Polystyrene
R6G	Rhodamine-6G
RAFT	Reversible addition fragmentation transfer
RES	Reticuloendothelial system
RI	Refractive index
SH	Sulfhydryl groups
$Sn(EH)_2$	Tin(II) 2-ethylhexanoate
SRD	Stimuli-responsive degradation
ssABP	Disulfide-labeled amphiphilic block copolymer

ssDMA	Dithiopropionyl poly(ethylene glycol) dimethacrylate
TEM	Transmission electron microscopy
THF	Tetrahydrofuran
UV/Vis	Ultraviolet-visible Spectroscopy

CHAPTER 1

INTRODUCTION

1.1 Brief overview of the research

My master's research is aimed at exploring stimuli-responsive degradation (SRD) of dynamic covalent bonds, particularly reduction-responsive disulfides, in the design and development of novel polymeric nanomaterials for biological applications. Atom transfer radical polymerization (ATRP), a versatile controlled radical polymerization (CRP) technique, has been used to synthesize well-controlled polymeric nanomaterials. These nanomaterials include self-assembled micelles of polyester-based block copolymers as drug delivery nanocarriers and rapidly thermoresponsive cross-linked hydrogels as tissue engineering scaffolds. In response to reductive reactions, the cleaved disulfide bonds led to either enhanced release of encapsulated drugs from micellar aggregates or rapid change in thermoresponsiveness of hydrogels.

1.2 Introduction to polymer biomaterials

Polymers are high molecular weight macromolecules with repeating units linked by covalent bonds; thus denoted as $-A_n-$ (A = repeating unit and n = degree of polymerization). They have existed in natural forms since life began as DNA, RNA, polysaccharides, proteins, etc. Some of these natural polymers are used today for commodity or food such as wool, silk, or gelatin. Synthetic polymers started to appear in the beginning of the 20^{th} century, mainly with the use of new forms of rubber for tires. Throughout the century, progress in polymer science has enabled the synthesis of a variety

of polymers to accommodate our needs. Typical examples include polyesters used in clothing, insulation and filters; polyurethanes in the construction and automobile industry; and poly(methyl methacrylate) (PMMA) in Plexiglas, plastics and medical technologies. While these polymers represent commodities, recent advances in functional polymers have gained significant attention as effective biomaterials for biological and biomedical applications. Biomaterials are defined as natural or synthetic substances that can interact with biological systems for medical purposes. They must be biocompatible and biodegradable in order to perform their functions without presenting negative side effects in a living host.[1-2] In addition, they need to meet several criteria to be injected and used in the body. First, the administration should be simple and safe; second, the delivery should be specific to the area of interest; lastly, the response must be adapted to the pathological event.[3] These biomaterials are mostly used in the forms of micelles, dendrimers and vesicles that can transport active molecules (drugs, contrast agents, proteins, DNA) or possess certain surface features for biosensing. Other types of biomaterials include microgels, hydrogels and fibrous meshes that can be used in tissue engineering, regeneration and wound healing.[3] One way to enhance the efficiency of some biomaterials is to design them to incorporate specific stimuli-responsive triggers that are only activated when the proper external stimuli is applied.

1.3 Stimuli-responsive polymeric materials

Stimuli-responsive polymers undergo a chemical or physical transition in response to external triggers. While a vast array of effects can be achieved by different transitions, this thesis will focus on two of them. Some transitions cause degradation involving the cleavage of dynamic covalent bonds, while others lead to a volume change involving coil-

globular transitions. Both degradation and volume change result in better localization to the compartment of interest; controlled release of encapsulates and other changes leading to desired biological functions.[3-6] A variety of external stimuli have been explored. As illustrated in Figure **1.1**, the stimuli can be classified into two types: physical stimuli including light, temperature or ultrasound, as well as either a magnetic or electric field; chemical stimuli including ionic strength or pH, and biological stimuli such as enzymes or receptors.[3]

Stimuli-responsive degradation (SRD) involves the introduction of cleavable linkages (dynamic covalent bonds) that are cleaved in response to specific stimuli. Typical dynamic bonds include reduction-responsive disulfides,[7] acid-labile linkages such as acetals, orthoesters, hydrazones and imines,[8] as well as photo-cleavable linkages such as coumarin dimers, pyrenylmethyl or o-nitrobenzyl.[9] In contrast, temperature-responsiveness is a typical stimulus, which can cause volume changes through hydrophilic-hydrophobic transitions (i.e. thermo-responsive nanomaterials).

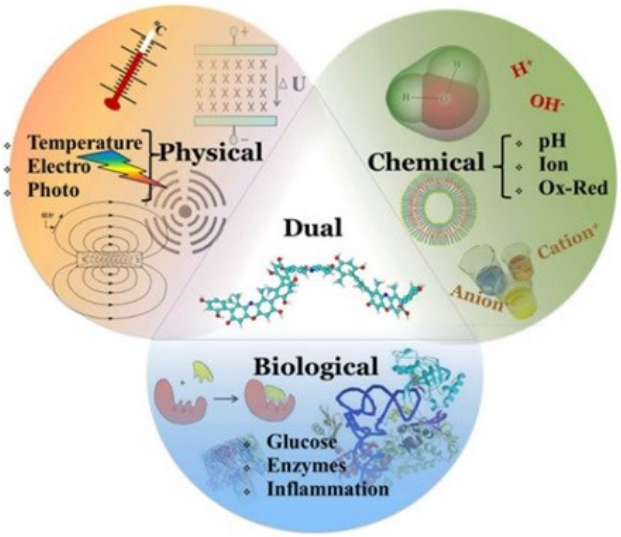

Figure 1.1. Types of stimuli-responsive triggers.[3]

1.4 Stimuli-responsive degradable micellar nanocarriers

1.4.1 Theoretical concepts for ABP-based nanocarriers

Amphiphilic block copolymers (ABPs) consist of hydrophobic and hydrophilic blocks and can self-assemble in aqueous solution to form micellar aggregates. These ABP based aggregates contain hydrophobic cores surrounded with hydrophilic coronas. Hydrophobic drugs can be encapsulated in the hydrophobic core, while the hydrophilic corona stabilizes the later with the external medium.[10] Consequently, micellar nanocarriers enhance the efficacy of therapeutics and reduce side effects. Towards effective tumor-targeting drug delivery applications, however, a number of properties of ABP-based micellar nanocarriers need to be considered.

1.4.1.1 Colloidal stability of aqueous micelles

Micelles have to be thermodynamically stable. Thermodynamic stability prevents micelles from disassembly when the total copolymer concentration is above the critical micellar concentration (CMC). The CMC of a copolymer is influenced by a number of parameters such as the nature and length of copolymer blocks. For example, higher hydrophobic/hydrophilic block ratio increases micelle stability and lowers CMC.[11]

Upon injection into the bloodstream, micelles are subject to "sink conditions", causing dissociation (or disassembly) of micelles.[10] Design of different polymers can tune the rates of disassembly. For example, hydrophobic blocks with high Tg values lead to slower disassembly in comparison with low Tg values at ambient temperature.[10] The hydrophobicity and length of both blocks can also influence micelle disassembly.[11-12]

1.4.1.2 Micelle size

Micelle size can be varied with the length and nature of hydrophobic and hydrophilic blocks.[13] Furthermore, micelle size influences circulation time and organ distribution, which determines their fate *in vivo*.[14] Opsonisation followed by recognition and phagocytosis from macrophages is related to size.[14-15] Compared to larger particles, those with a diameter <150 nm show an extended circulation time, thus being less susceptible to reticuloendothelial system (RES) clearance.[16]

1.4.1.3 Structure of ABP-based micelles

The nature of the micelle corona affects a number of properties including: biodistribution, pharmacokinetic parameters, biocompatibility, steric stability, specificity, surface adsorption to proteins, and adhesion to biosurfaces.[10] These properties can be

controlled by parameters such as the surface density of hydrophilic chains, the charge of the hydrophilic block, the hydrophilicity of the block, as well as the block length and bioconjugation of the polymer.[10] The most widely used polymer for the outer shell is poly(ethylene oxide) (PEO). PEO is biocompatible and FDA approved. PEO is soluble in water; such a high degree of hydration and large excluded volume induces repulsive forces contributing to stabilization of colloidal particles.[17-18] This property prevents micelle coagulation and surface adsorption of biological components. Adsorption of proteins to the micelle surface can cause a series of issues ranging from its lysis to premature release of encapsulated drugs or interference with some biochemical pathways.[17] The outer shell is also responsible for helping micelles to avoid detection by the immune system because opsonization of proteins (part of the RES) will attract macrophages, causing a reduction in circulation time of the vehicle which will not make it to its intended target.[19]

The micellar core can encapsulate hydrophobic drugs. There are several factors that influence the loading capacity and efficiency of micelles. These factors include the nature of drugs and core-forming polymers as well as the length and molecular weight of polymer blocks. In addition, the miscibility between drugs and core polymers can be estimated by the Flory-Huggins interaction parameter (χ_{sc}) since the encapsulation of the drugs in hydrophobic cores occurs through hydrophobic-hydrophobic interactions.[20] Consequently, it is critical to design micelles to be in synergy with a specific drug to maximize interactions with the polymer core as well as loading capacity and efficiency.

1.4.1.4 Micelles in the bloodstream

Once injected, micelles have to pass various obstacles before reaching their area of interest. They have to survive their journey in the bloodstream and arrive unscathed to the

target organ. During blood circulation, micelles have to be thermodynamically stable to avoid micelle disassembly upon dilution with blood and protect the encapsulated drug from the extracellular environment until the micelle is internalized in a cell. Furthermore, micelles could be designed to minimize uptake by the body's immune system. Opsonization of the micelle surface leads to the elimination of the micelle by the reticuloendothelial system (RES),[21] which includes Kupffer cells, hepatocytes of the liver and macrophages of the spleen.[22]

One concern is proteins in the serum that can influence drug delivery properties by changing the partitioning of drugs between the micelle and the external medium as well as the release kinetic profiles due to protein-drug interactions.[21, 23] This influence was analyzed by Kataoka et al., showing that a fraction of doxorubicin loaded in methoxy (polyethylene glycol)-b-poly(β-benzyl L-aspartate) (MePEG-b-PBLA) dissociated from the micelles and eluted with proteins using gel permeation chromatography (GPC).[24] Similar results were reported by Allen et al. using methoxy (polyethylene glycol)-b-poly(5-benzyloxy-trimethylene carbonate) (MePEG-b-PBTMC) with ellipticine as a model drug.[21] They have also showed that the presence of bovine serum albumin (BSA) increases the release kinetics of ellipticine in vitro. It was shown however, that using PEG at the surface of micelles reduces protein adsorption.[25] These findings show that serum proteins can influence various properties of a drug delivery system.

1.4.1.5 Passive vs active targeting

Once micelles are in the bloodstream, there are two ways they can reach the desired location: passive and active targeting. Passive targeting involves the extravasation of nanocarriers from the bloodstream through leaky vasculatures of irregularly aligned

endothelial cells in tumors (Figure **1.2A**).[26] The wide fenestration (opening) of tumor endothelial cells ranges from 300 to 4700 nm.[27] When the endothelium is perturbed by an inflammatory process or a tumor, particles with diameter <200 nm undergo enhanced vascular permeability. Furthermore, lymphatic vessels are not functional in tumor which leads to an accumulation of the nanocarriers in the tumor tissue. This characteristic is called the "Enhanced Permeability and Retention (EPR) effect".[28-30] This leaky vasculature can therefore be exploited for passive targeting of nano-sized drug carriers.

A promising approach is to use targeting ligands at the surface of nanocarriers (Figure **1.2B**). This is known as active targeting. Polymers can be bioconjugated to possess ligands that target specific receptors overexpressed on the surfaces of target cells. For example, folic acid ligands can interact with folate receptors on lung, kidney or brain tumors.[31] Ligands are chosen to have an affinity to cellular receptors present in excess on tumor cells.[32] Many different types of ligands have been used that include sugar moieties like galactose,[33] epidermal growth factor,[34] folate,[35] monoclonal antibodies[36] and peptides.[37] The coupling of bioconjugated ligands to the cell surface will induce accumulation of micelles in target cells by receptor-mediated endocytosis.[35-36] The use of actively targeted block copolymer micelles results in an enhanced efficacy in comparison with non-targeted micelles.[38-39] Mamot et al. showed that anti-EGFR immunoliposomes gained a 6-fold increase in cellular uptake compared to the nontargeted version 24 h following injection.[40]

Finally, after degradation, polymers are eventually excreted in the urine by the kidneys or in the feces.[41-43] In order to pass through the kidneys, materials must weigh less than 50 000 g/mol[44] and have a diameter less than 5.5 nm.[45]

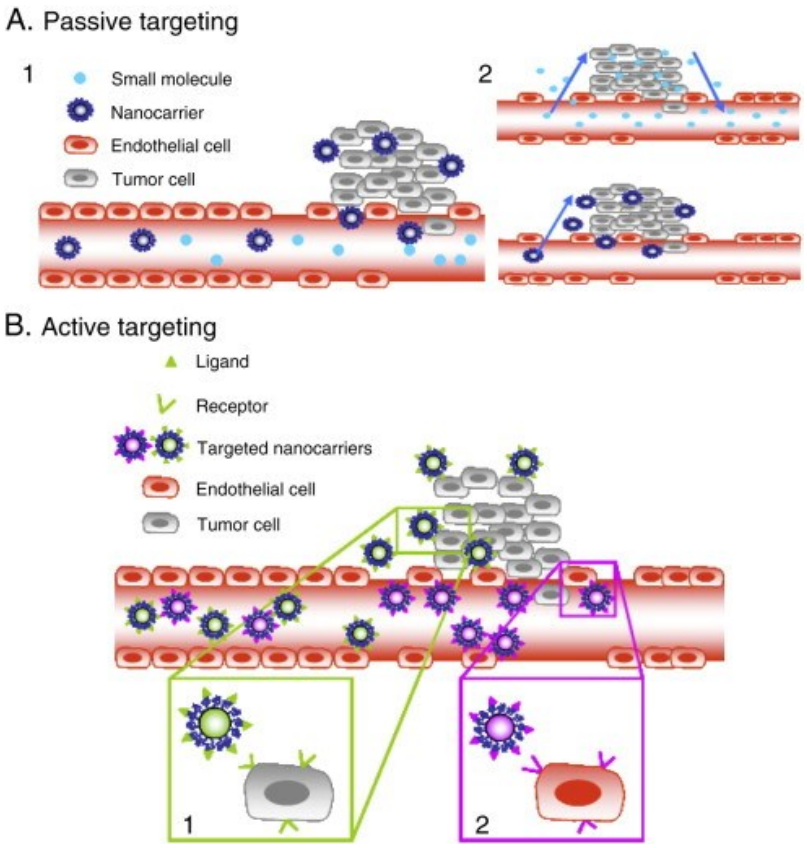

Figure 1.2. Active and passive targeting in tumors. Note that arrows designate diffusion of small molecules from bloodstream to cells and vice versa.[26]

1.4.1.6 Stimuli-responsive controlled release

Release kinetics can be influenced by the strength of the interaction between the polymers and the drugs. A stronger interaction will lead to higher loading levels, but slower release. In order to achieve a sustainable release profile, the desired drug would have to be matched with hydrophobic polymers that give better interaction. Depending on the location of the drug within the micelle, release kinetics can vary. The deeper the drugs are within the micelle, the slower the release.[46] Also, cross-linked hydrophobic cores were shown to slow down release kinetics in contrast with single chains.[46] Other factors that can influence the release kinetics include the length of the core-forming block, the molecular

volume (larger volume leads to smaller diffusion constant)[46] and the physical state (dissolved or crystallized in the core)[47] of the drug.

To achieve the desired controlled release rate, it is desirable for the drug's release to sustain a constant concentration over time (Figure **1.3)**. If the drug's concentration is above the toxic level or below the minimum effective level, ineffective delivery follows or in some cases, serious medical conditions could develop. Stimuli-responsive nanocarriers have been developed to address these issues by controlled release of encapsulated drugs in response to cellular triggers.

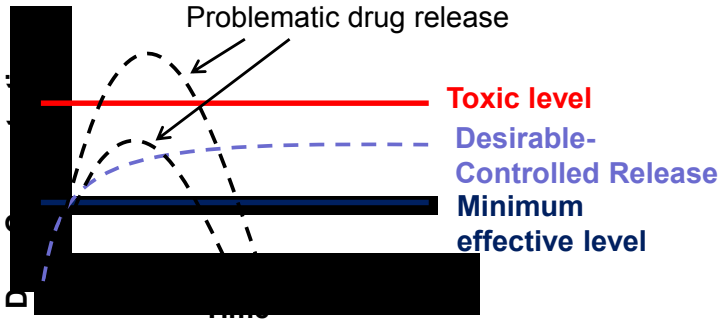

Figure 1.3. Desired drug release profiles in circulatory system over time.[48]

1.4.2 Approaches to SRD-micelle design

When designing SRD polymers, the position of the cleavable linkages affects micelle dynamics and functions. Polymers can possess either one or multiple cleavable linkages, and the cleavable linkage can be either in the micellar core or at the interface. One strategy involves the synthesis and self-assembly of degradable ABPs, having pendent multiple cleavable linkages along the hydrophobic block (Figure **1.4A**). Upon the proper

stimuli, these groups are cleaved, causing an increase in polarity which destabilizes the micelle structure. A second strategy is the presence of multiple cleavable linkages positioned regularly on the hydrophobic polymer backbone (Figure **1.4B**). Upon degradation, the hydrophobic backbone is disintegrated, leaving the hydrophilic block intact, destabilizing the micelle in the process.

Another strategy involves the synthesis of ABPs with functional groups that react with each other or with external cross-linkers, leading to the formation of cross-links (Figure **1.4C**). Depending on the location of the functional groups, this can lead to core-[49-50] or shell-crosslinked[51-52] micelles. This strategy inhibits the controlled release of encapsulated drugs but enhances the colloidal stability against micelle dissociation in the blood.[53] Degradation of cleavable linkages located inside cross-linkers leads to the destabilization of the micelle structure and its collapse. Mono-cleavable polymers (Figure **1.4D**) are based on triblock copolymers and having a single cleavable linkage in the middle. Its cleavage still leads to an amphiphilic polymer, but its molecular weight will be halved. This can lead to altered morphologies and sizes in aqueous solutions but also to slower release of trapped molecules possibly due to a lower concentration of cleavable linkages.[53] Finally, sheddable micelles (Figure **1.4E**) are formed when a single cleavable group is present at the interface, between the hydrophobic and hydrophilic block. An example of this system is the synthesis of a polylactide-SS-poly oligo (ethylene glycol) monomethyl ether methacrylate (PLA-SS-POEOMA) based micelle. A cleavage of the disulfide bond in this polymer leads to the loss of the hydrophilic corona and the precipitation of the hydrophobic PLA core.[54]

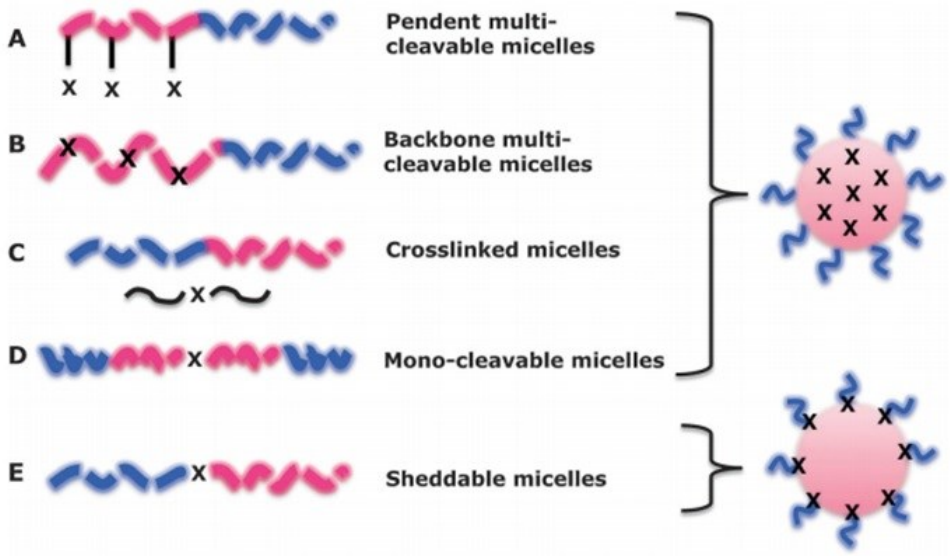

Figure 1.4. Different possible cleavable linkage positions and their outcome in a micelle structure.[53]

There are numerous design possibilities that can be useful for different goals. This thesis will mainly focus on the oxidation/reduction of disulfide bonds in polymers as well as discuss thermal polymer properties.

1.4.3 Reduction-responsive degradation platform

A disulfide bond (-S-S-) is a covalent bond between two sulfur atoms that is created by the oxidation of two sulfhydryl (SH) groups from SH-containing compounds. Naturally, disulfide bonds are present in bacterial and eukaryotic cells inside some secretory or membrane proteins. For example, cysteine is an amino acid that forms disulfide bridges in order to stabilize a protein's tertiary structure. Designing polymers to contain disulfide bonds can have interesting uses as will be discussed in more details in chapter 3. For example, the disulfide bond is an interesting one in drug delivery because of its reversibility and its stability in the plasma. Disulfides can be formed spontaneously by autoxidation of

sulfhydryls in the presence of air and can be reversibly cleaved in the presence of a reducing agent such as dithiothreitol (DTT) and β-mercaptoethanol[55]. Indeed, in the presence of DTT, disulfide bonds undergo thiol-disulfide exchange and two thiols will be generated (Figure **1.5**).

In biological systems, a large difference in redox potential between the oxidizing extracellular compartment and reducing intracellular compartment is present.[55] Inside the cell, the reducing environment is caused by the presence of glutathione (GSH), a tripeptide containing cysteine having a pendant thiol. The concentrations of GSH is ≈10 mM inside cells[56] while <10 μM outside cells.[55-57] This low concentration is caused by the rapid catabolism of GSH in the extracellular medium.[56] Interestingly, tumor cells have been found with elevated levels of GSH in their cytoplasm.[58] This is caused by up-regulation and down-regulation of various biological pathways that lead to an increase in GSH production in tumor cells.[59] Therefore, polymers based on disulfide stimuli have seen an increased interest from researchers for use in various biomedical applications such as the targeted delivery of drugs, proteins, DNA and imaging.[60] Disulfide bonds can also be used on materials to alter their properties by creating cross-links for example. The applications of disulfide bonds can vary depending on the need at hand.

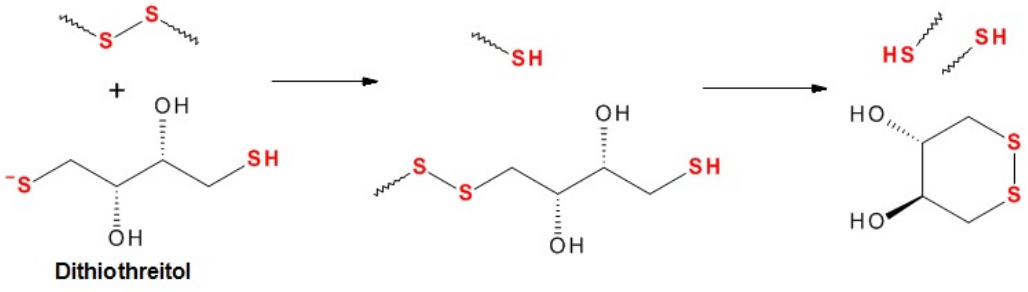

Figure 1.5. Thiol-disulfide exchange in the presence of DTT.

When the micelle crosses the cell membrane through receptor-mediated endocytosis, disulfide bonds can be cleaved by GSH and the micelle destabilized, releasing encapsulated drugs in the cytosol (Figure **1.6**).

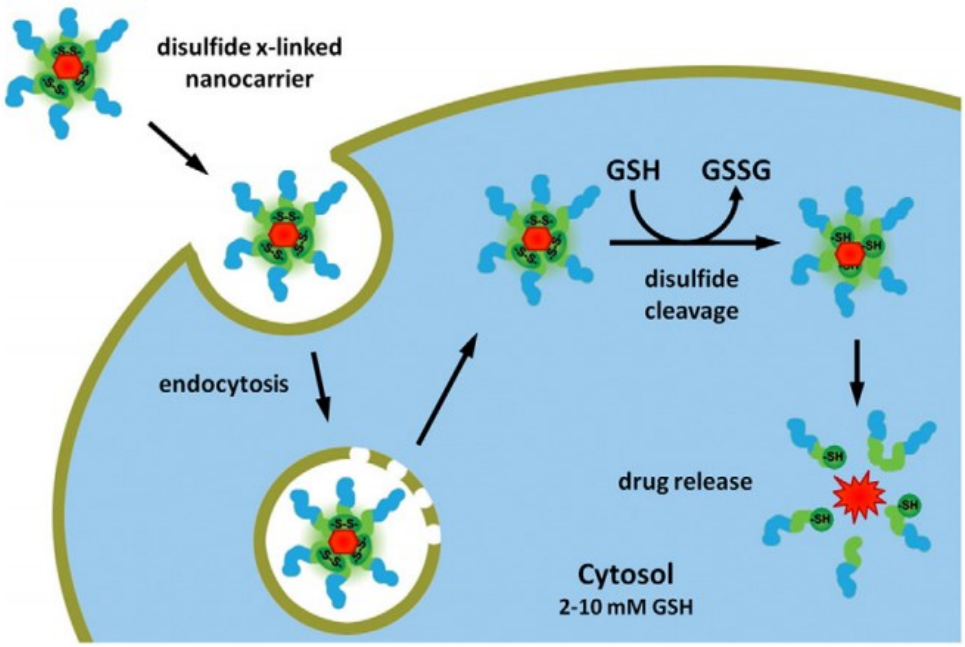

Figure 1.6. Schematic representation of disulfide cleavage mechanism in the cell by GSH.[61]

There are many ways to design disulfide containing block copolymers. Sun et al. developed a shell-sheddable micelle with PEG-SS-PCL having a disulfide bond at the interface. They show the release of DOX quantitatively within 12 h (>80 %) in an environment similar to that of the cytosol and cell nucleus (reducing environment). Without that disulfide bond, less than 20 % of the DOX was released within 24h in the same conditions, showing the benefit of the cleavable group.[62] Another group analyzed the release kinetics of DOX by fluorescence spectroscopy of a graft copolymer (SS-PAA-g-PEG). They show a nearly 100 % release of DOX using only 1 mM DTT in 10 h.[63] The

faster release can be attributed to the presence of repeating disulfide bonds in the main polymer chain, leading to faster degradation of the polymer and therefore disassembly of the micelle. Liu et al. synthesized a single disulfide containing hyperbranched multiarm copolymer using boltorn H40, PLA and poly(ethylene phthalate) (PEP) to obtain H40-*star*-PLA-SS-PEP. Addition of 10 mM DTT lead to an increase in particle size seen by DLS and a decrease in solution transparency within 8 hours. Particle size increased from 70 nm to several hundred nanometers. The loss of hydrophilic PEP causes the inner PLA core to aggregate. Also, DOX release using 0.1 mM DTT was doubled within the same 12 hours' time frame compared with samples untreated with reducing agent.[64] The same group has also synthesized another hyperbranched polymer. In this case however, they used copolyphosphates (HPHSEP-star-PEP) with disulfide bonds in the backbone. They found that upon degradation with DTT, particle size decrease with time from ~80 nm to 10 nm in 48 hours. Also, DOX release kinetics increased with an increase in DTT concentration.[65] Another design example is placing the disulfide bond in pendent groups. Zhang et al. synthesized a polymer (PEO-b-PHMSSEt) that possesses a disulfide bond in each pendent chain. These pendent chains give the block its hydrophobic property. If using less than 1 equivalent DTT to disulfides, they found that the polymer becomes hyperbranched by forming crosslinks with other polymer pendent chains through thiol-disulfide exchange reactions leading to a core-crosslinked micelle. If excess DTT is used however, the micelle is destabilized and crosslinks are unable to form. Also, release kinetics of a model encapsulated drug (Nile red) were comparable to the control (no DTT), for DTT lower than 1 equivalent. Moreover, at excess DTT, only 32% of Nile red was released after 70 hours. Below 1 equivalent DTT, due to core-crosslinking, Nile red is still confined within the

micellar core. When DTT is in excess, the micelle dissociates slowly because of hydrophobic interactions causing Nile red to preferably partition in those areas and therefore being released very slowly.[66] Han et al. developed a dual responsive SRD micelle containing both disulfide and *o*-nitrobenzyl linkages along the hydrophobic backbone. UV irradiation leads to 80% Nile Red release within 2 minutes while a 4/1 DTT to disulfide ratio reached a 25% release in more than 1000 minutes. The combination of both stimuli showed NR release of 50 % after 300 minutes.[67] Fan et al. showed that micelles of poly(amido-amine) labeled with backbone disulfides and grafted with PEO lead to slow degradation of disulfide bonds in response to DTT. Indeed, it took more than 120 h to reach >80% degradation.[68]

As seen, there are numerous ways to design polymers with disulfide bonds. They can be at the interface, in the hydrophobic main chain, in pendent chains or in relation with other stimuli. Every design decision leads to different polymer, micelle and drug delivery properties. In order to better understand structure-property relationships between the individual polymers and the micelle, more studies are required.

1.5 Thermoresponsive hydrogels leading to volume changes

1.5.1 Thermoresponsive polymers and LCST

The development of thermoresponsive polymers has recently received increased attention for biomedical applications;[69] particularly, drug delivery,[70-72] gene delivery[73-75] and tissue engineering.[76-78] Some diseases cause temperature differences that can be exploited to trigger designed changes in the physical polymer structure.[3] Thermoresponsive polymers are characterized by a temperature called *lower critical*

solution temperature (LCST) at which the hydrophilic and hydrophobic dynamics are reversibly changed according to their composition.[79] At temperatures below LCST, thermoresponsive polymers are hydrophilic and dissolve, while above the LCST they are hydrophobic and aggregate (Figure **1.7**).

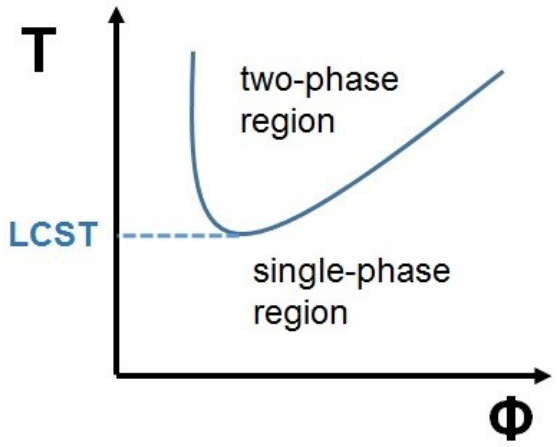

Figure 1.7. Graph of Temperature vs. polymer volume fraction, ϕ. Above the LCST, polymer is immiscible with water (hydrophobic) while below the LCST, it is miscible (hydrophilic).[48]

A typical example of thermoresponsive polymer is poly(N-isopropylacrylamide) (PNIPAM). In water, the LCST of PNIPAM is 32 °C, close to body temperature (37 °C), and is insensitive to environmental conditions.[80-83] Furthermore, its LCST can be tuned with a change in molecular weight, architecture or introduction of hydrophilic (or hydrophobic) moieties. When PNIPAM is copolymerized with 18% of acrylamide, its LCST increases to 45 °C. On the other hand, 40% of hydrophobic *N*-tert-butylacrilamide (N-tBAAm) decreases the LCST by 10 °C.[84] However, concerns about cytotoxicity and non-specific protein adsorption limit the use of PNIPAM-based materials in biological applications.[85-86]

A promising alternative is poly(oligo (ethylene glycol) monomethyl ether methacrylate) (POEOMA), which has an LCST between 20 °C to 80 °C depending on the lengths of pendent ethylene oxide (EO) repeating units as well as copolymerization with OEOMA units with different EO chain lengths.[87-88] More importantly, POEOMA is the analog of linear PEO, which is not toxic or immunogenic. It is also FDA approved for clinical trial use.[89-90] Advantages of POEOMA materials over PNIPAM include bio-repellency below LCST, reversible phase transitions (no hysteresis) and bio-inert properties.[91] Polymerization of POEOMA offers the best strategy for the synthesis of thermoresponsive polymers and permits facile conjugation with different polymeric backbones.[88, 92-93]

At the LCST, polymer chains undergo intramolecular collapse followed by intermolecular aggregation, thus increasing light scattering. Phase separation between the collapsed polymer and the solvent follows[94] (cloud point). This phenomenon is driven by the entropy of the water. Indeed, when the polymer comes out of solution, the water loses order and has higher entropy. Considering the Gibbs free energy equation $\Delta G = \Delta H - T\Delta S$, a higher entropy will lead to a more favorable reaction if temperature is high enough.[48]

1.5.2 Thermoresponsive hydrogels

Hydrogels are a porous three dimensional cross-linked network of hydrophilic polymers with tunable properties. There are two types of gels, physically linked gels and covalently linked gels. Physical hydrogels are generally formed by intermolecular associations through hydrophobic, ionic, or hydrogen bond interactions.[48, 95] In contrast, chemical gels are covalently linked to form cross-linked networks. They exhibit excellent

mechanical properties, high water content and biocompatibility.[95-98] An interesting application of these hydrogels has been found as tissue engineering scaffolds. Of our interest, thermoresponsive hydrogels can be set to swell or deswell depending on the temperature. As stated earlier, at temperatures below the LCST, certain polymers will become hydrophilic. Hence, hydrogels subject to temperatures above the LCST, become more hydrophobic and will expel the water, thus exhibiting a volume change. Naturally, below the LCST, the polymers forming the hydrogel become more hydrophilic, absorbing surrounding water, leading to an increase in volume (Figure **1.8**). The hydrogel will be explored in more details in chapter 4.

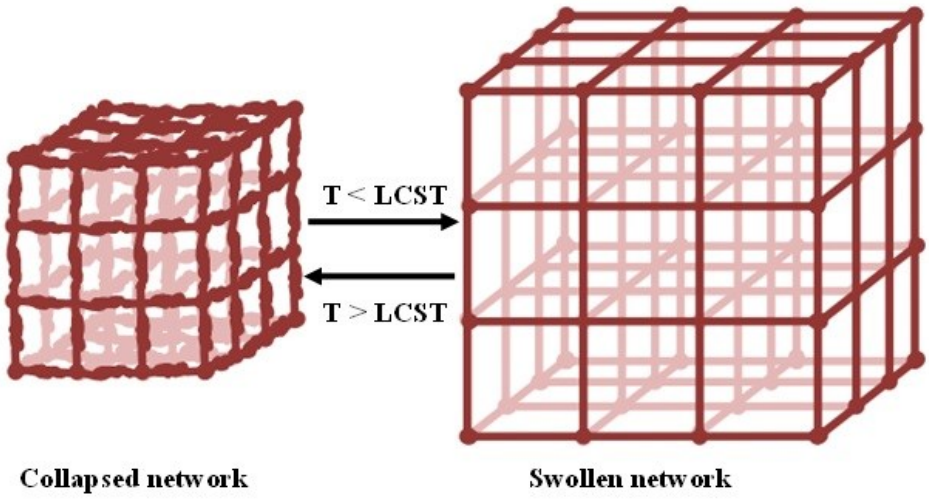

Figure 1.8. Effect of temperature on hydrogel swelling behaviour. Above the LCST, hydrogels will expel water and shrink. Below the LCST, they will absorb water and swell.[48]

1.6 Scope of the thesis

The purpose of this thesis is to provide an exhaustive study of the different strategies to synthesize a disulfide containing polyester based amphiphilic block copolymer and a thermoresponsive hydrogel with cleavable disulfide containing crosslinkers. Moreover, characterization of these polymers will be discussed thoroughly such as the CMC, encapsulate release, degradation, particle size for the micelle and swelling ratio, extent of degradation, water retention and rheology for the hydrogel. The goal is to analyze various polymer bionanomaterials for several properties. Both biomaterials explored (micelle and hydrogel) exhibit behavioural changes upon the cleavage of disulfide bonds within their molecular structure. This cleavage results in either destabilization of a micelle, enhancing drug release kinetics, or promotion of rapid thermoresponsive swelling and deswelling of a hydrogel system in water. Chapter 2 focuses on general protocols used, and the theory behind them as well as the principles necessary to understand and make an educated analysis of the data shown in the remainder of the thesis.

The first biomaterial, presented in chapter 3, is a polyester-b-POEOMA (PES-b-POEOMA) based block copolymer for drug delivery purposes. This polymer has repeating cleavable disulfide bonds in its hydrophobic polyester backbone. The synthesis and characterization of this polymer is explained. Micellization, CMC, particle size, morphology, degradation of the polymer and release of encapsulates are shown and explained. Upon cleavage of disulfide bonds, PES-b-POEOMA micelles exhibit enhanced release of a model drug. This cleavage also leads to the destabilization of the micelle over time. Moreover, functionalization of the polymer with biotin is shown and quantified using

a facile bioconjugation method. Additionally, cytoxicity data confirms the biocompatible nature of the polymer.

The second biomaterial covers the topic of tissue engineering and is explained in more details in chapter 4. A polymer hydrogel was synthesized by using PEO-b-MEO_2MA and a cross-linker containing a disulfide bond. The result is a thermoresponsive 3D polymer network that can absorb water below its LCST and expels water above that critical temperature. Swelling ratios are compared between samples synthesized using various amounts of cross-linkers. Deswelling kinetics are explored before and after degradation with DTT. Cleavage of the disulfide bridges lead to enhanced thermoresponsive properties but also weaker mechanical properties. Moreover, hydrogel degradation is quantified using Ellman's assay, calculating the concentration of thiols present in the structure after cleavage of disulfide bonds. Furthermore, the release profile of a model hydrophilic dye above LCST is investigated before and after cleavage. Initial cell viability studies prove the hydrogels are not toxic to cells.

Finally, chapter 5 will conclude with brief remarks and suggest pertinent future works that can further explain and explore the material presented in this thesis.

CHAPTER 2

PRINCIPLES AND THEORY OF POLYMER SYNTHESIS AND CHARACTERIZATION

2.1 Polymer synthesis

2.1.1 Polycondensation for polyester synthesis

Polycondensation is a step-growth polymerization which involves the growth of polymer chains in a step-wise fashion by mixing reactive multifunctional monomers. During the polymerization, small molecules such as H_2O and CH_3OH as byproducts are eliminated. Because of the step-growth mechanism, high molecular weight polymers are formed at very high conversion (> 99.5%). Figure **2.1** illustrates two typical processes to synthesize polyesters. First, a high temperature process involving a dicarboxylic acid and a diol is subject to high temperature (>350 °C) in the presence of Lewis acids as catalysts in bulk.[99] An alternative process utilizes a facile carbodiimide coupling polycondensation in the presence of a base as a catalyst at ambient temperature. This method (also called the Steglich esterification) was adapted by Wolfgang Steglich in 1978[100] and a typical mechanism is shown in Figure **A.1**. This method is advantageous because it requires mild reaction conditions. However, a challenge presents the difficulty to obtain high molecular weight polyesters due to low conversion. A more efficient method using ruthenium-based catalysts has been repeated to synthesize high molecular weight polymers under mild conditions.[101]

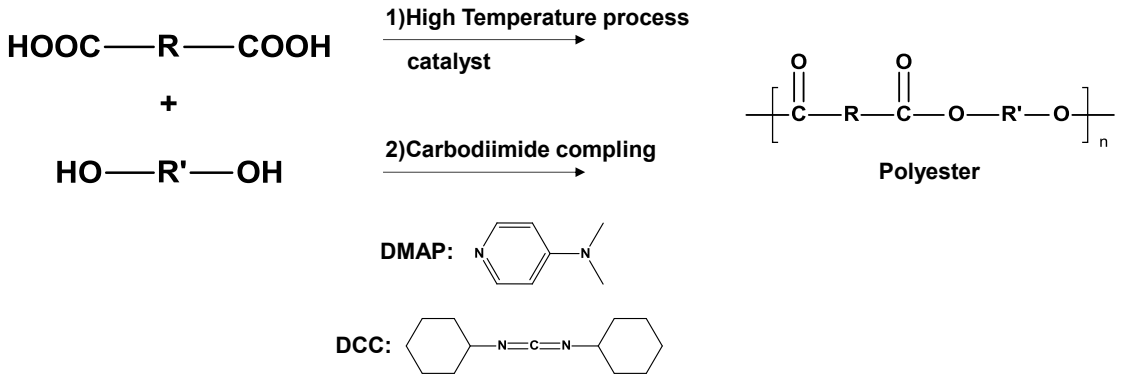

Figure 2.1. Polyester synthesis by reaction of a diacid and a diol through a high temperature process (1) or a carbodiimide coupling reaction (2).

2.1.2 ATRP for block copolymer synthesis

An important goal in polymer synthesis is to control molecular weight and polydispersity of synthesized polymers. For biological applications, it is essential to control their composition, architecture and end group functionalities.[102] Living polymerization is a technique that allows for the synthesis of well-controlled block copolymers. Typical processes include anionic, cationic, and ring-opening metathesis polymerizations. However, they require highly controlled environments and sophisticated catalysts as well as a high degree of purification of reagents.[102] Free radical polymerization (FRP) is more tolerant of impurities and functional monomers; however, its control is not easy due to irreversible termination and chain transfer reactions.[102] An alternative is the controlled radical polymerization (CRP) method as an effective means to synthesize well-defined block copolymers with narrow molecular weight distributions.[103] This method utilizes a reversible termination mechanism where the polymer chain switches between a propagating and dormant state. Typical methods include nitroxide-mediated polymerization (NMP),[104-106] atom transfer radical polymerization (ATRP)[107-109] and

reversible addition fragmentation chain transfer (RAFT) polymerization[110-113] utilized for the preparation of well-defined ABPs.

Figure **2.2** illustrates the mechanism of two ATRP processes. In a direct ATRP process, a lower oxidation state copper (Cu(I)Br/L) as an activator reacts with the dormant species (P_n-X). This activation expressed with the rate constant of activation (k_{act}) generates growing polymeric radicals (P_n*) and a higher oxidation state copper complex (X-Cu(II)Br/L) as a deactivator. The resulting P_n* radicals can undergo propagation by an addition of monomers with the rate constant of propagation (k_p). Preferably, the propagating polymeric radicals are deactivated by reacting with the deactivator to regenerate the dormant species and the activator. This deactivation can be expressed with the rate constant of deactivation (k_{deact}). This reversible process of activation and deactivation is shifted towards deactivation because $k_{deact} >> k_{act}$. This shift can minimize the concentration of radicals in the polymerization, thus suppressing irreversible termination and chain transfer reactions.[114]

First-order kinetics of ATRP leads to a linear relationship of increasing polymer molecular weight with monomer conversion. Propagation of the polymer chain leads to a rapid decrease of polydispersity with conversion. These unique attributes can be exploited to target a desired molecular weight or conversion for precise polymer synthesis. Furthermore, the living nature of chain ends (terminal bromines) allows for the synthesis of functional block copolymers for various applications, including biological applications. In my research, ATRP was used to synthesize degradable polyester-based block copolymer as nanocarriers for reduction-responsive drug release (chapter 3).

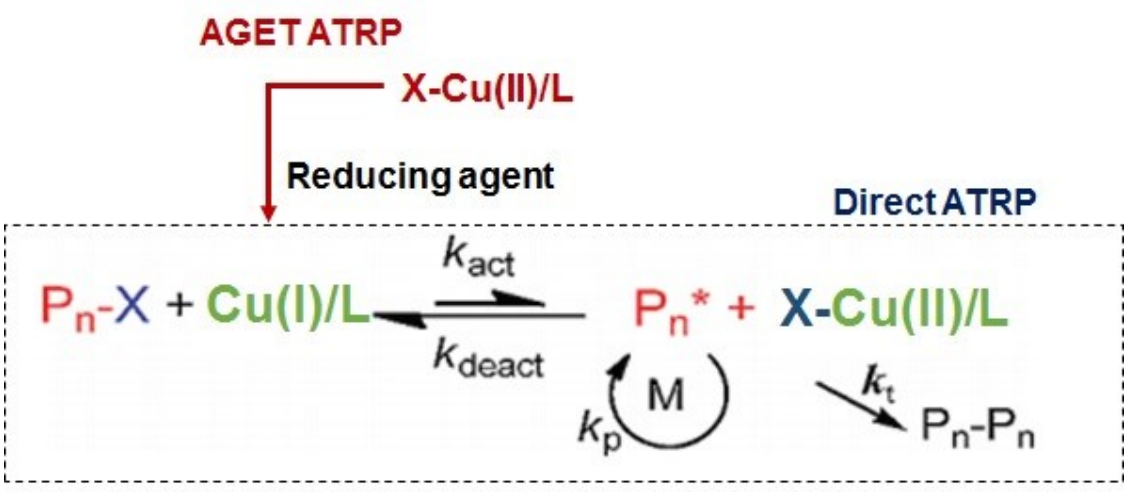

Figure 2.2. Mechanism of ATRP. Initiator functionalized with halide group (P_n-X) reacts with metal catalyst of low oxidation state (m) complexed with ligand (L). In AGET ATRP, polymerization is initiated by the reduction of a high oxidation state metal (m+1) like Cu(II) complexed with a ligand.[114]

A main limitation for the practice of the direct ATRP process is associated with the Cu(I) species being sensitive to oxygen. In order to overcome this limitation, a new process for ATRP called Activators Generated by Electron Transfer (AGET ATRP) has been recently developed.[115] In this method, the oxidatively-stable Cu(II) complexes react with a reducing agent such as Tin(II) 2-ethylhexanoate ($Sn(EH)_2$) or ascorbic acid to generate Cu(I) active species (Cu(I)/L), which then undergoes the normal ATRP process (Figure **2.2**). This method has all the benefits of ATRP but adds a stable catalyst to the reaction mixture.[115] In this thesis, the AGET ATRP process was used to synthesize three-dimensional cross-linked hydrogels exhibiting rapid thermo-responsiveness as tissue engineering scaffolds (chapter 4).

2.2 Polymer Characterization

2.2.1 Gel Permeation Chromatography (GPC)

Molecular weight and molecular weight distribution are important properties of polymers. The molecular weight of polymers is defined with the number-average molecular weight (M_n) and the weight-average molecular weight (M_w). The number average molecular weight is calculated by $M_n = \frac{\sum N_i M_i}{\sum N_i}$, where N_i is the number of polymers and M_i the molecular weight of each one. The absolute M_n value can be determined by osmometry.[116] The weight-average molecular weight (M_w) is given by $M_w = \frac{\sum N_i M_i^2}{\sum N_i M_i}$ and the absolute M_w can be determined by static light scattering (SLS).[116] The polydispersity (PDI) is defined by M_w/M_n (molecular weight distribution). Polydispersity (PDI) is a measure of the heterogeneity of polymer molecular weight. While a monodisperse sample will have a PDI of 1.0, higher PDI values reflect samples with varying polymer chain lengths.

Gel permeation chromatography (GPC) is a convenient method to determine relative molecular weights of polymers. Figure **2.3** shows a schematic illustration of GPC instrumentation. A diluted polymer solution is injected into a solvent stream in the sampling chamber. The polymers then travel through columns packed with porous beads whose porosity ranges between 5-10^5 nm. Molecules smaller than pore sizes reside longer in the pores, while larger polymers are excluded from the columns. Such size exclusion defines the elution times of each molecule. Consequently, polymer chains with different dimensions are separated depending on their molecular weight and conformations.[117] An RI detector is used to measure the presence and concentrations of polymers against the

elution time. For comparison, GPC columns are calibrated using a set of polystyrene or poly(methyl methacrylate) standards that represent a wide range of molecular weights. Molecular weight is determined by comparing the elution time and molecular weight of reference samples with the injected ones.

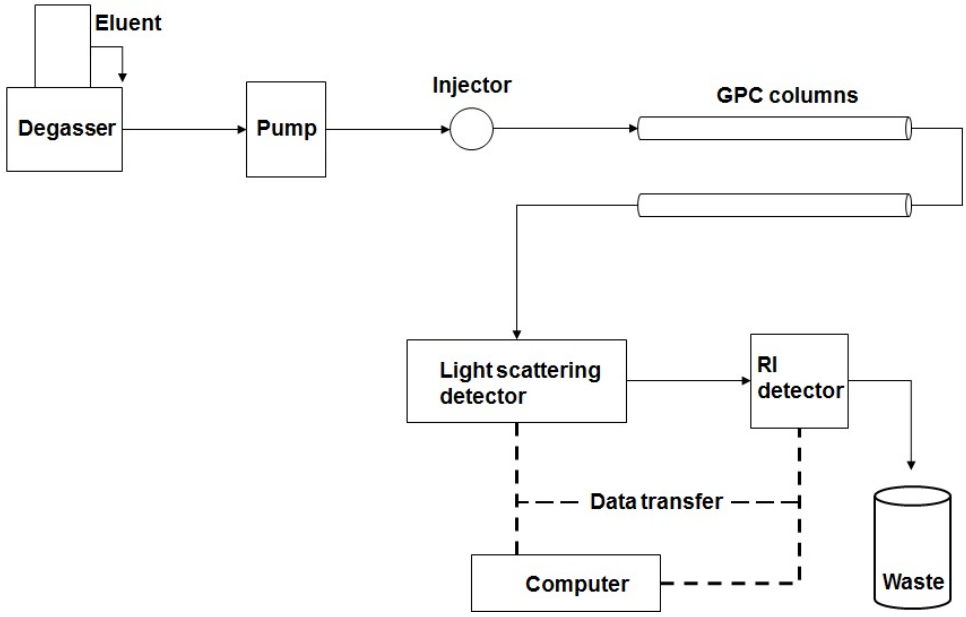

Figure 2.3. Schematic diagram of a typical GPC instrument setup with light scattering and RI detector.

2.3 Aqueous micellization and characterization

2.3.1 Aqueous micellization

In aqueous solution, amphiphilic block copolymers self-assemble to form micellar aggregates consisting of a hydrophobic core surrounded by a hydrophilic corona. There are different methods to facilitate the formation of micelles. One method, direct dissolution, involves dissolving the polymer directly in an aqueous solution. This method is used for polymers that are just moderately hydrophobic and somewhat soluble in water.[118] Another method is the solvent evaporation method used for polymers not directly soluble in

water.[118] In this method, the polymer is dissolved in volatile organic solvents such as tetrahydrofuran (THF) or acetone to form a clear solution. Water is then slowly added while stirring. Evaporation of solvents yields an aqueous micellar dispersion. The other method, called the dialysis method uses a dialysis tubing in outer water. In this method, the solvent used to dissolve the polymer is removed through intensive dialysis in water, yielding stable aqueous micellar dispersions. The micellization method used most readily in this thesis is the solvent-evaporation method.

2.3.2 Determination of Critical Micellar Concentration (CMC) by tensiometry

The critical micelle concentration (CMC) is defined as the concentration at which the first formed micelle appears. As the concentration of polymers increases in aqueous solution, unimers stay at the interface as well as in water. These unimers are in equilibrium between interface and water. A further increase in polymer concentration results in an increase in surface pressure as well as a decrease of the self-diffusion constant of the unimers in solution.[119]

Tensiometry is a technique to determine CMC. A series of polymer solutions at varying polymer concentrations are added in equal volume to wells on a plate (Fig. **2.5A**). After being zeroed both in air and in distilled water, the tip is lowered so it just touches the top of the well bubble. The tensiometer measures the surface tension and pressure of the solutions. The results are recorded and the protocol is repeated for the other solution going from the lowest concentration to the highest. Below CMC, surface pressure increases gradually, remaining almost flat (Figure **2.4B-1**). As the concentration is increased closer to the CMC, the surface pressure increases (Figure **2.4B-2**). Eventually, when reaching the CMC, surface pressure is at a maximum and further increase in concentration does not lead

to further increase in pressure (Figure **2.4B-3**). The point where the pressure becomes stable again is considered to be the CMC. Note that the instrument measures surface tension, which is converted to surface pressure by using the equation $\pi = \gamma_o - \gamma$, where π is the surface pressure, γ_o is the surface tension without any solutes and γ with the current concentration of solutes.

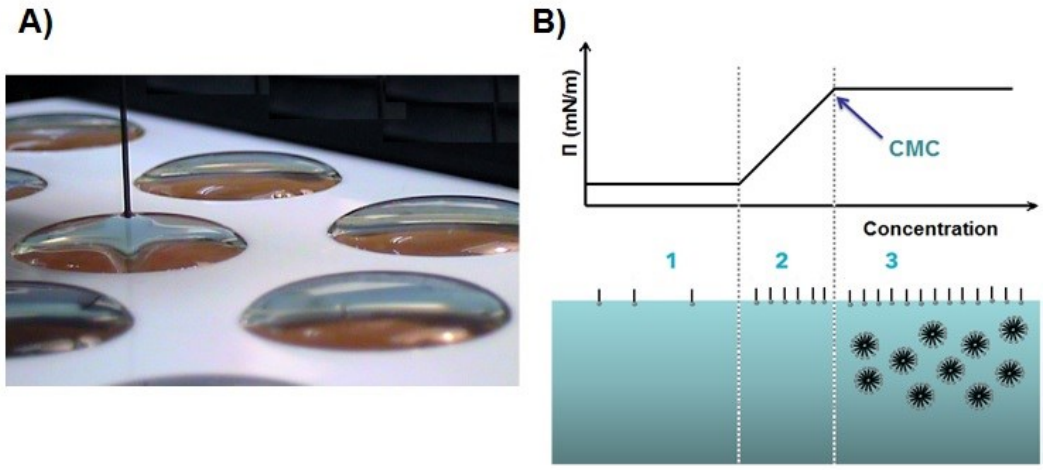

Figure 2.4. a) Tensiometer tip location in wells; b) Micelle formation evolution with increasing polymer concentration.[120]

2.3.3 Dynamic light scattering (DLS)

Dynamic light scattering (DLS) is a standard technique that measures particle size and particle size distribution of micellar aggregates. Micelles surrounded by water molecules undergo Brownian motion which causes fluctuations in light intensity. Fluctuation speed is related to micelle size and determines the diffusion coefficient *D*.[121] The larger sized micelles diffuse slower while smaller micelles diffuse faster. When temperature and solvent viscosity is known, the Stokes-Einstein equation $R_H = \frac{k_B T}{6\pi\eta D}$ can

be used to determine the particle size (R_H) (k_B is Boltzman's constant, T is the temperature and η is the solvent viscosity).

2.3.4 Imaging techniques

Transmission electron microscopy (TEM) and atomic force microscopy (AFM) are used to investigate the morphologies of dried micelles on carbon grids or mica surfaces. TEM studies the morphologies of micellar aggregates in a dehydrated state providing absolute measurement of particle size, while AFM visualizes the scanned sample surface using a cantilever. Analysis of particle size is done using third-party software by looking at the diameter of each surface feature detected. TEM images were taken using a Philips CM200 HR-TEM, operated at 200kV electrons and equipped with thermionic LaB6 cathode filament, anti-contamination cold finger, Genesis EDAX system, and AMT V600 2k X2K CCD camera. The point-to-point resolution and the line resolution of the machine are 0.24 nm and 0.17 nm, respectively. AFM studies of distinct micelles were carried out in the tapping mode with the aid of a Nanoscope IIIa (Digital Instruments, Santa Barbara, CA) in air at room temperature at a scan rate of 1 to 4 Hz using etched silicon cantilevers (TAP300, Innovative Solutions Bulgaria) with a resonance frequency of about 300 kHz, a nominal spring constant of 40 N/m, and tip radius of <10 nm. Medim damping (about 30%) was employed for these measurements.[122]

2.4 Hydrogel characterization

This section describes how thermoresponsive hydrogels are characterized: including swelling ratio, deswelling kinetics and viscoelastic properties. The most interesting property of hydrogels is their swelling in the presence of a solvent. Swelling is

a continuous transition from a dry glassy state to a swollen rubbery state upon absorption of a solvent.[123]

2.4.1 Gel swelling ratio (GSR)

When gels are placed in aqueous solutions below LCST, they become hydrophilic, swell and absorb water. Consequently, wet gels gain weight due to their water content. The GSR is defined as the ratio of the weight of wet gels over dry gels (w_t/w_d). To determine GSR experimentally, pieces of gels are submerged in aqueous solution to reach absorption equilibrium at room temperature. Wet gels are then taken and blotted to remove residual water. The wet weight is then measured (w_t) and the gel is then put in a small oven at 120 °C for 4 hours to remove all solvent traces. The dry weight (w_d) is then taken and the ratio calculated.

2.4.2 Gel Deswelling Kinetics

When swollen gels are exposed to temperatures above their LCST, they become hydrophobic, shrink and expel water. In my research, deswelling kinetics of hydrogels were followed by characterizing water retention above LCST. Water retention at time *t* was calculated by $\frac{wt-wd}{w_0-wd}$, where w_t is the weight of swollen gels at time *t*, w_d is the weight of dried gels, and w_o is the initial weight of swollen gels. A sample experimental procedure is as follows: pieces of swollen gels are weighed at room temperature before being submerged in a water bath preset at 45 °C, above LCST. At a given time *t*, they were blotted to remove residual water on their surfaces and weighed. Each sample was analyzed for one hour, where no more significant change in weight was observed, and was then dried in an oven to obtain dry weight.

2.4.3 Viscoelastic Measurements by Rheometry

Matter, including polymeric materials, is deformed when a force (or stress) is applied to it. There are two types of stresses: extensional stress and shear stress. Extensional stress is applied when a certain force pulls or pushes an object in an up or down direction such as a weight attached on a string. Shear stress is defined as force applied parallel to a certain object. When shear stress is applied on an object, there is also a strain on it which is defined as the deformation per unit length (units of stress are Pascals). As seen in Figure **2.5**, the elastic modulus *E* (or Young's modulus *Y*) is determined by the slope of the stress-strain curve of a certain stressed object.[124] At lower strain values, the elastic modulus is constant. However, at higher values, the modulus increases up to a fracture point; a phenomenon called "strain hardening". This observation is prevalent in cross-linked polymeric networks.

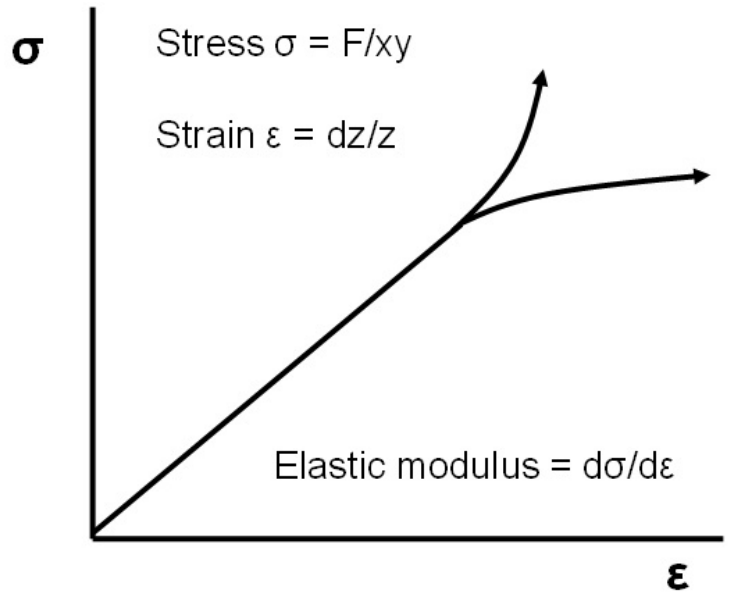

Figure 2.5. Stress-strain curve of a stressed object.[124]

Viscoelastic properties of hydrogels are often measured in oscillatory shear mode. In my research, thermo-responsive hydrogels are subject to oscillating stress and strain. Using a plate to plate geometry, an oscillating strain is applied to the gel which creates a stress, and both of them oscillate with time (Fig. **A.2**). The information contained in the oscillation graph must be interpreted differently to be understood. At a given frequency ω, the maximum stress σ_o divided by the maximum strain γ_o is constant and is called the complex modulus G^*. This equation is similar to the equation that represents the elastic modulus seen previously. Indeed, the elastic modulus and the complex shear modulus have only the type of stress to differ them.[125]

$$|G^*(\omega)| = \frac{\sigma_o}{\gamma_o}$$

Here, ω is the radial frequency and is equal to 2πf where f is the applied frequency in Hz. The phase difference δ between the peak values of stress and strain is also constant. Moreover, G^* and δ are characteristic of a specific material. If we have two plates, and a displacement is applied to the lower plate, a strain is produced. This displacement will go through the sample and the upper plate will react accordingly, giving a stress response. If the strain is an oscillation, the stress response will be the same, leading both of them to be inphase and a δ value of 0. However, if the sample is a Newtonian liquid they are out of phase. Therefore, because the hydrogel is considered as a viscoelastic material, some energy is stored (inphase) and some is dissipated (out of phase).[124] The mathematical models and simplifications that follow from here are beyond the scope of this thesis, but can be found in the references. In the end, the complex modulus with a given frequency ω for a Maxwell model is given by: $G^*(\omega) = G'(\omega) + G"(\omega)$, where G' is the storage

(elastic) modulus and G" is the loss (viscous) modulus.[125] The storage modulus represents the "solid" portion of the sample while the loss modulus represents the "liquid" portion. A higher G' for example means that the sample is much more "solid" than liquid. For hydrogels, G' should always have a greater contribution than G". In "ideal" solids, G' is equal to the elastic modulus and G" is 0. For a Newtonian "Ideal" liquid, G' is 0 and G"= $\omega\eta$. In order to understand how elastic the sample is, the ratio of viscous modulus to elastic modulus is calculated and designated as Tan δ (tangent of the phase angle).

CHAPTER 3

REDUCTION-RESPONSIVE DEGRADABLE POLYESTER-BASED MICELLES

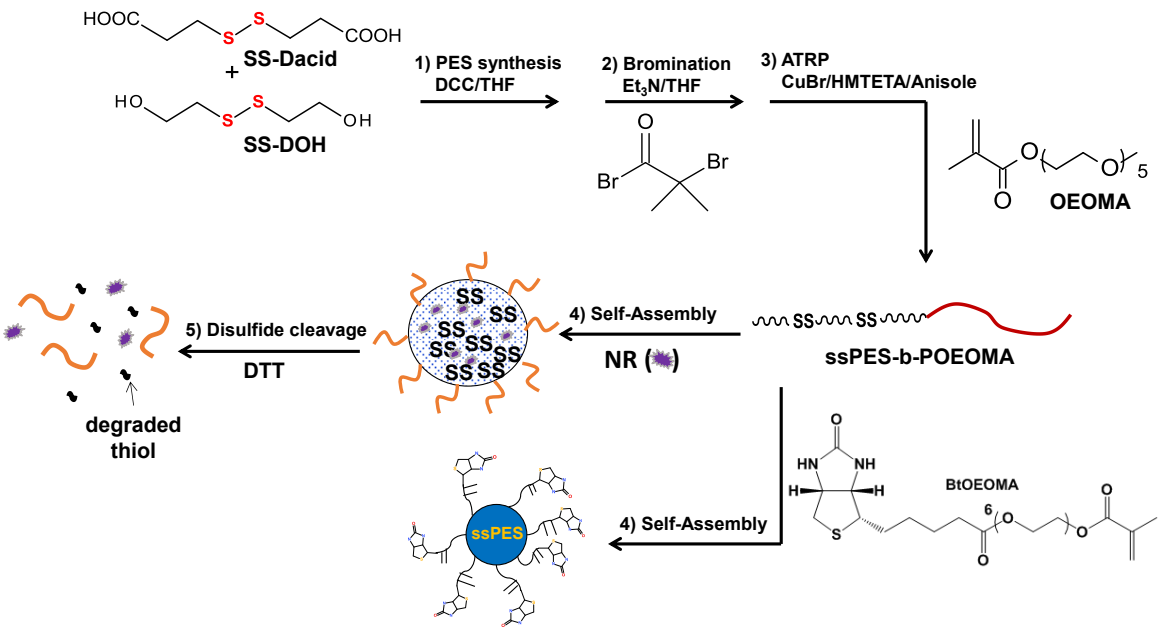

Degradation of amphiphilic block copolymer (ABP) micelles in response to external stimuli (stimuli-responsive degradation) is a desired property in the design of controlled delivery vehicles. In this chapter, a versatile methodology that combines facile carbodiimide coupling polycondensation with controlled radical polymerization to synthesize thiol-responsive degradable ABP micelles is described. These smart micelles consist of a hydrophobic degradable polyester block with disulfide linkages labeled repeatedly along the main chain; more importantly, in response to thiols they exhibit rapid

and controlled degradation, thereby leading to enhanced release of encapsulated model drugs. Moreover, the proposed method allows for a facile bioconjugation of hydrophilic coronas using cell-targeting biomolecules during polymerization.

3.1 Introduction

Amphiphilic block copolymers (ABPs) self-assemble in aqueous solution to form micellar aggregates consisting of a hydrophobic core, enabling the physical encapsulation of non-polar biomolecules, and a hydrophilic corona, ensuring biocompatibility and colloidal stability.[22, 126-127] Extensive research has explored the effectiveness of these micelles for use as drug delivery carriers.[128-130] However, control over several properties is still required. Bioconjugation with cell targeting biomolecules can promote active targeting to specific malignant cells through, for example, specific ligand-receptor interactions.[32] Stimuli-responsive degradation of ABP micelles in response to external stimuli is a more desirable approach.[131]

Stimuli-responsive ABP micelles are generally designed to have degradable linkages, which are cleaved in response to external triggers such as low pH, light, or ultrasound, as well as reductive, oxidative, or enzymatic reactions.[132] Thiol-responsive disulfide linkages are of particular interest as a degradable platform, because they are cleaved into corresponding thiols in a reducing environment or through a disulfide-thiol exchange.[133-134] Moreover, glutathione (GSH) is found at different concentrations between the intracellular and extracellular environments[55], and even at elevated levels in cancer cells.[58]

Many approaches have been proposed for the preparation of reductively degradable ABP-based micelles.[53] Examples include mono-cleavable micelles having single disulfides in the middle of triblock copolymers,[135-136] sheddable micelles having disulfides at the junction of hydrophilic and hydrophobic blocks,[7, 54, 64, 137] and crosslinked micelles with disulfide linkages.[138-139] Incorporating disulfides repeatedly along the

backbone of the hydrophobic main chain is a promising approach. Examples of this type of architecture include redox-responsive hyperbranched multiarm copolyphosphate[140] and poly(ethylene oxide)-grafted poly(amido amine)[68] as well as dual-responsive poly(β-amino ester).[141] Despite these advances, strategies to precisely control the speed and extent of degradation, thus release of encapsulates, remain limited.

We have recently developed a versatile method to synthesize reductively degradable polyester-based polymethacrylate block copolymers.[142] The method employs a combined polycondensation with ATRP, a successful controlled radical polymerization (CRP).[143] Figure **3.1** illustrates our approach consisting of 1) carbodiimide coupling polycondensation for synthesis of disulfide-labeled degradable polyester (ssPES-OH), 2) bromination of ssPES-OH to ssPES-Br, and 3) ATRP for the chain extension of ssPES-Br with water-soluble polymethacrylate. These thiol-responsive degradable ssABPs (ssPES-b-polymethacrylates) self-assembled in an aqueous environment to form micellar aggregates, consisting of degradable ssPES cores surrounded with water-soluble and biocompatible polymethacrylate coronas. Our use of this methodology allows for the preparation of multifunctional nanomaterials having several features. The method uses commercially available diols or diacids, and thus does not require monomer synthesis. A broad selection of monomers allowed for tunable degradation of ssPESs by varying diols or diacids in the polyester synthesis.[144] Furthermore, degradable ssPES blocks having disulfide linkages labeled along the main chain at regular intervals results in fast degradation of the ssABPs and their micellar aggregates, enhancing the release of encapsulated model drugs. More importantly, the method ensures facile bioconjugation during ATRP: functionalization of hydrophilic coronas with biomolecules for active

targeting.[145] These unique properties suggest that the multifunctional stimuli-responsive micelles hold great potential as controlled drug delivery carriers.

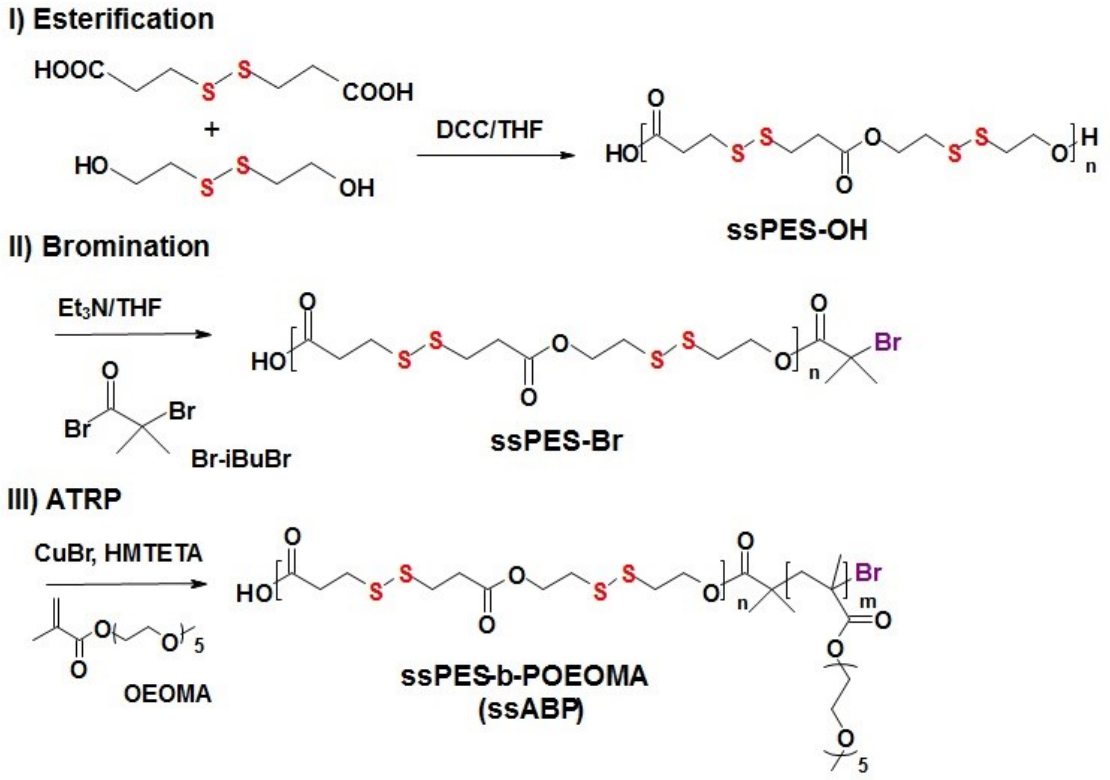

Figure 3.1. Synthetic route for reductively degradable ssABPs consisting of ssPES block labeled repeatedly with disulfide linkages along hydrophobic main chains and a water-soluble POEOMA block.

This chapter explores thiol-responsive ssABP micelles with rapid degradation and facile bioconjugation that have a potential for controlled drug delivery applications. A block copolymer was synthesized consisting of a poly(oligo(ethylene oxide) monomethyl ether methacrylate) (POEOMA) hydrophilic block and a disulfide containing polyester (ssPES) hydrophobic block. The hydrophobic core-forming block polyester contains repeating disulfide units and is biocompatible and biodegradable. The micelles were characterized with size and morphology using DLS, TEM, and AFM. Fast thiol-responsive

degradation of ssABPs caused their micellar aggregates to be destabilized, which was confirmed by a significant decrease in chain length as well as a change in molecular structure and hydrodynamic diameter. Such disruption of micelles upon degradation of the hydrophobic ssPES core in response to a water-soluble thiol at millimolar concentrations enhanced the release of an encapsulated model drugs. Furthermore, an applicability of thiol-responsive degradable micelles toward the facile bioconjugation of the ssABP during ATRP was demonstrated by the synthesis of a new biotin (vitamin H)-functionalized, water-soluble methacrylate (BtOEOMA). The incorporation of BtOEOMA into ssABP through copolymerization allowed for the preparation of biotin-conjugated degradable micelles. The availability of biotin was determined by both competitive binding assay and fluorescence microscopy. Cell viability assay revealed the non-cytotoxicity of both the non-conjugated and biotin-conjugated forms of the ssABP micelles.

3.2 Experimental section

3.2.1 Materials

2-Hydroxyethyl disulfide (SS-DOH), 3,3'-dithiodipropionic acid (SS-Dacid), dicyclohexylcarbodiimide (DCC), 4-dimethylaminopyridine (DMAP) as a catalyst, triethylamine (Et_3N), α-bromoisobutyryl bromide (Br-iBuBr), copper(I) bromide (CuBr, >99.99%), 1,1,4,7,10,10-hexamethyltriethylenetetramine (HMTETA, 97%), Nile Red (NR), 1-ethyl-3-(3-dimethylaminopropyl) carbodiimide (EDC), oligo(ethylene glycol) methacrylate (HO-OEOMA with MW = 326 g/mol), Avidin from egg white, biotin (>99%, lyophilized powder), 2-(4-hydroxyphenylazo)benzoic acid (HABA), and anisole from Aldrich were used as received. DL-dithiothreitol (DTT, 99%) was purchased from Acros Organics. Oligo(ethylene glycol) monomethyl ether methacrylate (OEOMA with MW =

300 g/mol and pendent EO units DP ≈ 5) from Aldrich was purified by passing it through a column filled with basic alumina to remove inhibitors.

3.2.2 Instrumentation

^{1}H-NMR spectra were recorded using a 500 MHz Varian spectrometer. The $CDCl_3$ singlet at 7.27 ppm and DMF-d_7 singlet at 8.01 ppm were selected as reference standards. Molecular weight and molecular weight distribution were determined by gel permeation chromatography (GPC) with a Viscotek VE1122 pump and a refractive index (RI) detector. Three PolyAnalytik columns (PAS-103L, 105L, 106L, designed to determine molecular weight up to 2,000,000 g/mol) were used with THF as eluent at 30 °C at a flow rate of 1 mL/min. Linear poly(methyl methacrylate) (PMMA) standards were used for calibration. Conversion was also determined using GPC by following the decrease of macromonomer (OEOMA) peak area relative to the increase of polymer peak area.[146] The sizes of micelles in hydrodynamic diameters by volume were measured by dynamic light scattering (DLS) at a fixed scattering angle of 175° at 25 °C with a Malvern Instruments Nano S ZEN1600 equipped with a 633 nm He-Ne gas laser. All micellar dispersions without dilution were filtered by 0.45 μm PES filter to remove large aggregates. Fluorescence spectra were recorded on Varian Cary Eclipse Fluorescence spectrometer using a 1-cm wide quartz cuvette.

3.2.3 Synthesis of ssABP

The dried, purified ssPES-Br (1.4 g, 0.67 mmol), OEOMA (10.0 g, 33.3 mmol), HMTETA (90 μL, 0.33 mmol), and anisole (7.2 mL) were added to a 50 mL Schlenk flask. Freeze-thaw cycles were performed to deoxygenate the samples. CuBr (47.8 mg, 0.33

mmol) was added to the reaction flask when frozen and filled with nitrogen. After another deoxygenation step, the mixture was thawed and an initial sample was taken via syringe. Polymerization was started when the flask was immersed in an oil bath preheated to 47 °C. The polymerization was stopped at 15 min by exposing the reaction mixture to air.

To purify the resulting ssABP, the as-prepared green polymer solution was drop-wise added into hexane (500 mL) under magnetic stirring to remove unreacted OEOMA and ssPES macroinitiators. Note that OEOMA monomer is miscible with hexane. Precipitates were further purified by gravity filtration through basic aluminium oxide with THF as an eluent to remove copper species. The solvent was removed by rotary evaporation and the product further dried overnight in a vacuum oven at 50 °C.

3.2.4 Aqueous micellization of ssABP

Micellar aggregates were prepared by adding deionized water drop-wise into clear polymer solutions consisting of aliquots of the purified, dried ssABP dissolved in THF (2.5 mL). The resulting dispersions were stirred for 24 hrs to remove THF. Using the procedure, micellar dispersions at 0.1 mg/mL were prepared with ssABP (10 mg) and water (100 mL) for DLS, AFM, and TEM measurements. Micellar dispersions at 3.3 mg/mL were also prepared with ssABP (50 mg) and water (15 mL) for thiol-responsive degradation and release of NR.

3.2.5 CMC determination

The purified, dried ssABPs (20 mg) was dissolved in THF (2.5 mL). The resulting clear polymer solution was drop-wise added into deionized water (20 mL). The resulting dispersion was kept under stirring overnight to remove THF, yielding colloidally stable

micelle dispersion in water at a concentration of 1 mg/mL. Then, aliquots of the aqueous stock solution were diluted with different amounts of deionized water to form a series of ssABP solutions at different concentrations from 10^{-5} to 1.0 mg/mL. The pressure (mN/m) of the solutions were measured using tensiometer as follows; An aliquot of each ssABP solution (600 μL) was carefully placed on each well and let to equilibrate before the measurements. The tensiometer was zeroed with air and water.

3.2.6 Thiol-responsive degradation of ssABP

For GPC measurements, aliquots of the dried, purified ssABP (19.2 mg) dissolved in DMF (5 mL) were mixed with DTT (5.3 mg, 1 mole equivalent to disulfides). At different time intervals, aliquots of polymer solutions were taken to analyze molecular weight of their degraded products. For ^{1}H-NMR measurements, a solution of ssABP (8.4 mg) dissolved in DMF-d_7 (600 μL) was analyzed before and after it was mixed with a solution of DTT (2.3 mg) dissolved in DMF-d_7 (300 μL).

3.2.7 Thiol-responsive degradation of micelles in water

Aliquots of micellar dispersion (3.3 mg/mL, 5 mL) were mixed with 5 mM DTT (4.5 mg) under stirring. Aliquots were taken at different time periods to be analyzed using DLS. For ^{1}H-NMR measurements, a second equivalent aliquot (for each time period) was dried by rotary evaporation, the product dissolved in $CDCl_3$ and analyzed over time.

3.2.8 Release of Nile Red for NR-loaded micelles upon thiol-responsive degradation

NR-loaded micelles were prepared similarly to previous dispersions but with one added component. A stock solution of NR in THF (5 mg/mL, 10 μL) was added to the polymer prior to addition of water. After THF was removed from the micelle solution, non-

dissolved NR was removed by filtration using 0.45μm PES filters. The final concentration of ssABP was 3.3 mg/mL. A series of NR-loaded micelles at 0, 0.01, 0.05, and 0.1 mg/mL were prepared to measure their emission spectra (λ_{ex} = 480 nm) as described in the literature. For release experiments, a NR-loaded micellar dispersion at 3.3 mg/mL was then divided into two equivalent aliquots (3 mL each) in 20 mL vials. One aliquot was used as a control (no DTT) and to another was added DTT (2.3 mg). Their emission spectra were recorded over time and the fluorescence intensity at 620 nm was analyzed.

3.2.9 Synthesis of biotin-functionalized ssABP copolymers

The dried, purified ssPES-Br (0.5 g, 0.33 mmol), OEOMA (5.6 g, 18.7 mmol), HMTETA (45 μL, 0.17 mmol), and anisole (6 mL) were added to a 25 mL Schlenk flask. The same ATRP protocol previously described was used with Cu(I)Br (23.9 mg, 0.17 mmol). 20 minutes after the polymerization was initiated (conv = 0.52), a nitrogen-purged solution of BtOEOMA (586 g/mol, 220 mg, 0.38 mmol) in DMF (1 mL) was added via syringe to the reaction mixture. After another 5 min, the polymerization was stopped by exposing the reaction mixture to air.

3.3 Results and discussion

3.3.1 Synthesis of ssPES-b-POEOMA (ssABP)

As illustrated in Figure **3.1**, a reductively-cleavable polyester having a terminal hydroxyl group, ssPES-OH, was prepared by polycondensation through a facile carbodiimide coupling reaction of a SS-DOH (a diol) and a SS-DCOOH (a diacid). The resulting ssPES-OH had a molecular weight = 1900 g/mol with M_w/M_n = 1.6 (Figure **B.1**). Bromination of ssPES-OH with Br-iBuBr resulted in the synthesis of ssPES-Br

macroinitiator with molecular weight = 2100 g/mol and M_w/M_n = 1.5. ^{1}H-NMR was used to confirm the successful synthesis of ssPES-OH and ssPES-Br having disulfides positioned on main chains (Figure **B.2**). Synthesis and characterisation of ssPES-OH and ssPES-Br were conducted by Andrew Nelson-Mendez (in our laboratory) and the details are described in our publication.[99]

After successful bromination of ssPES-OH with Br-iBuBr, the chain extension of the resulting ssPES-Br with water-soluble POEOMA was performed by direct ATRP to synthesize well-defined ssPES-b-POEOMA (ssABP). The conditions include the initial mole ratios of $[OEOMA]_0/[ssPES\text{-}Br]_0/[CuBr]_0/[HMTETA]_0$ = 50/1/0.5/0.5 and OEOMA/anisole = 1/1 w/w in anisole at 47 °C. After 15 minutes, polymerization was stopped by subjecting the polymer mixture to air. Resulting ssABP was purified by precipitation from hexane to remove unreacted monomer, followed by elution through a basic alumina column to remove unreacted initiator and Cu species. ^{1}H-NMR and GPC were used to analyze the final polymer. As seen in Figure **3.2A**, ^{1}H-NMR spectrum shows new peaks: a singlet appeared at 3.3 ppm corresponding to methoxy protons (h) and the multiple peaks at 0.8-1.1 ppm corresponding to the methyl protons (g) from POEOMA chains. EO protons appeared between 3.5 and 3.8 ppm. GPC results indicate a shift towards higher molecular weight from 2,100 g/mol of ssPES-Br to 12,000 g/mol for ssABP (Figure **3.2B**). Interestingly, molecular weight distribution became narrower as decreasing from M_w/M_n = 1.5 to 1.2. A plausible reason is the small weight-fraction of ssPES block compared to POEOMA blocks (~17%), which cannot contribute significantly to molecular weight distribution. These results suggest that the new method utilizing a combined carbodiimide coupling polycondensation reaction and ATRP enables the synthesis of well-

controlled ssABPs consisting of a hydrophobic ssPES block with disulfide linkages positioned repeatedly along the main chains and a water-soluble POEOMA block.

3.3.2 Aqueous micellization of ssABPs

The resulting ssABP is amphiphilic, and thus can self-assemble to form micellar aggregates consisting of a ssPES core and POEOMA coronas.[147] The critical micellar concentration (CMC) of ssABP was determined by tensiometry. A stock solution of ssABP in water at 1.0 mg/mL was prepared by mixing ssABP in THF with water, followed by evaporation of THF. Aliquots of the stock solution was diluted with different amounts of water to obtain final concentrations between 10^{-5} to 1 mg/mL. Figure **B.4** shows the plot of surface pressure values measured using a tensiometer vs. various concentrations of ssABPs in water. At low concentrations, pressure does not change; however it increases as ssABP concentrations increase. From two equations obtained by fitting each dataset to linear relationships, the CMC of ssABP with 11,000 g/mol was determined to be 8 μg/mL.

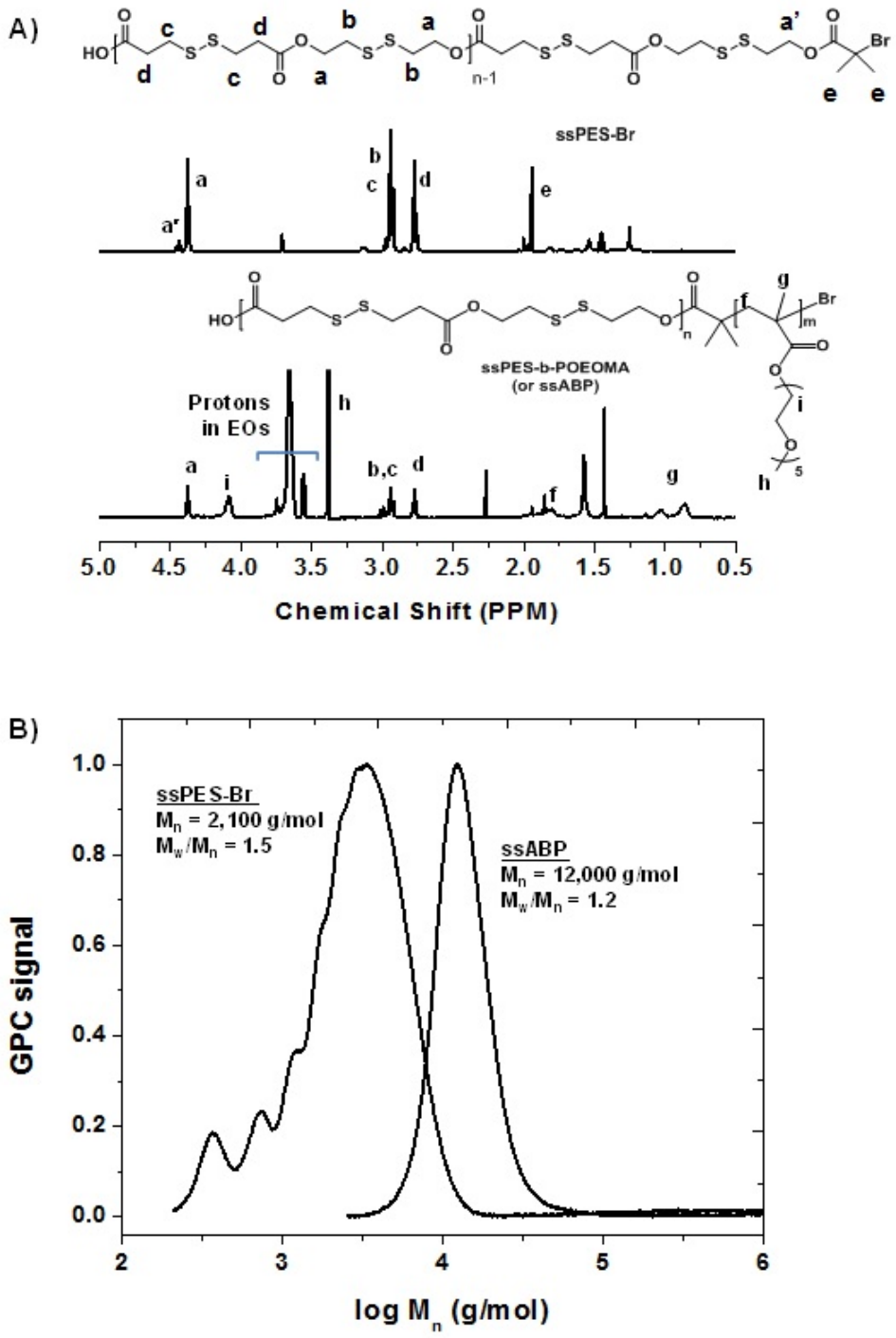

Figure 3.2. ^{1}H-NMR spectra (A) and GPC traces (B) of ssPES-Br and ssABP after purification. Conditions for ATRP: $[OEOMA]_0/[ssPES\text{-}Br]_0/[CuBr/HMTETA]_0 = 50/1/0.5$ and OEOMA/anisole = 1/1 w/w.[122]

Next, a micellar dispersion at 0.1 mg/mL, a concentration above CMC, was prepared using a solvent-evaporation method.[148] After filtration using a 0.45 μm PES filter, the size and morphologies of micellar aggregates were examined using DLS, TEM and AFM (Figure **3.3**). Note that AFM and TEM measurements were performed by Dr. R. Schmidt in the (Center for NanoScience Research) and B. Khorsand (in our laboratory), respectively. DLS results indicate that the micelles had a diameter = 68.4 ± 6.2 nm with a monomodal distribution (Figure **3.3A**). The average diameter and standard deviation was calculated from three measurements of one sample, each being the average of 10 scans. For the AFM measurements, the micellar dispersion at 0.1 mg/mL was spin-cast (1000 rpm x 10s) on to freshly cleaved mica, followed by allowing the sample to dry in air. AFM images suggest spherical morphologies of the dried micelles with a diameter of 105.3 ± 22 nm, on mica surfaces. The size is larger than that determined by DLS due to flattening of micelles on mica as suggested by the height of 4 ± 1 nm (Figure **3.3B**). To prepare samples, the micellar dispersion at 0.1 mg/mL was dropped onto the TEM copper grids (400 mesh, carbon coated). The grids were dried in air. TEM images suggest that diameter = 14.4 ± 2.9 nm (Figure **3.3C-D**). This smaller diameter is caused by dehydration of micelles causing POEOMA chains to compact into a collapsed state.[149] The results of DLS, AFM and TEM suggest that ssPES-b-POEOMA ssABPs formed spherical monomodal micelles with an ssPES degradable core surrounded by hydrophilic stabilizing POEOMA coronas in aqueous solution.

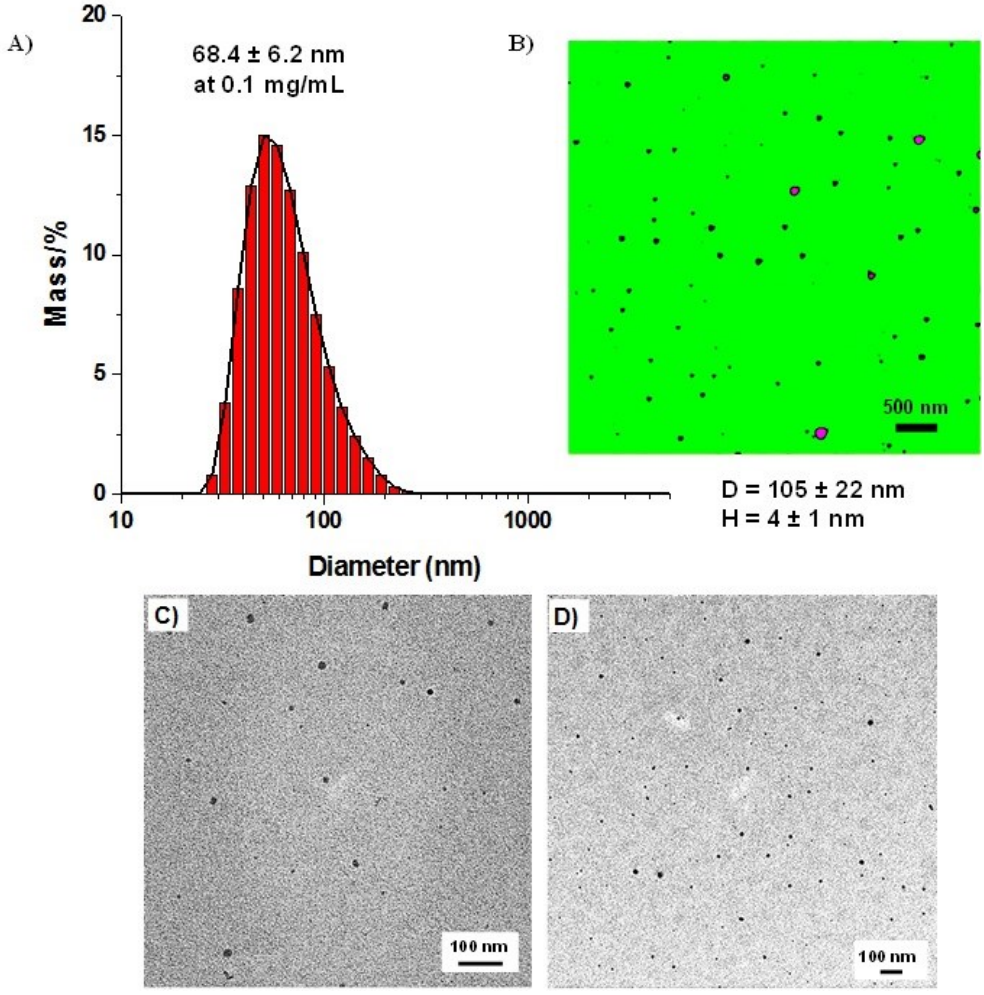

Figure 3.3. DLS diagram (A), AFM image with size = 5 µm x 5 µm and scale bar = 500 nm on mica (B) and TEM images with different magnifications (C) of self-assembled ssABP micellar aggregates at 0.1 mg/mL.[122]

3.3.3 Reductive degradation of ssABPs and their micelles

ssABPs and their ssPES precursors are labeled with disulfide linkages along their main chains. To examine the reductive cleavage of disulfide into their corresponding thiols, aliquots of ssPES and ssABPs were first mixed with DTT whose amount was 1:1 mole equivalent to disulfides. GPC was used to follow the degradation. For ssPES precursors, the GPC traces taken after 10 minutes significantly evolved to low molecular weight

regions with the decrease of molecular weight from M_n = 2500 g/mol to M_n < 150 g/mol, as a result of rapid cleavage of multiple disulfides labeled on polyester main chains (Figure **3.4A**). Similarly, the molecular weight of ssABP decreased from 12 000 g/mol to 8 300 g/mol in the presence of DTT within 15 min. (Figure **3.4B**). The relatively larger molecular weight after degradation can be attributed to the generation of POEOMA-SH degraded products.

Furthermore, the degraded product was analyzed by ^{1}H-NMR in DMF-d_7 inside an NMR tube, 30 minutes before and after the addition of DTT. As seen in Figure **3.5**, disulfide linkages of ssPES were cleaved upon thiol-disulfide exchange reactions with DTT. A peak at 4.4 ppm representative of ssPES methylene protons disappeared after 30 minutes and a new peak at 4.2 ppm can be seen. Moreover, other methylene protons that define the ssPES block between 2.5 ppm and 2.8 ppm have shifted positions. Linear ssPES and ssABP degradation results show that multiple disulfides along the hydrophobic main chain leads to fast degradation of the polymer chain in less than 15 minutes. As shown before, repeated cleavable linkages in the polymer backbone lead to faster degradation.

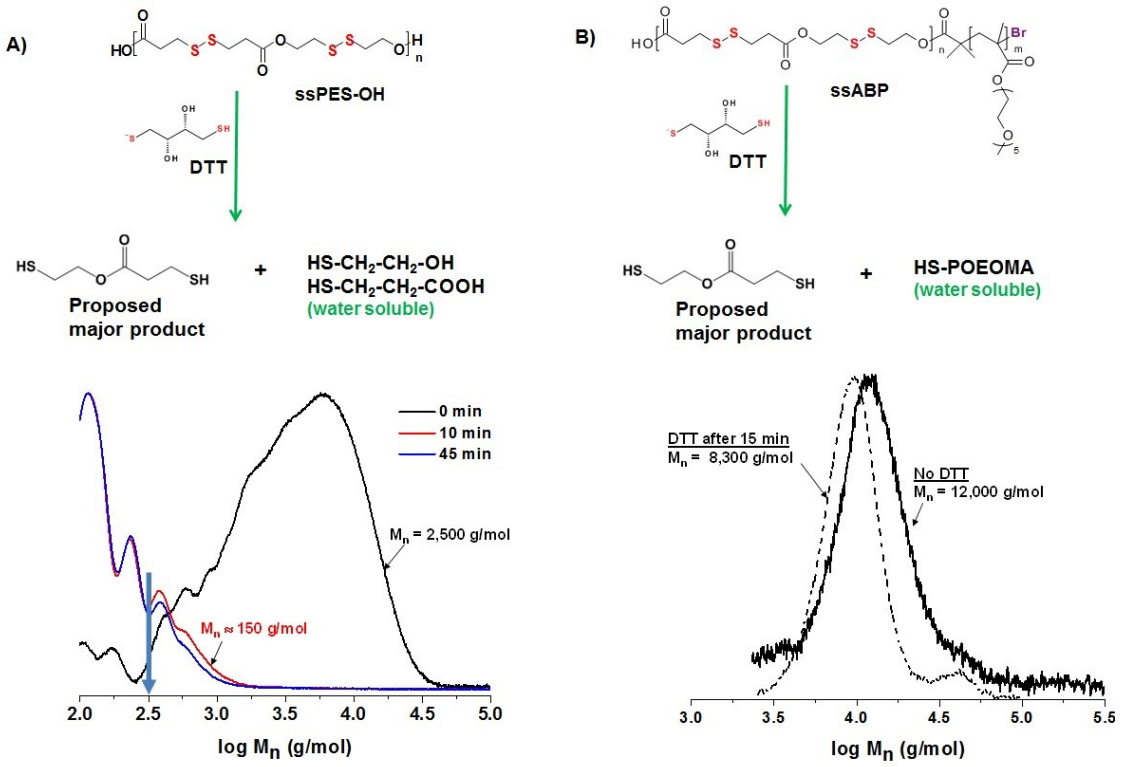

Figure 3.4. Thiol-responsive degradation and GPC traces of ssPES-OH (A) and ssABP (B) with their degraded product.

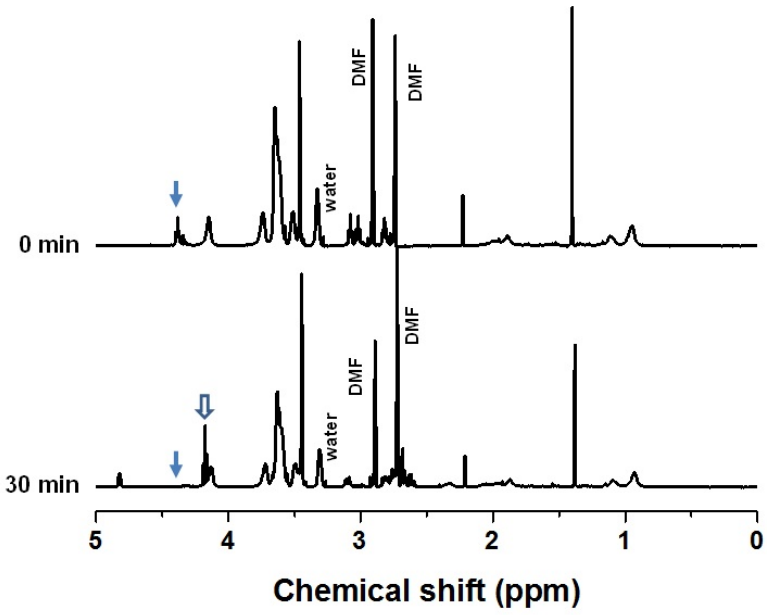

Figure 3.5. ^{1}H-NMR spectra of ssABP before and 30 minutes after addition of DTT (1 mole equivalent ratio to disulfides) in DMF-d_7.

Next, degradation of ssABP-based micelles in aqueous solution upon the cleavage of disulfides in response to DTT, was investigated. Aliquots of aqueous micellar aggregates at 3.3 mg/mL in aqueous solutions were prepared using the solvent evaporation method. Aliquots of the micellar dispersion were mixed with 5 mM DTT in different vials under stirring. At different time intervals, the dispersions were divided into two aliquots. One aliquot was immediately analyzed to measure micelle size distribution by DLS and the other was analyzed for chemical composition by ^{1}H-NMR and molecular weight by GPS after evaporation of solvents. Figure **3.6** shows ^{1}H-NMR spectra of samples in $CDCl_3$ before and after the addition of DTT over time. The peaks at 4.4 ppm (a) and 2.9 ppm (b and c), corresponding to methylene protons, disappeared steadily with time upon addition of DTT. New peaks appeared at 4.2 ppm (a′) and at 2.7 ppm (b′ and c′), which are attributed to the proposed major degraded product. The extent of the degradation was estimated using integration ratios of peaks a and e. Within 10 minutes, 55% of disulfide linkages were cleaved and more than 99% cleavage was seen after 90 minutes. GPC results also suggest the rapid decrease in molecular weight from 12 000 g/mol to 8 200 g/mol (Figure **B.4**). The ^{1}H-NMR and GPC results suggest the significant rapid degradation of ssPES cores in ssABP micelles upon the cleavage of disulfides in the main chains, compared to other micellar systems labeled with disulfide linkages along backbones. Indeed, Fan et al. show that micelles containing poly(amido amine) grafted with PEO take >120 hours to achieve 90% degradation.[68] Another example is the hyperbranched multiarm polyphosphate discussed earlier which also has disulfide bonds positioned repeatedly in its backbone. Release of DOX was slow as even after 45 hours, fluorescence intensity failed to plateau.

Furthermore, samples without DTT added showed DOX leakage indicating high micelle permeability.[65]

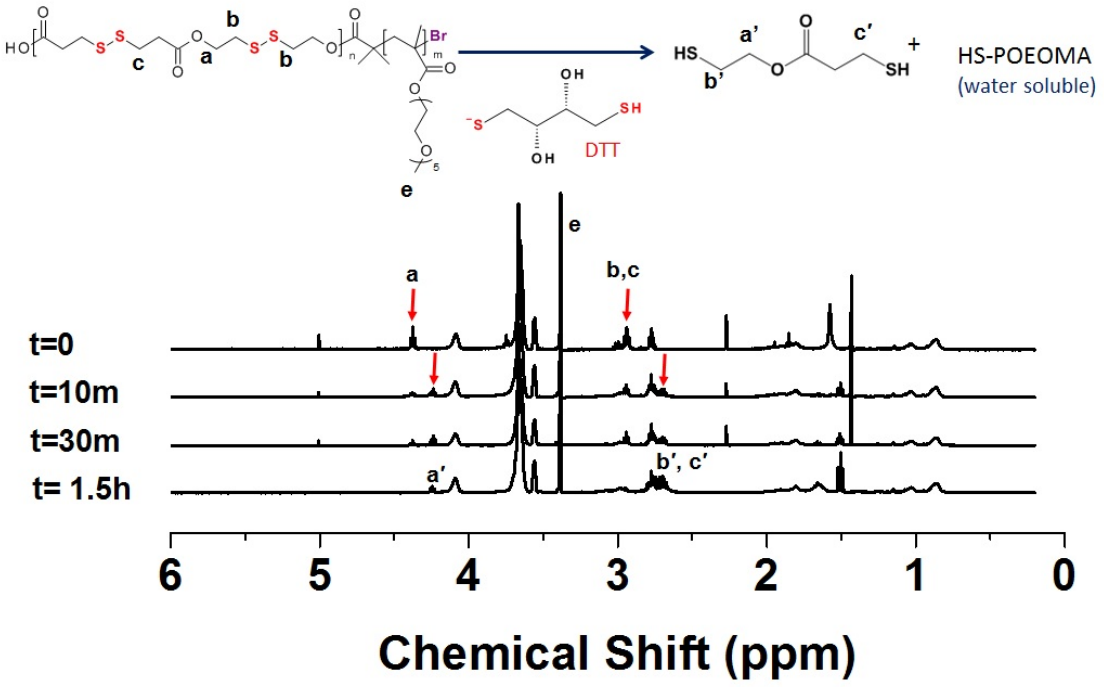

Figure 3.6. ^{1}H-NMR spectra in $CDCl_3$ for mixtures of ssABP micellar aggregates with DTT in water over degradation time.

DLS was also used to monitor the change in size distribution of aqueous micellar aggregates at 3.3 mg/mL in the absence and presence of 5 mM DTT. Figure **3.7** shows the evolution of size distribution in volume% of ssABP micelles over time. In the absence of DTT as a control, no significant change in size distribution occurred over 5 hrs. When 5 mM DTT was added, the size distribution of micellar aggregates became bimodal with the occurrence of a new smaller-sized population within 30 min. The distribution became broader and further aggregated to larger particles (> 1 μm). The hydrophobic nature of the cleaved product might induce aggregation, leading to large particle formations over

extended period of times. These results suggest that the degradation of ssPES cores in response to water-soluble thiols caused micellar aggregates to be destabilized and disintegrated over time. Similar results are reported for other degradable ABP micelles.[65, 150]

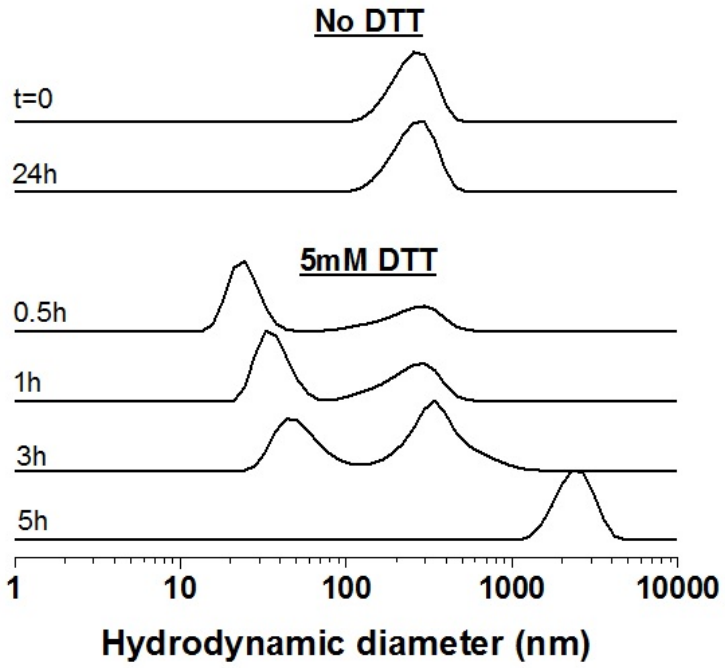

Figure 3.7. Evolution of DLS diagrams (normalized volume %) for ssABP micellar aggregates (3.3 mg/mL) mixed without and with 5 mM DTT over time.

Another experiment was designed to explore the DTT-responsive degradation of ssABP micellar aggregates in a mixture of 6/4 wt/wt THF/water. Water was gradually added into a clear solution of ssABP dissolved in THF until the mixture became turbid, suggesting the formation of micellar aggregates with a diameter = 569 nm. When DTT (1 mole equivalent to disulfides) was added, the mixture turned clear after 45 min. As seen in Figure **B.5**, the DLS results indicate the significant decrease in diameter to <10 nm,

suggesting the complete dissociation of micellar aggregates in the presence of DTT. As proposed in Figure 3.5B, degraded products of ssABP include HS-terminated POEOMA (HS-POEOM, $M_n \approx 9{,}500$ g/mol) soluble in water and THF, while the proposed major species are insoluble in water. Upon degradation of micellar ssPES cores in water, hydrophobic major species could be stabilized by relatively high molecular weight HS-POEOMA chains, resulting in micelle-like structures with a diameter = ca. 100 nm. In contrast, the same major degraded species could be dissolved in THF/water mixture (6/4 wt/wt), resulting in clear solution.

3.3.4 Thiol-responsive enhanced release of model drugs

In order to assess an application of ssABP micelles as controlled drug delivery nanocarriers, the release of encapsulated Nile Red (NR), a hydrophobic model drug in response to reduction reactions was investigated. NR is a solvatochromic fluorescent dye whose emission wavelengths are varied with the polarity of solvents.[151] Nile Red emits a stronger fluorescence intensity (FI) and is blue shifted in hydrophobic environments, while it is red shifted in more hydrophilic environments, with a lower fluorescence intensity. This property has been exploited to qualitatively characterize the release kinetics of NR from micelles.[152-153] This method monitors the change in the FI of NR as it is released from the hydrophobic micellar core into the surrounding water. This change in environment polarity causes a dramatic decrease in the FI of NR due to a higher polarity and lower solubility of NR in water.

First, several control experiments were designed to learn the change in the emission of Nile Red in hydrophobic vs hydrophilic environments. In the first set of experiments, a series of samples with equal amounts of Nile Red in organic solution of different volume

ratios of THF/water from 0/100 to 100/0 V/V were prepared and their emission spectra recorded with λ_{ex} = 480 nm. As seen in Figure **B.6**, fluorescence intensity decreased and λ_{max} was red shifted as the amount of water increased. These results are consistant with literature.[154] Figure **B.7** shows an increase in the amount of PEO also affects fluorescence intensity by increasing the solubility of NR in the sample. However, no shift is present in this case because PEO is hydrophilic. Other experiments we conducted have confirmed that only when the hydrophobic core of a micelle is present, a blue shift is observed in Nile Red's emision spectra.

A series of mixtures of the same amount of NR with different amounts of ssABP were prepared using the solvent evaporation method after removal of THF. As seen in Figure **B.8**, the FL intensity of NR increased with an increasing amount of ssABP, suggesting that more NR molecules are entrapped in micelles. The slight red shift could be caused by a more polar environment due to the presence of relatively larger concentrations of POEOMA in the medium, rendering the overall environment more hydrophilic. To test NR release in response to thiols, a NR-loaded micellar dispersion at 3.3 mg/mL concentration (diameter = 220 nm by DLS) was divided into two samples: one without DTT (as control) and with 5 mM DTT. Figure **B.9** shows the overlaid fluorescence spectra of NR in the two mixtures and Figure **3.8A** shows the evolution of normalized FL intensity at λ_{max} = 620 nm over time. In the absence of DTT, no significant change in FL intensity was observed, suggesting neither release nor photobleaching of a significant amount of NR from micelles. NR is confined in small micellar cores (digital image **B1** in Figure **3.8**). When 5 mM DTT was added, the FL intensity decreased significantly within 40 min. Such FL decrease is attributed to enhanced release of NR from hydrophobic micellar cores to

aqueous solution as a result of thiol-induced degradation of micelles by cleavage of disulfides. Because of the low solubility of NR in water, the resulting micellar dispersion containing released free NR became turbid (digital image **B2** in Figure **3.8**). The turbid dispersion became translucent when the dispersion was subjected to centrifugation, upon which free NR was precipitated in aqueous solution (digital image **B3** in Figure **3.8**). These results indicate that the thiol-responsive degradation of micellar aggregates of ssABPs having disulfide linkages positioned repeatedly on the hydrophobic main chains enhanced the release of encapsulated model drugs.

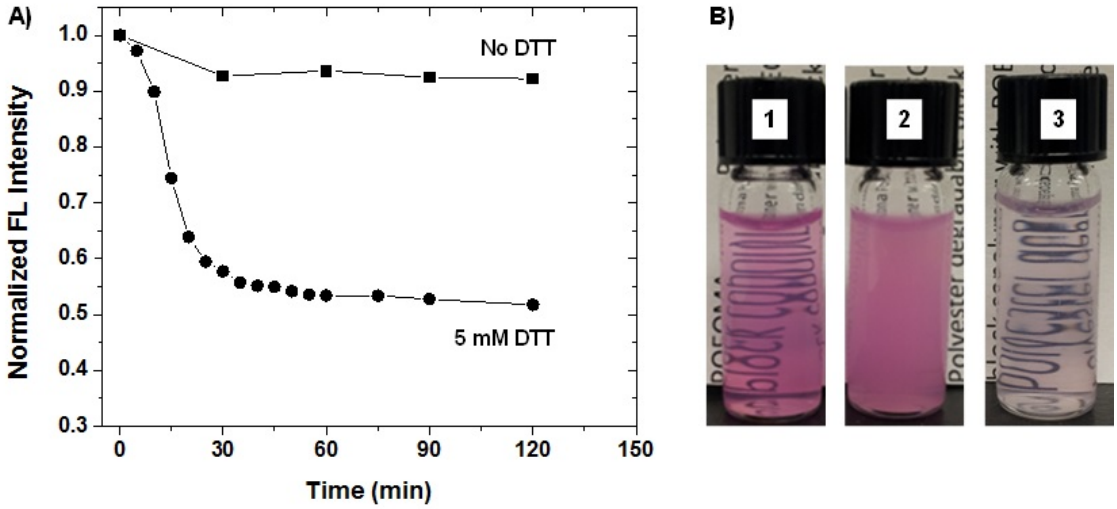

Figure 3.8. Release profile of NR from NR-loaded ssABP-based micelles in water without and with 5 mM DTT (A) and digital images for NR-loaded micelles (B) mixed without (1) and with DTT before (2) and after (3) centrifugation to remove free NRs released from micelles in water.

3.3.5 Bioconjugation with biotin

Applicability of the new method towards bioconjugation during ATRP was explored. The first step involves the synthesis of a biotin-functionalized methacrylate (BtOEOMA), synthesized by the carbodiimide coupling of a COOH group of biotin with

an OH group of HO-OEOMA. Next, BtOEOMA (2 mol% of OEOMA) was introduced at 52% conversion during the ATRP of OEOMA in the presence of ssPES-Br macroinitiators. In this way, the resulting biotin-functionalized ssABP (ssABP-Biotin) is a triblock copolymer of ssPES-b-POEOMA-b-P(OEOMA-co-BtOEOMA) having pendent biotin moieties positioned mostly at the end of the hydrophilic block (Figure **3.9**). GPC results indicate an increase in conversion from 52 to 60% (increased by ≈ 8%) as well as an increase in molecular weight from 11,400 g/mol to 13,000 g/mol after the addition of BtOEOMA. The resulting ssABP-Biotin self-assembled toward degradable micellar aggregates bioconjugated with biotin molecules localized at the end of POEOMA corona chains by aqueous micellization. The CMC of ssABP-Biotin was 7 μg/mL determined by tensiometry. This value is similar to that (8 μg/mL) of ssABP with M_n = 11,000 g/mol but without biotin conjugation.

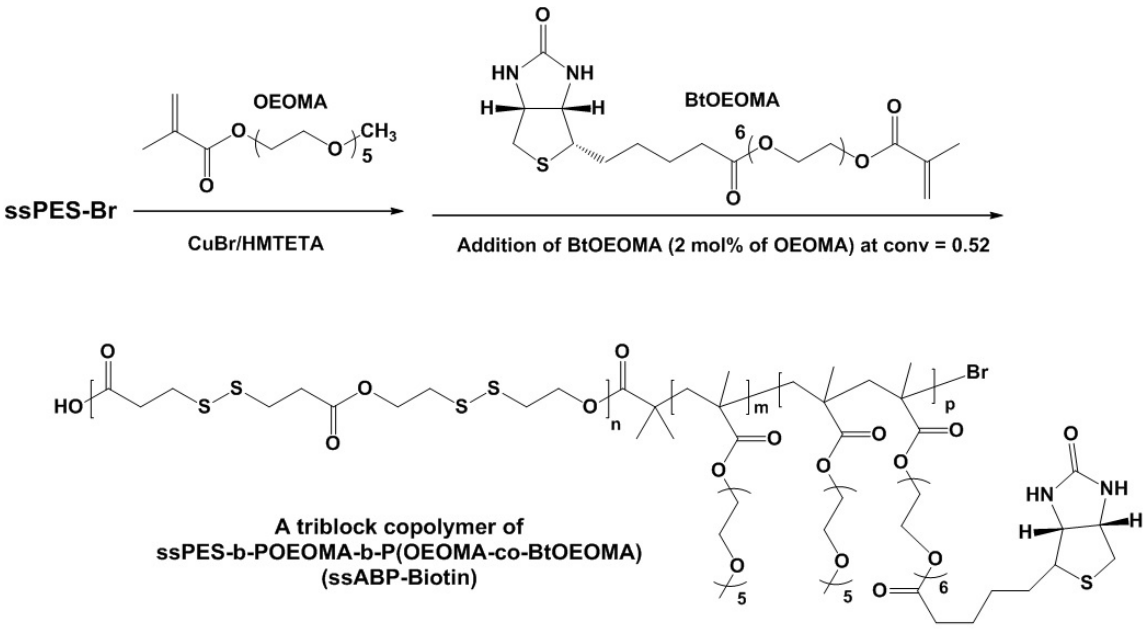

Figure 3.9. Pathway for synthesis of ssABP-biotin by ATRP.

The availability of biotin presented from ssABP-Biotin copolymers was evaluated by a competitive binding assay and fluorescence microscopy. The amount of available biotin in copolymers was quantified by the Avidin-HABA assay using UV/vis spectroscopy. Avidin is a protein having four binding pockets. Because of the stronger affinity of biotin to Avidin ($K_d = 10^{-15}$M) as opposed to HABA, biotin molecules replace HABA molecules in an Avidin-HABA complex. In fact, the biotin-avidin complex is the strongest known non-covalent bond interaction between a protein and a ligand.[155] In our experiments, aliquots of ssABP-Biotin micellar dispersion were mixed with aqueous Avidin-HABA complex. Figure **3.10** shows an example of the decrease in absorbance at 500 nm by $\Delta A = 0.17$, which is attributed to Avidin-HABA complexation upon addition of ssABP-Biotin. Using the calibration curve reported elsewhere,[156-157] the availability of biotin in ssABP-Biotin was calculated to be 0.40 ± 0.03 mg biotin/g polymer on average (three measurements). The incorporation of BtOEOMA into ssABP-Biotin polymer was also calculated to be 8.9 ± 0.8 wt%. This value is close to 8 wt% of OEOMA conversion, which corresponds to ≈ 100% incorporation efficiency at the given time interval (5 min). As illustrated in Figure **3.9**, pendent biotins are positioned locally at the end of hydrophilic coronas in degradable micelles. It can be anticipated that such localization of biotin molecules can enhance the active targeting ability of ssABP-Biotin micelles toward cancer cells *in vivo*.

The avidin-biotin-ssABP complexation was further investigated with NR using fluorescence microscopy. NR-loaded micelles of ssABP-Biotin were prepared using an extensive dialysis with MWCO = 3,500 g/mol over water to remove any free NR molecules. Dialyzed NR-loaded micelles and their mixture with Avidin were spin-cast on

glass plates and allowed to be dried overnight at room temperature. Figure **B.10A** shows the FL image for NR-loaded ssABP-Biotin micelles, in which FL signals are individually localized. However, upon the addition of Avidin, the FL image for the mixture shows that fluorescence signals are aggregated, suggesting the formation of a biocomplex of micelles with Avidin (Figure **B.10B**). These results show a facile bioconjugation method for ssABP, which could therefore be used for active targeting of micelles toward cancer cells in vivo.[158]

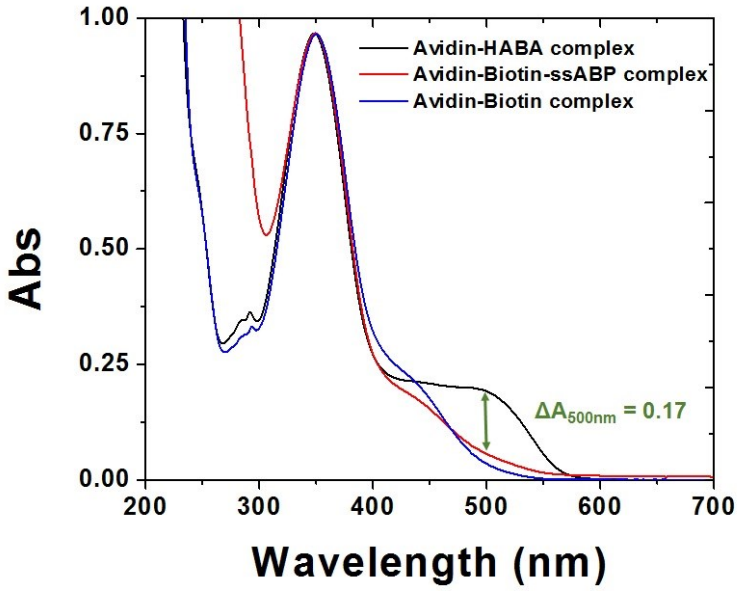

Figure 3.10. UV/Vis spectra of avidin-HABA complex before and after addition of ssABP-biotin micelles.

3.3.6 MTS cytotoxicity assay

Furthermore, a 3-(4,5-dimethylthiazol-2-yl)-5-(3-carboxymethoxyphenyl)-2-(4-sulfophenyl)-2H-tetrazolium (MTS) cell viability assay of ssABP micelles was performed by Behnoush Khorsand, using human embryonic kidney cells (HEK293T). Cells were cultured with different concentrations of micelles of ssABP and ssABP-Biotin after their

extensive dialysis over water. Cells without polymers as controls were also included. After 48 hr incubation, absorbance was measured using an absorbance-based plate reader and corrected for an increase due to light scattering of micelles to determine viability. Figure **3.11** suggests >90% viability of HEK cells, with no significant difference compared to control cells, indicating that both ssABP and ssABP-Biotin block copolymers up to 110 μg/mL are nontoxic to cells, and thus are biocompatible.

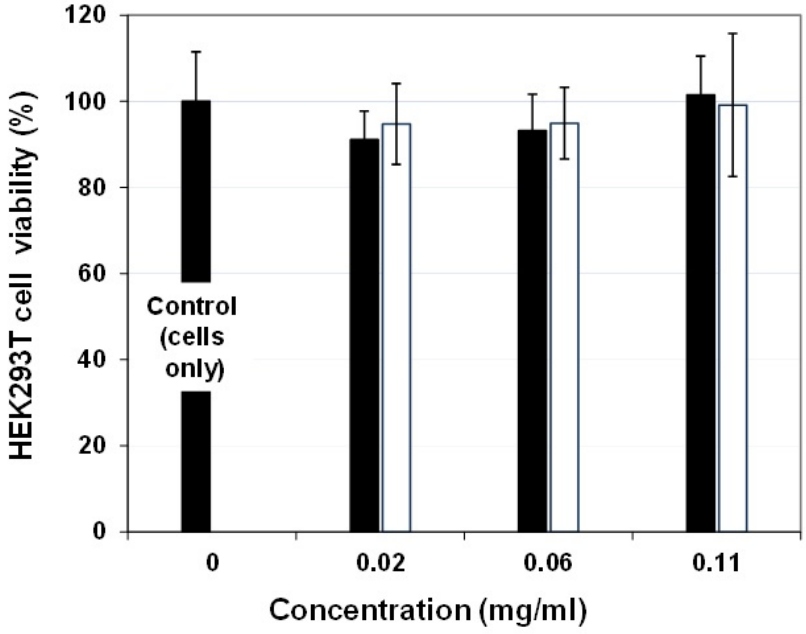

Figure 3.11. Viability of HEK293T cells cultured with various amounts of ssABP (filled) and ssABP-biotin (empty) for 48 h using the MTS assay.

3.4 Conclusion

The facile method utilizing carbodiimide coupling polycondensation combined with ATRP allowed for the synthesis of well-defined thiol-responsive degradable ssABPs. These ssABPs consist of a water-soluble polymethacrylate block, ensuring enhanced colloidal stability and non-cytotoxicity, and a hydrophobic degradable ssPES block with

disulfide linkages positioned repeatedly along the main chains, enabling rapid degradation in response to reducing conditions. GPC and ^{1}H-NMR spectra confirmed the synthesis of well-defined ssABP with $M_w/M_n < 1.2$. A combination of DLS, AFM, with TEM results indicate that ssABP formed, through aqueous micellization, monomodal spherical micellar aggregates having a degradable ssPES core surrounded with hydrophilic POEOMA long corona.

In response to reductive reactions, both ssPES-containing ssABP and their micellar aggregates rapidly degraded. DLS results suggest the degradation of ssPES cores caused the destabilization and disintegration of micellar aggregates, leading to enhanced release of encapsulated model drugs. Furthermore, the coronas were easily decorated with biomolecules during ATRP for active targeting. A facile bioconjugation was demonstrated via the synthesis and incorporation of new BtOEOMA, resulting in ssPES-b-POEOMA-b-P(OEOMA-co-BtOEOMA) triblock copolymers with biotin positioned at the end of the water-soluble corona during the ATRP. The availability of biotin was determined to be 0.40 ± 0.03 mg biotin/g polymer using Avidin-HABA assays. These significant results, combined with non-toxicity to cells, suggest that well-defined thiol-responsive ssABP micelles offer versatility in multifunctional drug delivery

CHAPTER 4

THERMORESPONSIVE HYDROGELS WITH DISULFIDE BRIDGES

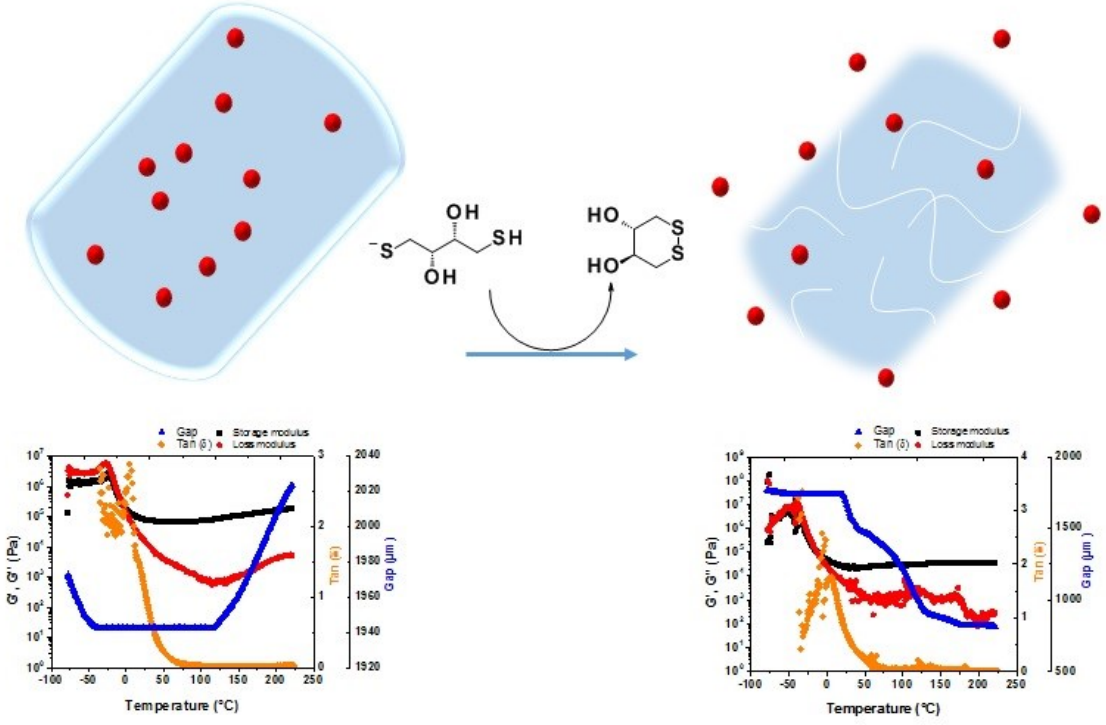

Chapter 3 investigated the use of degradable disulfide linkages in drug delivery strategies. Disulfide bonds can also be used in other types of systems and be strategically positioned to confer enhanced properties once cleaved. One other such system is the hydrogel. In this chapter, a facile strategy to fabricate thiol-responsive thermoresponsive hydrogels able to rapidly change their volume in response to temperature is reported. The strategy utilizes crosslinking atom transfer radical polymerization to synthesize well-

defined hydrogels of thermoresponsive oligo(ethylene oxide)-based polymethacrylates with uniform network crosslinked with dynamic disulfides. Thiol-responsive cleavage of disulfide linkages to the corresponding pendant thiols allow for the generation of hydrophilic dangling chains in the hydrogels as well as the increase in hydrophilicity of hydrogel network. The degraded hydrogels exhibit rapid change of thermoresponsiveness (deswelling kinetics) with a slight sacrifice in mechanical properties. Evaluating the hydrogels from a biomedical perspective, rapid thermoresponsive hydrogels are non-cytotoxic and exhibit enhanced release of encapsulated model drugs.

4.1 Introduction

Thermoresponsive hydrogels undergo volume change in response to temperature. They shrink and expel water above the LCST, while above the LCST they swell and absorb water.[94, 131] This unique property makes thermoresponsive hydrogels effective candidates for various biomedical applications in tissue engineering,[159-160] drug delivery,[161-162] as biosensing and detection,[163-165] intracellular thermometry[166] and bioconjugation.[167-168]

A repeating problem of covalently-linked thermoresponsive hydrogels involves the formation of an impenetrable hydrophobic "skin layer" on the surface of the gel. The skin layer is attributed to a faster transition of the gel surface from hydrophilic to hydrophobic compared to inside the gel, upon heating at above LCST.[169] To circumvent this problem, a rapid response for water release is required in the hydrogel matrix. Several approaches involve the introduction of hydrophilic chains or domains to enhance water release rate. They include grafting dangling chains with surface active molecules,[170-173] adjusting hydrophilic/hydrophobic balance,[174] forming interpenetrating polymer networks (IPN)[175] and heterogeneous crosslinked networks.[176-179] However, these approaches are often associated with a decrease of the hydrogel swelling ratio.[171, 178]

Stimuli-responsive degradation (SRD) is a dynamic and powerful platform that involves the cleavage of covalent bonds in response to external stimuli such as low pH, light, or ultrasound, as well as reductive, oxidative, or enzymatic reactions.[53, 180] Disulfides are cleaved to the corresponding thiols in a reducing environment or through a disulfide-thiol exchange.[181] Disulfide-thiol degradation chemistry offers an advantageous SRD platform in constructing reductively-responsive degradable nanomaterials desirable for various biomedical applications; these include self-assembled micellar

nanocarriers,[182-183] nanocapsules,[184] nanogels,[185-187] hydrogels,[188-189] and bioconjugates.[190-192] Furthermore, this type of degradation chemistry has been explored for tuning lower critical solution temperature (LCST) of polymeric materials[193-194] and changing morphologies of self-assembled nanostructures.[195] Moreover, disulfide crosslinked-hydrogels that can undergo reductively-responsive cleavage would be interesting as smart precursors for the synthesis of unique thermoresponsive nanomaterials with rapid change of thermoresponsive properties.

This chapter describes thiol-responsive thermosensitive PEO-based hydrogels chemically cross-linked via a degradable disulfide containing cross-linker for the enhancement of thermoresponsive properties. Thermoresponsive hydrogels were synthesized by AGET ATRP of di(ethylene glycol) methyl ether methacrylate (MeO_2MA) using a PEO-Br initiator in the presence of a degradable (ssDMA) cross-linker. ATRP ensures the synthesis of hydrogels with more uniform networks and higher swelling ratios compared to hydrogels prepared by free radical polymerization.[157, 195] Indeed, hydrogels synthesized by CRP undergo fast initiation, slow propagation and reduced chances of termination reactions leading to more relaxed primary chains, increasing the chances to react with pendent vinyl groups and form branching points.[196] On the other hand, free radical polymerization chains can react with their own pendent vinyl groups which can lead to a dense nanogel network possessing a very low swelling ratio. Moreover, linkage of preformed hyperbranched polymers is the cause of gelation in CRP gels. These branched chain ends create dangling chains that increase swelling ratio.[196-197]

Using degradable crosslinkers, after hydrogel formation, reductive cleavage of the disulfides into corresponding thiols will generate dangling chains in the network (Figure

4.1). These hydrophilic pendent thiols increase the polarity of the hydrogel and create pores within the structure, resulting in enhanced thermoresponsiveness but lowering mechanical properties. Further applicability of these porous hydrogels towards biomedical applications was assessed with studies on cell viability and release of encapsulated dyes. Swelling ratio and mechanical properties are further compared with hydrogels containing permanent cross-linkers.

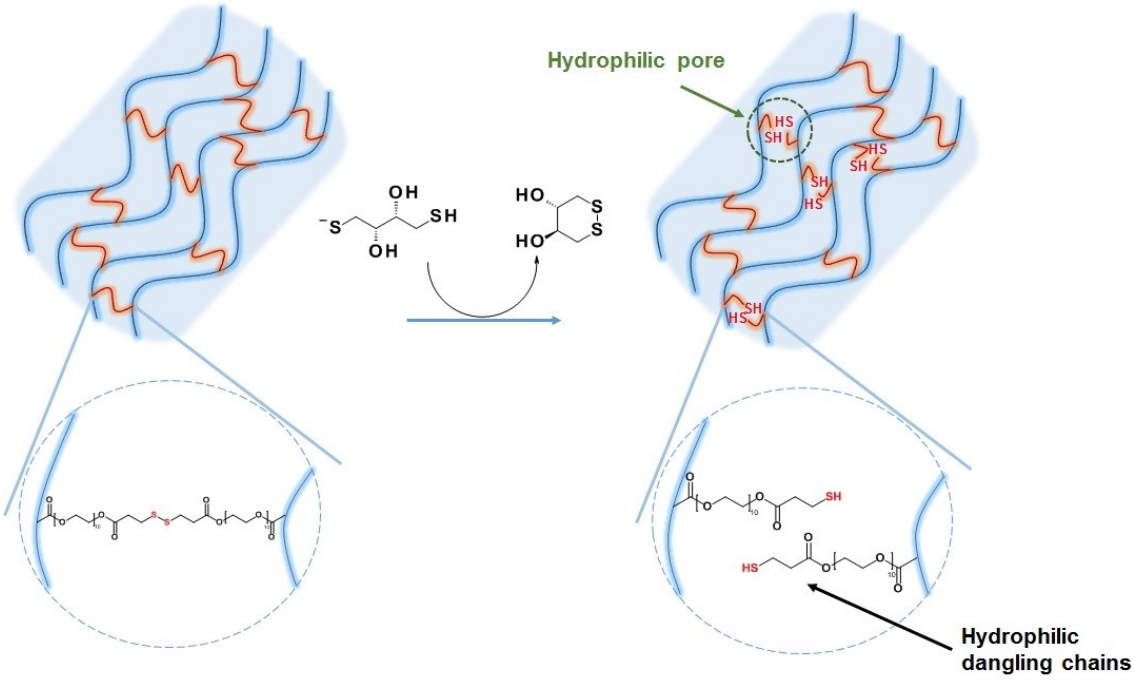

Figure 4.1. A facile strategy utilizing disulfide-thiol degradation chemistry to synthesize thiol-responsive hydrogel scaffolds for enhanced thermo-responsive properties.

4.2 Experimental section

4.2.1 Materials

Poly (ethylene glycol) monomethyl ether (PEO-OH, MW = 5000 g/mol with ethylene oxide (EO) # ≈ 113), 2-bromoisoburylic acid (BriBuA, 98%), poly(ethylene glycol) methacrylate (POEOMA526, MW = 526 g/mol with EO# ≈ 10), 3,3′-dithiopropionic acid (ssDCOOH, 99%), N,N′-dicyclohexyl carbodiimide (DCC), N,N-dimethylaminopyridine (DMAP), Tin(II) 2-ethylhexanoate ($Sn(EH)_2$, >95%), 2,2′-bipyridine (bpy, 98%), Rhodamine-6G (R6G, 99%), and 5,5′-dithiobis(2-nitrobenzoic acid) (DTNB, Ellman reagent, ≥98%) from Aldrich Canada, copper(II) bromide ($CuBr_2$, >99.99%) from Acros Organics and dithiothreitol (DTT, ≥99%) from fisher scientific were purchased and used as received. Di(ethylene glycol) methyl ether methacrylate (MEO_2MA, 95%) from Aldrich was purified by passing it through a column filled with basic alumina to remove inhibitors. An aqueous buffer solution at pH = 8.0 was prepared by dissolving sodium phosphate dibasic (0.1 mM) and EDTA (1 mM) in deionized water.

4.2.2 Instrumentation

^{1}H-NMR spectra were recorded using a 500 MHz Varian spectrometer. The $CDCl_3$ singlet at 7.26 ppm was selected as the reference standard. Spectral features are tabulated in the following order: chemical shift (ppm); multiplicity (s - singlet, d - doublet, t – triplet, m - complex multiple); number of protons; position of protons. Molecular weight and molecular weight distribution were determined by gel permeation chromatography (GPC). An Agilent GPC was equipped with a 1260 Infinity Isocratic Pump and a refractive index (RI) detector. Two Agilent columns (PLgel mixed-D and mixed-C) were used with DMF containing 0.1 mol% LiBr at 50 °C at a flow rate of 1.0 mL/min. Linear poly(methyl

methacrylate) (PMMA) standards from Fluka were used for calibration. Aliquots of polymer samples were dissolved in DMF/LiBr. The clear solutions were filtered using a 0.25 μm PTFE filter to remove any DMF-insoluble species. A drop of anisole was added as a flow rate marker. Conversion was determined by ^{1}H-NMR for linear polymers and by gravimetry for hydrogels. UV/Vis spectra were recorded on Agilent Cary 60 UV/Vis spectrometer.

4.2.3 Synthesis of PEO-Br macroinitiator

PEO-functionalized 2-bromoisobutyrate (PEO-Br), a water-soluble ATRP macroinitiator, was synthesized as described elsewhere.[198] Briefly, PEO-OH (20 g, 4 mmol) was reacted with BriBuA (740 mg, 4.4 mmol) in the presence of DCC (900 mg, 4.4 mmol) and a catalytic amount of DMAP in dichloromethane (DCM, 200 mL). The formed solids were removed by filtration under vacuum. The product was isolated via rotary evaporation of the solvent and further dried in a vacuum oven at 50 ºC for 12 hrs. ^{1}H-NMR ($CDCl_3$, 7.26 ppm): 1.9 (s, 6H, -C(CH_3)$_2$Br), 3.4 (s, 3H, -OCH_3), 3.45-3.80 (m, EO protons), 4.2 (m, 2H,-CH_2-O(O)C-).

4.2.4 Synthesis of ssDMA cross-linker

Dithiopropionyl poly(ethylene glycol) dimethacrylate (ssDMA) was synthesized as described in the literature.[199] Briefly, 3,3′-dithiopropionic acid (4.6 g, 20 mmol) in THF (60 mL) reacted with POEOMA526 (20 g, 38 mmol) in the presence of DCC (7.8 g, 38 mmol) and a catalytic amount of DMAP in DCM (120 mL). The product was purified by vacuum filtration and solvent evaporation. ^{1}H-NMR ($CDCl_3$, 7.26 ppm): 1.9 (s, 6H, -CH_3), 2.7 (t, 4H, -C(O)-$\underline{CH_2}$-CH_2-SS-), 2.9 (t, 4H, -C(O)-CH_2-$\underline{CH_2}$-SS-), 3.5-3.8 (m, PEO

protons), 4.0-4.3 (m, 8H, -C(O)O-CH_2- and –CH_2-O(O)C-), 5.6 (s, 2H, CH=), and 6.1 (s, 2H, CH=).

4.2.5 AGET ATRP of MEO_2MA in DMF

For kinetic studies, AGET ATRP of MeO_2MA in the presence of PEO-Br was carried out in DMF at 47°C. MEO_2MA (5 g, 26.6 mmol), PEO-Br (272.8 mg, 0.053 mmol), $CuBr_2$ (35.6 mg, 0.16 mmol), bpy (49.8 mg, 0.32 mmol), and DMF (3.5 mL) were mixed in a 50 mL Schlenk flask at room temperature. The resulting solution was stirred for 30 min, while being purged under nitrogen to remove oxygen. A nitrogen-purged anisole solution of $Sn(Oct)_2$ (375 mg/mL, 120 μL, 0.11 mmol) was added to the flask in order to reduce the Cu(II) complex to the activator Cu(I) complex and start the polymerization. Samples were withdrawn at different time intervals during the polymerization to determine conversion by NMR and provide molecular weight data by GPC. The polymerization was stopped by exposing the catalyst to air.

For purification, the as-synthesized solutions were diluted with acetone and then passed through a basic alumina column to remove residual copper. Acetone was removed by rotary evaporation at room temperature. The residues were precipitated from cold hexane three times and then dried under vacuum at room temperature for 18 hrs.

4.2.6 Synthesis of cleavable thermoresponsive hydrogel

The recipe optimized for the AGET ATRP of MEO_2MA in the presence of PEO-Br in DMF at 47 °C was used with various amounts of ssDMA crosslinker. Typically, to synthesize ssH2 gels in Table 1, MEO_2MA (5 g, 26.6 mmol), PEO-Br (272.8 mg, 0.053 mmol), $CuBr_2$ (35.6 mg, 0.16 mmol), bpy (49.8 mg, 0.32 mmol), ssDMA (2 mol% based on MEO_2MA, 290 mg, 0.53 mmol), and DMF (3.5 mL) were mixed in a 50 mL Schlenk

flask at room temperature. Pieces of glass tubing (8 mm diameter and 2 cm length) were placed in the flask to act as cylindrical-shaped templates. The resulting solution was stirred for 30 min, while being purged under nitrogen to remove oxygen. A nitrogen-purged anisole solution of $Sn(Oct)_2$ (375 mg/mL, 120 μL, 0.11 mmol) was added to the flask in order to reduce the Cu(II) complex to the activator Cu(I) complex and start the polymerization. The polymerization was stopped at 8 hrs by exposing the catalyst to air.

The formed cylindrical hydrogels were purified as follows; the as-synthesized gels were immersed in fresh acetone (20 mL) five times for two days to remove remaining monomers and DMF solvent. They were then immersed in fresh deionized water to remove residual Cu species and acetone four times for two days. The purified gels were stored in water before use.

4.2.7 Determination of swelling ratio

Aliquots of swollen hydrogels were immersed in water at room temperature (RT) for 16 hrs. They were blotted against tissue paper to remove residual water (w_t, ≈100 mg). They were then dried at 120 °C for 4 hrs (w_d). The SR was determined by the weight ratio of swollen (w_t) to dried hydrogels (w_d).

4.2.8 Determination of hydrogel LCST using Differential Scanning Calorimetry (DSC)

The hydrogel was swollen in water for 24 hrs. Aliquots of the swollen gels were then placed in a hermetic sample pan filled with water (30 μL). Thermal properties of the gels were measured against a sealed reference pan filled with water (30 μL) with a TA

Instruments DSC Q20 differential scanning calorimeter over a temperature range of 5 to 50 °C, at a heating rate of 2 °C/min from 5 to 50 °C under a nitrogen flow rate of 50 mL/min.

4.2.9 Deswelling kinetics by gravimetry

Water retention of hydrogels was measured as follows; Aliquots of swollen hydrogels were placed in water at 45 °C for a given period time and weighed after being blotted against tissue paper to remove residual water (w_t). The procedure was repeated at specified time intervals over the course of 1 hr. Water retention is calculated by $\frac{wt-wd}{w0-wd}$, where w_t is the weight of swollen gels at time t, w_d is the weight of dried gels, and w_0 is the initial weight of swollen gels.

4.2.10 Reductive cleavage of disulfide linkages of ssH hydrogels

Aliquots of swollen hydrogels were immersed in an aqueous DTT solution under magnetic stirring at RT for 48 hrs. The degraded gels were extensively washed with water more than four times at 4 °C to remove excess DTT, yielding ssH-d gels.

4.2.11 Ellman assay for quantitative analysis of disulfide cleavages

A stock solution of DTNB at pH = 8 was prepared at 4 mg/mL concentration by dissolving DTNB (8 mg) in aqueous buffer solution (2 mL). Aliquots of the swollen, purified ssH-d gels were further washed with aqueous buffer solution (10 mL) more than five times to remove residual DTT. The complete removal of residual DTT in the final wash was monitored with DTNB. The further purified ssH-d gels were placed in fresh buffer solution (5 mL) and then mixed with aqueous DTNB stock solution (200 μL) at 4 ºC for 1 hr. The hydrogels were taken and washed with fresh buffer solution three times to

remove residual NTB anions trapped inside the gels. The UV/Vis spectra of the solutions were then recorded.

4.2.12 Viscoelastic measurements

Mechanical properties of ssH hydrogels were measured on a DHR-2 rheometer (TA Instruments, USA) in either temperature sweep mode or small amplitude oscillatory shear mode with a parallel plate geometry (8 mm diameter). For the temperature sweep mode, hydrogel samples dried in a vacuum oven at 60 °C for 24 hrs were loaded on the plates. The gap was set to obtain an axial force around 5 N, and temperature was varied in the range of -80 and 220 °C with a 1% strain at 1 rad/sec frequency. For the oscillation mode, swollen hydrogels were loaded on the plates. The gap set to 2 mm and the oscillation frequency was varied in the range of 0.1 - 100 rad/sec at a 1% strain.

4.2.13 Cell viability using MTT assay

HeLa cells were plated at $5x10^5$ cells/well into a 96-well plate and incubated for 24 hrs in DMEM (Dulbecco's modified Eagle's medium) containing 10% FBS (fetal bovine serum) and 1% antibiotics (50 units/mL penicillin and 50 units/mL streptomycin) at 37 °C in a humidified atmosphere containing 5% CO_2. They were then incubated with three pieces of each ssH4-d (21.7 ± 2 mg) and ssH4 (20 ± 1 mg) gels for 48 hrs. Prior to the incubation, gels were immersed in fresh PBS buffer (5 mL) three times for 12 hrs. Controls without gels (cells only) were run simultaneously. Cell viability was measured using CellTiter 96 Aqueous Non-Radioactive Cell Proliferation Assay kit (Promega) according to manufacturer's instruction. Briefly, 3-(4,5-dimethylthiazol-2-yl)-2,5-diphenyltetrazolium bromide (MTT) solutions (15 μL) was added into each well and after 4 hrs incubation the medium containing unreacted MTT was carefully removed. The

formed blue formazan crystals were dissolved in stop solution (100 μL), the absorbance was measured at 570 nm using Powerwave HT Microplate Reader (Bio-Tek). Viability was calculated as the percent ratio of absorbance of mixtures with gels to control (cells only).

4.2.14 Loading and release of R6G using UV/Vis spectroscopy

An aqueous stock solution of R6G at pH = 6 was prepared at a concentration of 0.17 mg/mL. The stock solution was diluted with different volumes of water, yielding a series of aqueous solutions with different concentrations of R6G. Their UV/Vis spectra were recorded to determine its extinction coefficient at λ_{max} = 527 nm to be 79,800 M^{-1} cm^{-1}. Then, aliquots of hydrogels (30 mg in dried states) were immersed in the aqueous R6G stock solution (5 mL) at 4 °C for 48 hrs. After the R6G-loaded hydrogels were taken, UV/Vis spectra of the solutions were recorded. The loading level of R6G was determined as the weight ratio of loaded R6G to dried gels. For the release of R6G from R6G-loaded hydrogels, the resulting R6G-loaded ssH and ssH-d gels were placed in a dialysis tubing with MWCO = 12 kDa and immersed in water at 45 °C. The absorbance was followed using a UV/vis spectrometer equipped with an external probe at 527 nm over time.

4.3 Results and discussion

4.3.1 Synthesis of PEO-b-MEO$_2$MA by AGET ATRP

Activators Generated by Electron Transfer (AGET) is an effective initiating process for atom transfer radical polymerization (ATRP).[115, 199-201] AGET ATRP uses oxidatively stable Cu(II) complex which reacts with reducing agents such as $Sn(EH)_2$ to generate active Cu(I) complex for normal initiation with the added alkyl halide initiator. In the experiments, DMF formed a homogeneous reaction mixture with $CuBr_2$/bpy complexes. A hydrophilic PEO-based bromine macroinitiator (PEO-Br) was synthesized by a facile carbodiimide

coupling reaction of PEO-OH with BriBuA. AGET ATRP of MEO_2MA was initiated with PEO-Br in the presence of $CuBr_2$/bpy complexes in DMF at 47 °C. The conditions were $[MEO_2MA]_0/[PEO\text{-}Br]_0/[CuBr_2]_0/[bpy]_0$ = 500/1/3/6 with $[Sn(Oct)_2]_0/[CuBr_2]_0$ = 0.7/1 and MEO_2MA/DMF = 1.5/1 wt/wt.

Figure **C.1** shows the kinetic results for synthesis of linear polymer chains in two successive ATRP reactions. Polymerization was first-order, suggesting constant concentration of active centers during the polymerization. An induction period of 1 hr was observed. A similar induction period has been reported for AGET ATRP of 2-hydroxyethyl methacrylate (HEMA) with $CuBr_2$/bpy complex in a mixture of methyl ethyl ketone/MeOH (3/2 v/v) at 50 °C.[201] The occurrence of an induction period can be attributed to the slow reduction of Cu(II) to Cu(I) by $Sn(EH)_2$ and the induction period decreased as the reaction temperature increased. Molecular weight increased linearly with conversion and molecular weight distribution was as narrow as $M_w/M_n < 1.2$ up to 60% conversion. These results suggest that polymerization proceeded in a living manner. Above 60% conversion, kinetics lose their first-order characteristic because diffusion-controlled radical deactivation caused by diffusion limitations experienced by the reactants due to an increase of the solution viscosity, slow down termination while leaving initiation and propagation reactions unaffected, leading to autoacceleration of the polymerization.[202] The resulting diblock copolymers were purified by removal of Cu species and unreacted monomers. GPC results show the evolution of GPC trace to a higher molecular weight region with no significant traces of PEO-Br macroinitiator remaining, thus yielding well-controlled PEO-b-$PMEO_2MA$ block copolymers (Figure **C.2**).

4.3.2 Hydrogel synthesis

The similar procedure as described above for AGET ATRP of MEO_2MA was applied to the synthesis of $PMEO_2MA$-based hydrogels crosslinked with disulfide linkages. A disulfide-labeled dimethacrylate (ssDMA) was synthesized using a facile carbodiimide coupling reaction. Various amounts of 2, 4, and 6 mol% ssDMA cross-linker were introduced into an AGET ATRP to synthesize well-defined disulfide-labeled cleavable thermo-responsive hydrogel precursors. The final reaction scheme is presented in Figure **4.2**. Table **4.1** presents the characteristics of the cleavable hydrogels named as ″ssHx″, where x denotes the mol% of cross-linker in monomer mixtures. Monomer conversion and swelling ratio (SR) were both determined by gravimetry.

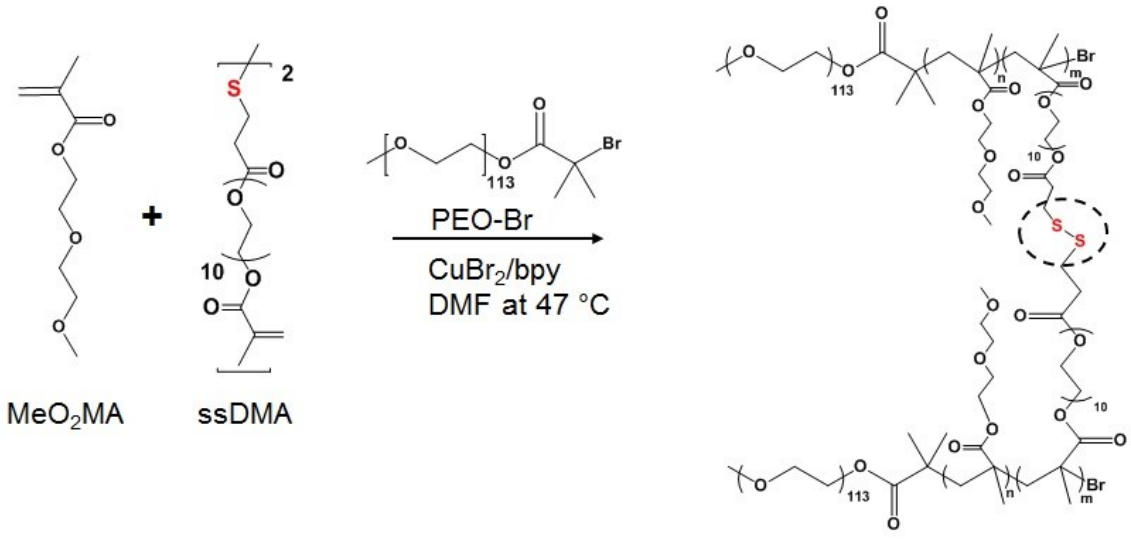

Figure 4.2. Synthesis of $PMEO_2MA$-based thermo-responsive hydrogels cross-linked with disulfide linkages by AGET ATRP of MEO_2MA in the presence of ssDMA in DMF at 47°C

Table 4.1. Characteristics of thermoresponsive hydrogel precursors synthesized using AGET ATRP of MEO_2MA in the presence of cleavable ssDMA in DMF at 47 °C.

Hydrogels	ssDMA/mol%	Conv.	SR	LCST (C°)
ssH2	2	43.9 ± 6.8	10.2 ± 2.3	32.2
ssH4	4	48.4 ± 4.8	3.8 ± 1.1	32.3
ssH6	6	49.3 ± 3.9	3.6 ± 0.9	32.6

4.3.3 Gel swelling ratio (SR) and viscoelastic properties

Monomer conversion determined using gravimetry was close to 44-50%. Such low conversion suggests the presence of dangling chains of double bonds. The SR is defined as the weight ratio of swollen to dried hydrogels in water. Table **4.1** shows that ssH2 hydrogels have a SR as high as 10.2 compared with ssH4 (3.8) and ssH6 (3.6), showing a decrease in SR as the amount of ssDMA increased. This is presumably attributed to the increasing in cross-linking density as evidenced by the results of viscoelastic measurements of the dried hydrogels in the temperature sweep mode. Temperature was varied from -80 to 220 °C with 1% strain at 1 rad/s shear rate. Figure **C.3** shows the viscoelastic properties of storage or elastic (G′), loss or viscous (G″) moduli, and tan δ (G″/G′) over the full range of temperatures. A higher crosslinking density increases the elastic component of the gel with the increase in the storage modulus. Figure **4.3** compares the G′ values of the hydrogels at 37°C (close to body temperature) and 75 °C, after they have reached a plateau after undergoing glass transition. At both temperatures, the G′ value increased with an increasing amount of ssDMA (ssH2 vs ssH4 hydrogels). The larger G′ modulus is due to higher crosslinking densities of gel networks, which decreases the SR. Upon a further

increase of ssDMA to 6 mol%, however, the G′ value remained unchanged (ssH4 vs ssH6 gels). Note that their SR is also similar.

In Figure **C.3**, during temperature sweep experiments, the instrument was set to always keep the axial force on the peltier plate around 5 N. Because of the large temperature differences between -80°C and 220 °C, the gel contracts or expands depending on its properties during the measurements. This option was chosen in order to ensure that the plate would always be in contact with the gel. Figure **C.3.** shows that gap size of ssH2 gels started going down after a certain temperature. The gap difference in ssH2 gels started at around 1740 μm at 170 °C down to almost 1650 μm at 220 °C. This decrease is the result of the gel collapsing under high temperature, effectively reducing strain. ssH4 gels showed a completely reversed situation where gap size actually increased when the sample was heated. The reason for this sudden expansion of the gel is unknown. However, ssH4 results show that after this expansion, at around 150 °C, the gap size starts to sharply decrease, indicating that the gel is collapsing. Finally, the gap variation profile of ssH6 is similar to ssH4, but only affected at higher temperatures. In this case, even at 220 °C, the gel did not collapse, suggesting a more robust hydrogel. These results suggest that the amount of crosslinkers is an important parameter that influences the SR and mechanical properties of thermoresponsive hydrogels.

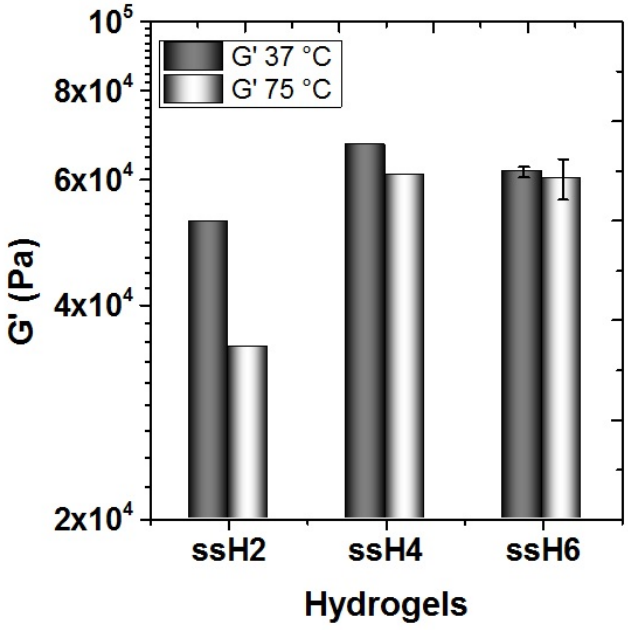

Figure 4.3. Viscoelastic properties of storage modulus (G′) at 37 °C and 75°C of thermo-responsive ssH hydrogels. Note that the G′ for ssH6 was averaged from three measurements with fresh gels.

4.3.4 Thermoresponsive properties and deswelling

LCST of $PMEO_2MA$ ssH4 hydrogels was obtained by DSC (measured by Dr. Nicky Chan) and was found to be 32.3 °C. Similar values were obtained for ssH2 and ssH6 gels. These values are close to that of their linear analog (PEO-b-$PMEO_2MA$, LCST = 33°C), measured by DLS. Light scattering intensity increased sharply with an increasing temperature, due to a coil-globular transition by hydrophilic/hydrophobic transition upon heating. The resulting cleavable thermoresponsive hydrogels undergo a volume change caused by a transition in hydrophobic/hydrophilic balance at the LCST. The rate of volume change (i.e. shrinking) of the hydrogels was examined by measuring the amount of water retained in hydrogels at a temperature of 45 °C, well above the LCST. The water retention is defined as the ratio of the amount of water retained in hydrogels at t to that at t = 0. As

seen in Figure **4.4**, the water retention of ssH hydrogels decreased to reach a plateau over time. After 40 min, the water retention was 0.2 for ssH2, 0.3 for ssH4, and 0.45 for ssH6, suggesting slower shrinking kinetics with an increasing amounts of ssDMA crosslinker. The slow kinetics is presumably attributed to the increase in crosslinking densities of hydrogel networks.

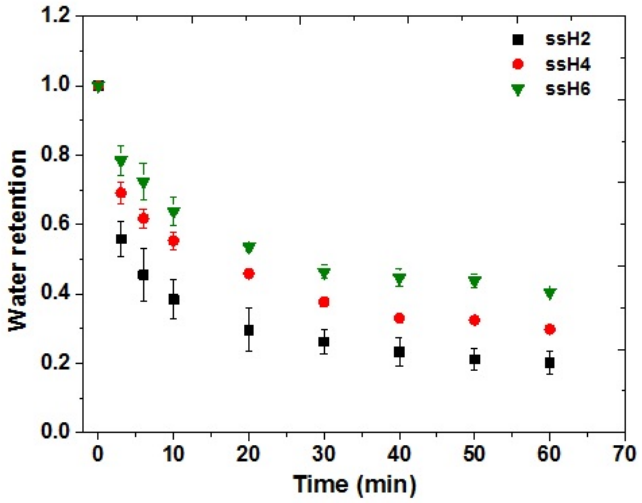

Figure 4.4. Deswelling kinetics at 45 °C expressed by water retention cleavable ssH hydrogels prepared with 2, 4, and 6 mol% ssDMA in water.

4.3.5 Reductive cleavage of disulfides in ssH hydrogels and quantitative analysis

One way to quantify the degradation of disulfides is by using Ellman's assay. Ellman's assay is used to determine the concentration of sulfhydryl (-SH) groups after the cleavage of disulfide bonds.[203] Analysis involves the spectroscopic determination (412 nm) of 2-nitro-5-thiobenzoate (NTB anion, yellow color) released from DTNB upon the cleavage of disulfide linkages by its reaction with a reducing agent (Figure **4.5**).

A stock solution of DTNB (4 mg/ml) was prepared in a pH = 8.0 buffer containing 0.1 mM sodium phosphate dibasic and 1 mM EDTA. After disulfide cleavage, hydrogels

were washed with buffer solution multiple times to remove residual DTT, whose presence was monitored by using DTNB. The purified degraded gels were placed in fresh buffer and mixed with DTNB and incubated for 1 hr at 4 °C. The UV-Vis spectra was recorded and analyzed for the presence of NTB^{2-} at 412 nm. Hydrogels were then taken, washed with fresh buffer to remove any trapped NTB anions and analyzed again. The absorption at 412 nm is used to calculate the extent of degradation of the gel with an extinction coefficient of 14 150 $M^{-1}cm^{-1}$ in the buffer.

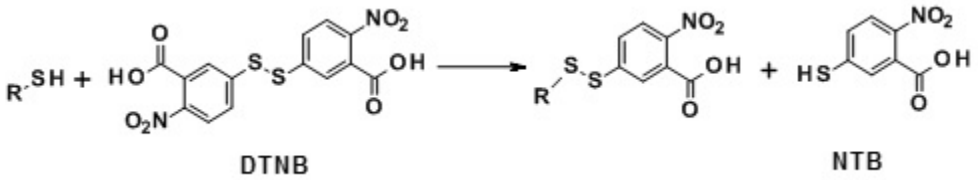

Figure 4.5. Mechanism of action of DTNB in the presence of sulfhydryl groups (unionized molecules shown).

As seen in Figure **4.6**, the UV/Vis spectrum of DTNB exhibits a maximum absorption at λ = 326 nm. When ssH4-d gels were mixed with DTNB in aqueous solution, a new absorption peak at 400-500 nm appeared. The occurrence of the absorption is caused by the formation of NTB anions, indicating the cleavage of disulfide linkages in ssH-d gels in response to DTT. Using the Beer-Lambert equation with the absorbance and extinction coefficient at λ = 412 nm, the extent of cleavage of disulfides was determined to be 9.5% for ssH4-d gels and 19.4% for ssH2-d gels. The partial cleavage of disulfides results in ssH-d hydrogels which retain a solid shape and mechanical properties.

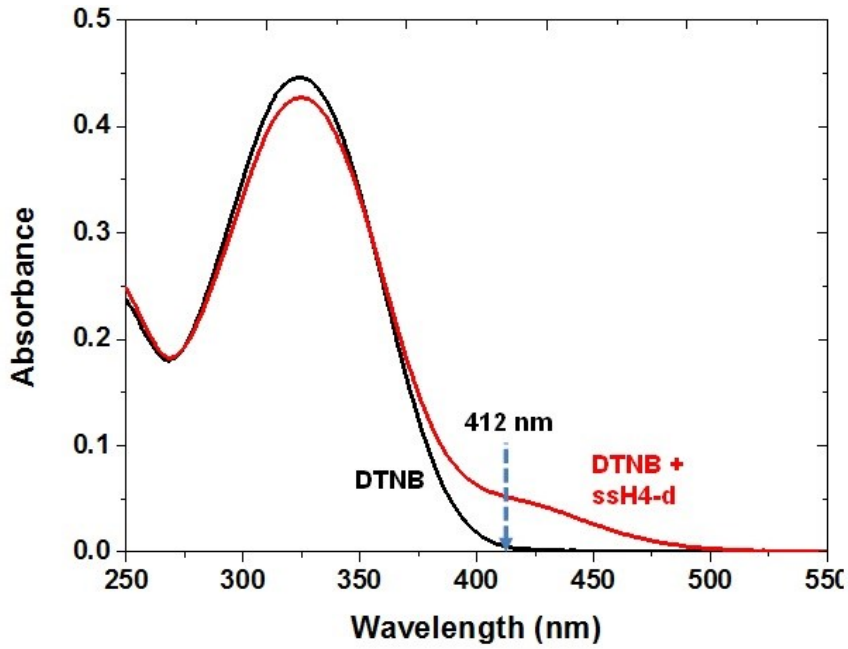

Figure 4.6. UV/Vis spectra of DTNB (black) and its mixture with ssH4-d (red) in aqueous buffer solution at pH = 8.0.

4.3.6 Analysis of degraded ssH-d gels

Because no significant cleavage of disulfide linkages is determined in ssH2 and ssH4 gels, the resulting ssH4-d gels were typically characterized for LCST, deswelling kinetics, and viscoelastic properties. Their LCST using DSC was determined to be 33.9 °C, slightly higher than the 32.3 °C of ssH4 precursor gels (Figure **C.4**). This difference is attributed to the increase in hydrophilicity of ssH gels to some extent as resulted from the formation of SH groups upon partial cleavage of disulfide linkages.

Deswelling of ssH2 and ssH4 was analyzed after degradation with 10eq. DTT. Enhanced deswelling kinetics of ssH4-d gels, compared to ssH4 gels at 45 °C is shown in Figure **4.7**. The water retention after 40 min decreased to 0.2 for ssH4-d gels, significantly lower than 0.4 for ssH4 precursor gels. Such enhancement is also observed with ssH2 gels:

the water retention = 0.2 for ssH2-d gels vs 0.23 for ssH2 gels (Figure **4.7**). The enhanced thermoresponsiveness of ssH-d gels could be attributed to the generation of hydrophilic dangling chains with terminal SH groups and the increase in hydrophilicity of hydrogel network as resulted from the cleavage of disulfide linkages.

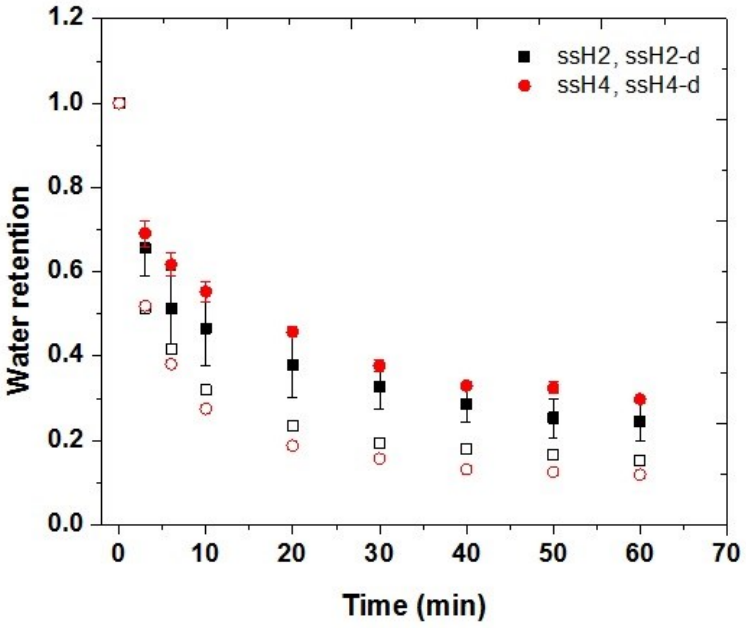

Figure 4.7. Deswelling kinetics at 45 °C expressed by water retention of ssH-d gels (blank symbols), compared with ssH precursor gels (filled symbols).

Mechanical properties of degraded ssH4 gels were analyzed. The decreased mechanical properties of the ssH4 hydrogel are shown in Figure **4.8**. The G′ modulus of wet ssH4-d gels were relatively lower than that of wet ssH4 gels in the oscillatory shear mode ranging from 0.01 to 100 rad/s at room temperature. The lower mechanical property of ssH4-d gels is attributed to the presence of partial cleavage of disulfide cross-links to

generate hydrophilic dangling chains in the hydrogels, thus increasing hydrophilicity of the hydrogel network.

The G′ modulus of ssH4 gels, before degradation, at 75 °C was 60 800 Pa (Figure **4.3**) but after degradation, storage modulus values went down to 28 800 Pa. In a temperature sweep viscoelastic measurement (Figure **C.5**), the gap profile shows that after degradation, ssH4-d gels are much more viscous and shrink more than ssH4 precursor gels. Indeed, after degradation, gap values go from 1735 µm down to approximately 800 µm. This gap difference is the largest seen in all my experiments.

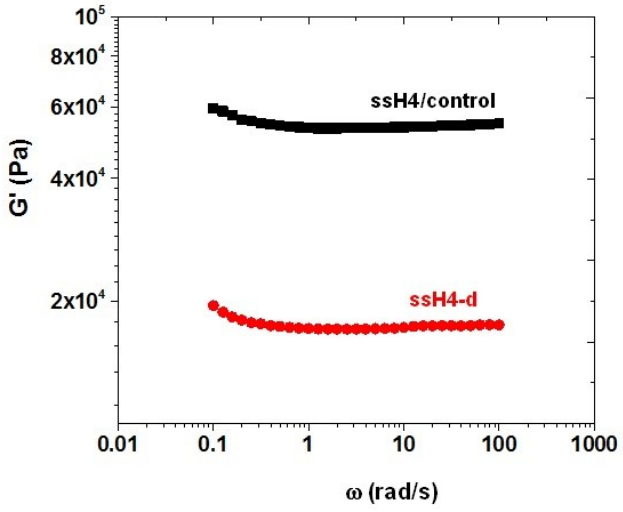

Figure 4.8. Viscoelastic properties of G′ modulus for wet ssH4-d gels, compared with wet ssH4 precursor gels in oscillatory shear mode.

4.3.7 Biomedical perspectives

To preliminarily assess the ssH-d hydrogels toward biomedical applications, particularly drug delivery, *in vitro* cytotoxicity with HeLa cells were examined using MTT assay (a colorimetric method to measure cell toxicity) by Yifen Wen. ssH4-d gels were cultured with HeLa cells, along with ssH4 gels for comparison and cells only as controls.

After 48 hr incubation, the absorbance was measured using absorbance-based plate reader and used to calculate cell viability. Figure **C.6** shows >90% viability of HeLa cells in the presence of both ssH4 and ssH4-d gels, suggesting their non-cytotoxicity.

The rate of release of rhodamine-6G (R6G) dye as a model hydrophilic drug was examined with ssH4-d gels, compared with ssH4 gels. Using the extinction coefficient of R6G at λ_{max} = 527 nm in water (ε = 79,800 M^{-1} cm^{-1}, Figure **C.7**), the loading level of R6G was determined to be 1.5% for ssH4-d gels, which is slightly higher than 1.3% for ssH4 gels. The release of R6G from these gels was examined using UV/vis spectrometer equipped with an external probe. Figure **4.9** shows % release of R6G over time, indicating that ssH4-d gels enhanced the release over 200 min, compared to ssH4 gels. These results indicate that ssH-d gels exhibited higher loading and enhanced release of encapsulated hydrophilic model drugs.

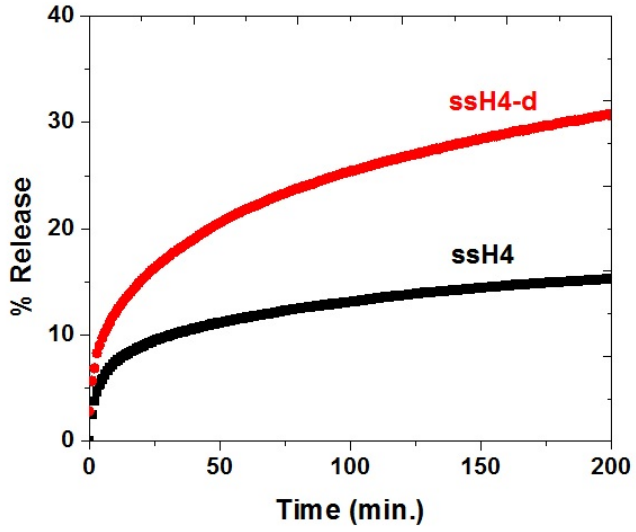

Figure 4.9. Release of R6G as a model hydrophilic drug from R6G-loaded ssH4-d and ssH4 hydrogels in aqueous solution.

4.4 Conclusion

Cleavable thermoresponsive hydrogels based on $PMEO_2MA$ crosslinked with disulfide linkages were prepared by crosslinking AGET ATRP of MEO_2MA and ssDMA in the presence of PEO-Br. In the absence of cross-linkers, polymerization proceeded in a living fashion as evidenced with first-order kinetics, linear increase of molecular weight with conversion, and narrow molecular weight distribution. Introduction of ssDMA allowed for the preparation of well-defined ssH precursor hydrogels exhibiting LCST = 32.5 °C as determined by DSC. The properties of ssH hydrogels were varied with their network crosslinking densities; when the amount of ssDMA and conversion increased, SR and deswelling kinetics expressed by water retention decreased, while mechanical properties increased. Reductive cleavage of disulfide linkages of ssH gels yielded ssH-d gels with hydrophilic pores containing SH groups. A 10-20% cleavage of disulfide linkages by quantitative analysis using Ellman assay increased LCST, enhanced deswelling kinetics, while slightly decreasing mechanical properties. With the balance of thermoresponsive and mechanical properties, combined with non-toxicity and enhanced release of encapsulated hydrophilic model drugs, ssH-d gels can find out their biomedical applications as effective tissue scaffolds.

CHAPTER 5

CONCLUSION AND FUTURE WORKS

The design and development of effective stimuli-responsive polymeric nanomaterials is a research area showing great promise. A desired property for their use towards biological and biomedical applications is their ability to undergo a chemical or physical change in response to external stimuli. Such changes lead to degradation of dynamic covalent bonds upon cleavage or volume change through hydrophilic/hydrophobic coil-globule transitions. In this thesis, two stimuli-responsive biomaterials designed with reduction-responsive disulfide linkages were studied for their potential in biomedical research: stimuli-responsive degradable block copolymer nanocarriers and temperature-responsive cross-linked hydrogels.

First, well-defined reduction-responsive degradable ssABPs were synthesized by utilizing a facile carbodiimide coupling polycondensation combined with ATRP. The novel block copolymer consists of a water-soluble polymethacrylate block to ensure enhanced colloidal stability and non-cytotoxicity, and a hydrophobic degradable ssPES block with disulfide linkages positioned repeatedly along the main chain for rapid degradation response. Confirmation of ssABP synthesis was analyzed by GPC and ^{1}H-NMR. Amphiphilic block copolymers can self-assemble in aqueous solution to form micellar aggregates. Size and morphology analysis, done by DLS, TEM and AFM, confirmed the formation of monomodal spherical micelles of 68.4 ± 6.2 nm at 0.1 mg/mL. In the presence of a reducing agent, disulfide bonds contained within the micellar core were

cleaved into their corresponding thiols and the micelle was destabilized. DLS and ^{1}H-NMR results confirmed the degradation of the polyester core, leading to micelle destabilization and enhanced release of the encapsulated model drug Nile Red. Furthermore, bioconjugation of ssABP with biotin was done by ATRP during polymerization with biotin positioned at the end of the water-soluble corona. Biotin availability was analyzed using an Avidin-HABA assay. This study has shown that well-defined thiol-responsive ssABP micelles are an interesting candidate for potential drug delivery applications.

However, in the current design, the short hydrophobic main chain led to a small core size, causing relatively low loading of encapsulated dyes. In future works, the hydrophobic ssPES core should be expanded by synthesizing longer polyester chains in order to increase loading and particle size. Further experiments are also needed to test the colloidal stability of the nanoparticles in the long term, to assess their over the counter stability. This stability should also be tested in biological conditions. The facile bioconjugation method investigated can be applied to other conjugates such as folic acid. Testing the micelle's ability to accumulate at tumor tissues after functionalization with a specific ligand is also an important part of the characterization process for drug delivery vehicles.

Second, using AGET ATRP, a thermo-responsive hydrogel was synthesized with a degradable cross-linker containing a disulfide bond. In the presence of a reducing agent, the disulfide bond is cleaved, lowering cross-linking density, increasing pore size and generating hydrophilic dangling chains, increasing the overall hydrophilicity of the hydrogel. This results in higher gel swelling ratio, but lower mechanical properties. Hydrogel degradation was not complete even at 100 DTT/disulfides as the gel still kept a

solid shape with only 10-20% of disulfides cleaved. Degradation has also led to an increase in LCST and enhanced release of an encapsulated hydrophilic model drug. These results, combined with confirmed non-toxicity show that this hydrogel has potential in being used as a tissue engineering scaffold.

Future work on this project should include the tuning of the gel swelling ratio and mechanical properties by utilizing a permanent non-cleavable cross-linker to confer better mechanical properties after cleavage of disulfide bridges in ssDMA. The desire in tissue engineering is to synthesize a gel that is able to readily absorb and release water and also be sturdy enough to hold its shape. In another experiment, growing cells inside and out of the hydrogel would show if it can be used in situ as cells would be able to properly attach themselves on the material. Finally, biodegradability tests can be conducted to estimate the amount of time the hydrogel will take to be completely degraded.

The biomaterials explored in this work are just an example of the many types and uses stimuli-responsive degradable polymers can take. Significant work is needed in order to accept these unique polymers in the applications of modern medicine. Some drug delivery systems are already undergoing clinical trials but they are very few. New stimuli-responsive polymers are being investigated and they could one day revolutionize the medical industry by offering specific and affordable health care to people around the world.

APPENDIX A

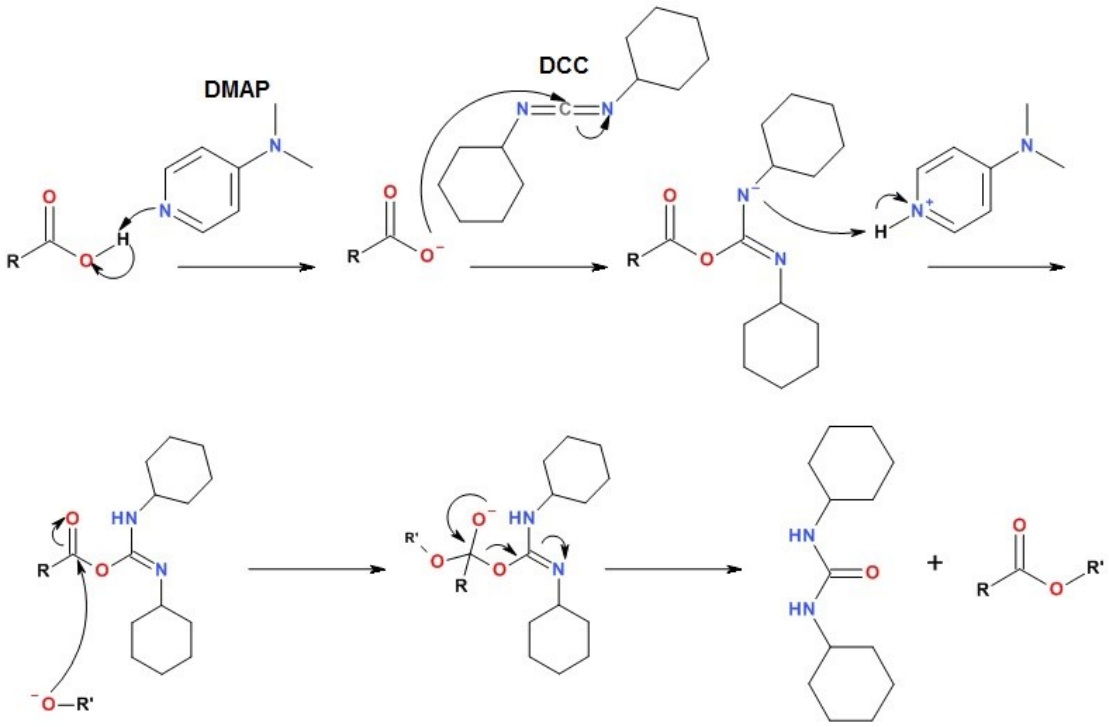

Figure A.1. Steglich Esterification mechanism with DCC and DMAP.

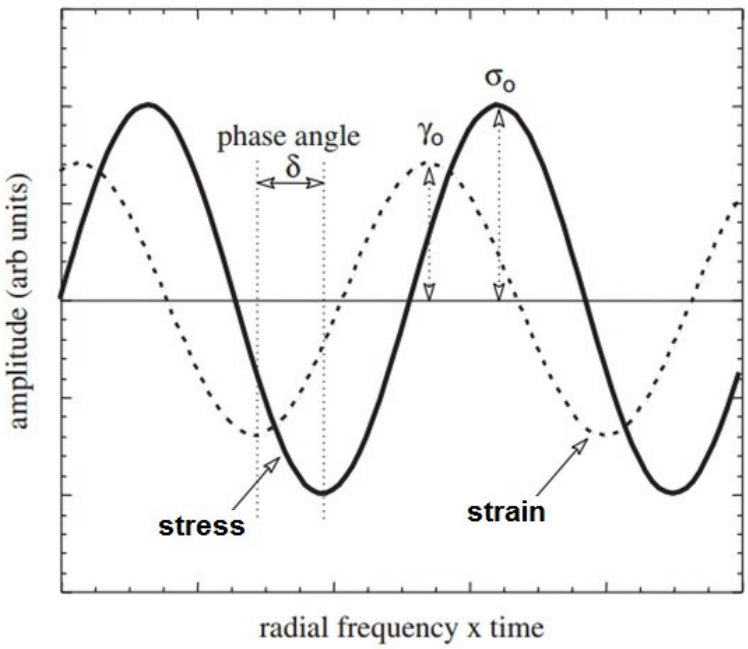

Figure A.2. Oscillating stress and strain response for a viscoelastic material.[124]

APPENDIX B

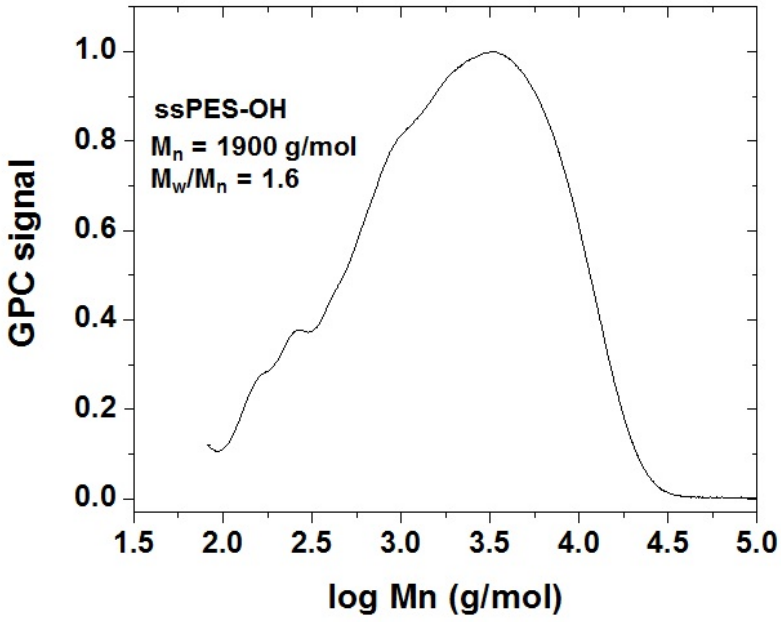

Figure B.1. GPC trace of ssPES-OH.

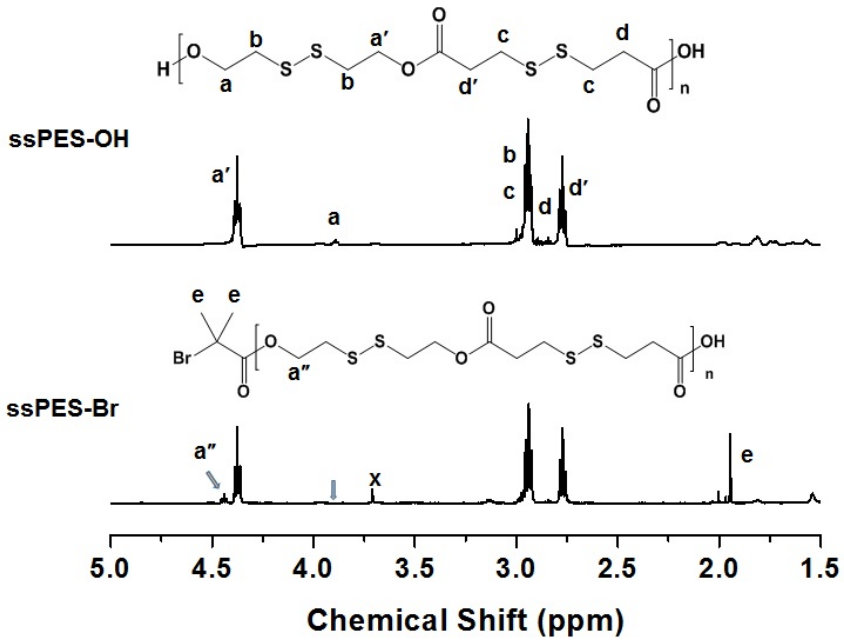

Figure B.2. ^{1}H-NMR spectra of ssPES-OH and ssPES-Br in $CDCl_3$.

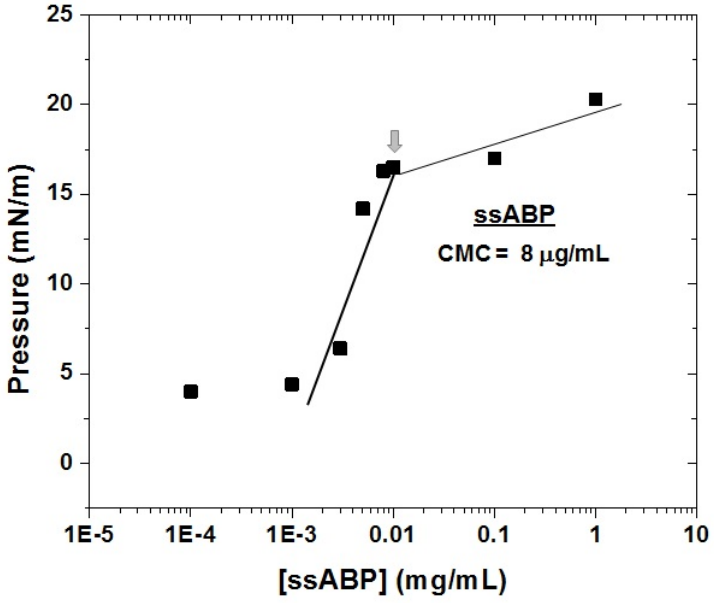

Figure B.3. Determination of CMC of ssABP (11 000 g/mol) using tensiometry by measuring pressure vs concentration.

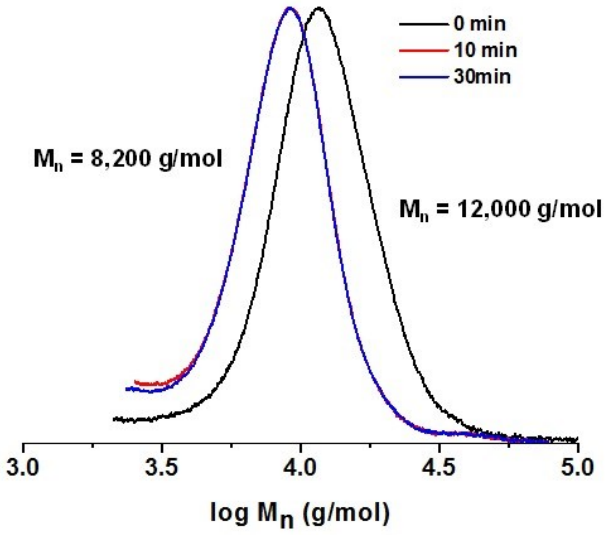

Figure B.4. GPC traces of ssABP micellar aggregates mixed with DTT in aqueous solutions over degradation time. For GPC measurements, micellar aggregates were dissolved in THF after evaporation of water at given time intervals.

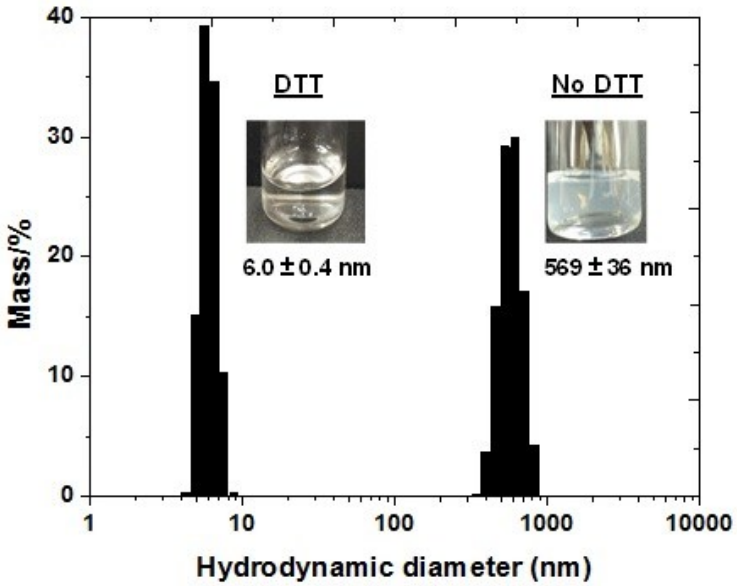

Figure B.5. DLS diagrams by volume% of micellar aggregates before and 45 min after addition of DTT in a mixture of 6/4 wt/wt THF/water. Insets are their digital images.

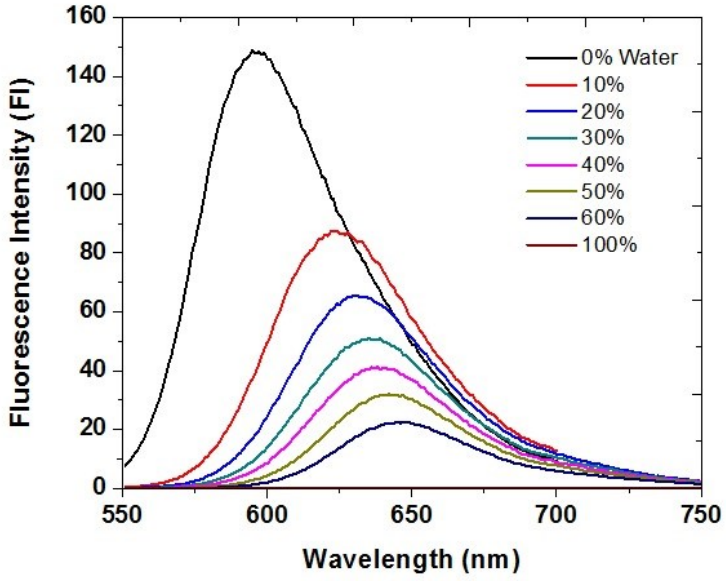

Figure B.6. Overlaid fluorescence spectra of NR in solution at different Water/THF ratios.

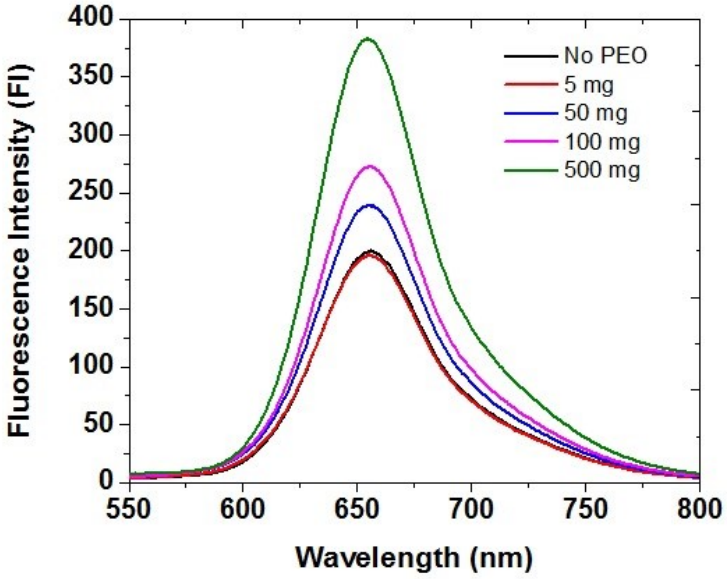

Figure B.7. Overlaid fluorescence spectra of NR with increasing concentration of PEO.

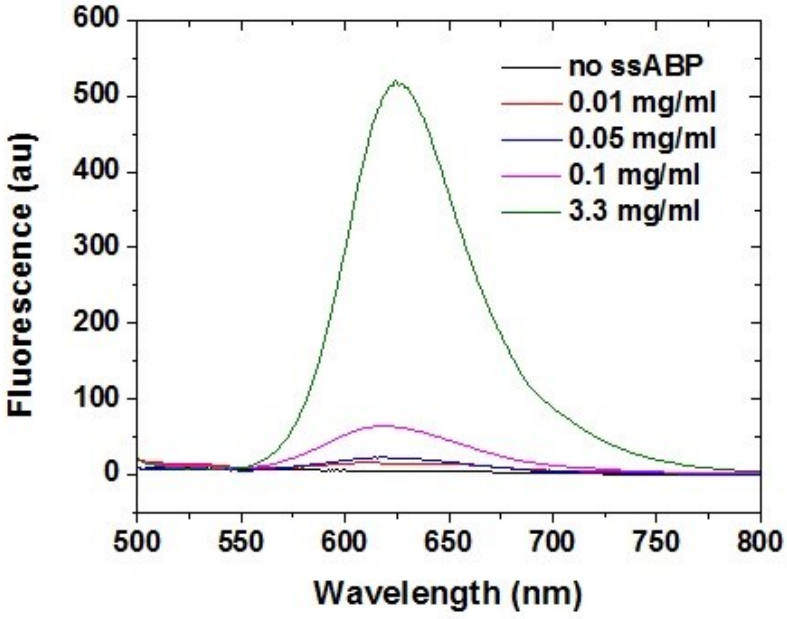

Figure B.8. Evolution of fluorescence spectra of NR in mixtures of the same amount of NR with an increasing amount of ssABP-based micelles.

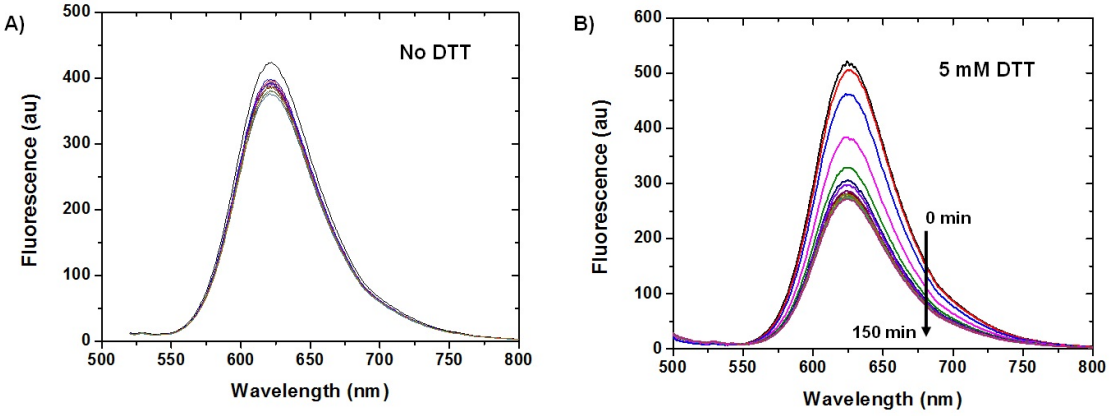

Figure B.9. Overlaid fluorescence spectra of NR in mixtures of ssABP-based micelles without (A) and with 5 mM DTT (B) in water.

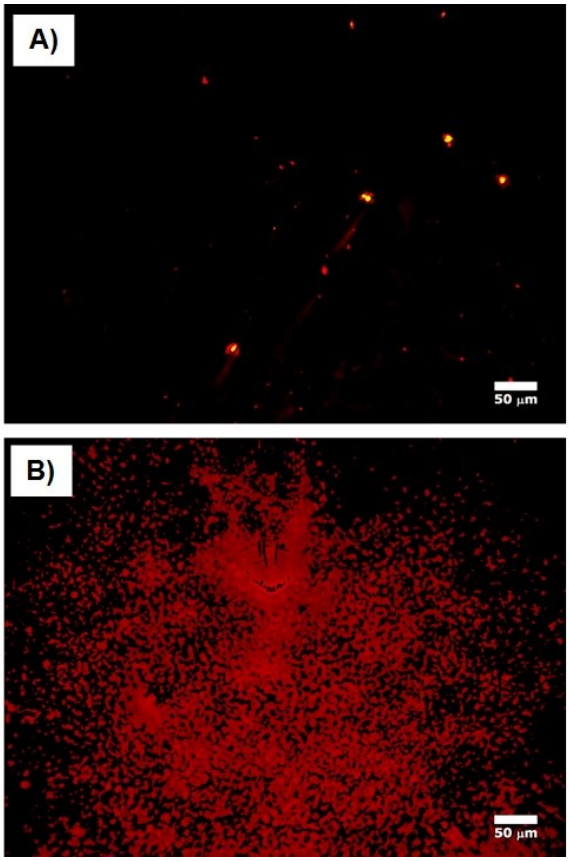

Figure B.10. Fluorescence images of NR-loaded ssABP-Biotin micelles (A) and their biocomplex with Avidin (B). Scale bar = 50 µm.

APPENDIX C

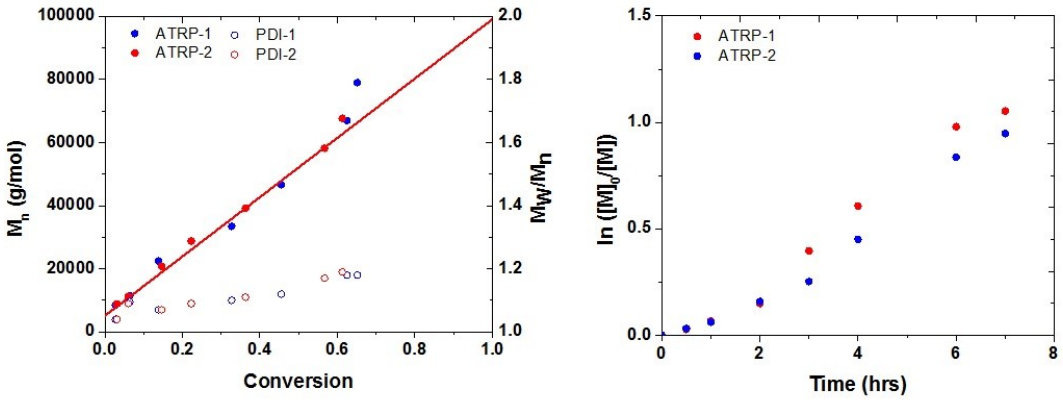

Figure C.1. Kinetic plot (left) and evolution of molecular weight and molecular weight distribution with conversion (right) for AGET ATRP of MEO_2MA in the presence of PEO-Br macroinitiator in DMF at 47 °C. Conditions: $[MEO_2MA]_0/[PEO\text{-}Br]_0/[CuBr_2]_0/[bpy]_0$ = 500/1/3/6; $[Sn(Oct)_2]_0/[CuBr_2]_0$ = 0.7/1; MEO_2MA/DMF = 1.5/1 wt/wt.

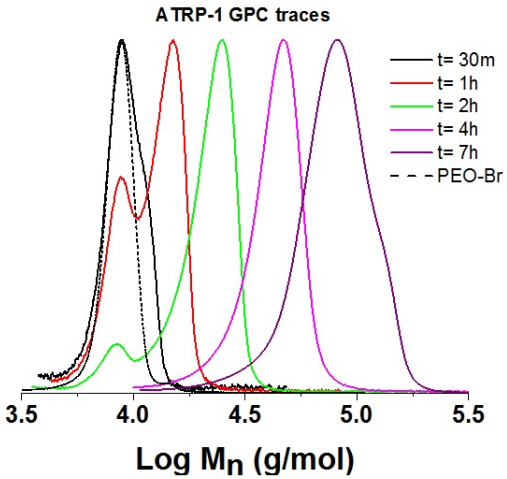

Time/ hrs	Conv	M_n (g/mol)	M_w/M_n
0.5	0.03	8,826	1.04
1	0.06	11,171	1.09
2	0.15	20790	1.07
4	0.36	39200	1.11
7	0.61	67700	1.19

Figure C.2. GPC traces of ATRP-1 PEO-b-$PMEO_2MA$ block copolymers, compared with that of PEO-Br macroinitiator. PEO-Br: M_n = 8.3 kg/mol, M_w/M_n = 1.03.

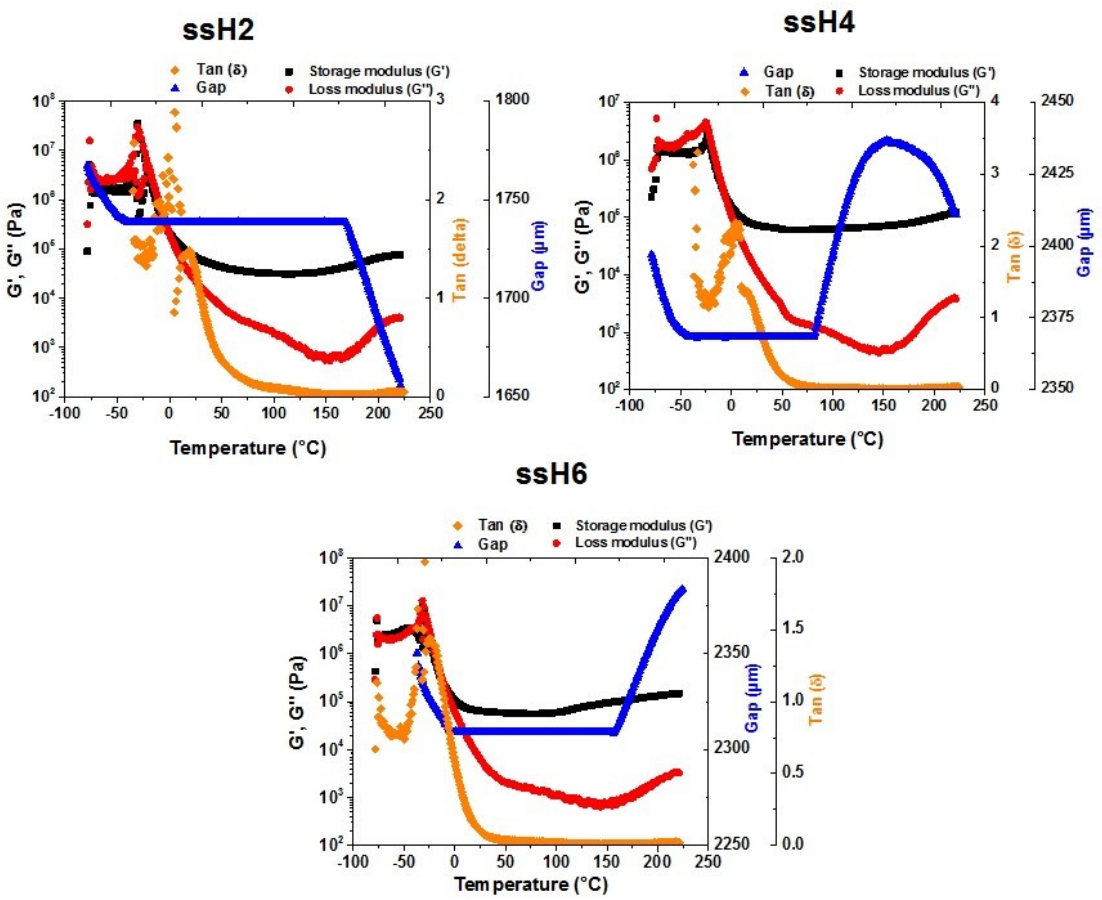

Figure C.3. Temperature-dependent viscoelastic properties of ssH2, ssH4 and ssH6.

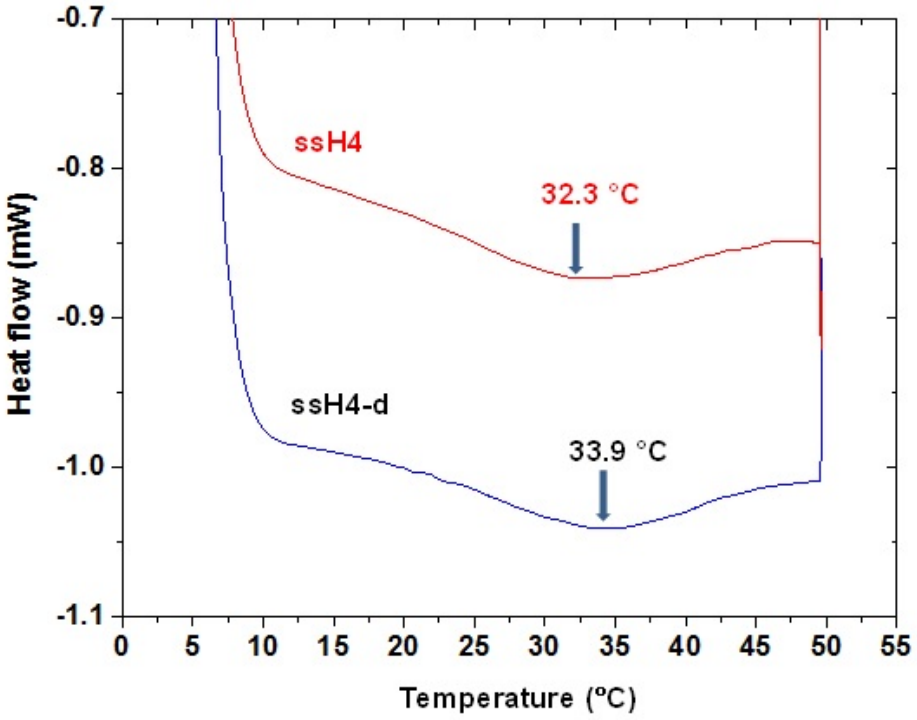

Figure C.4. DSC thermograms of ssH4 and ssH4-d hydrogels before and after treatment with excess DTT.

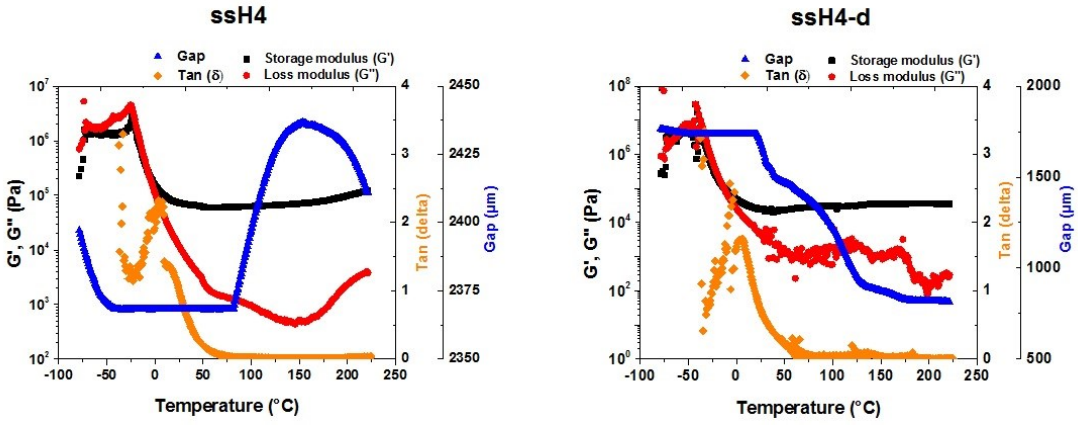

Figure C.5. Temperature-dependent viscoelastic properties of ssH4 and ssH4-d.

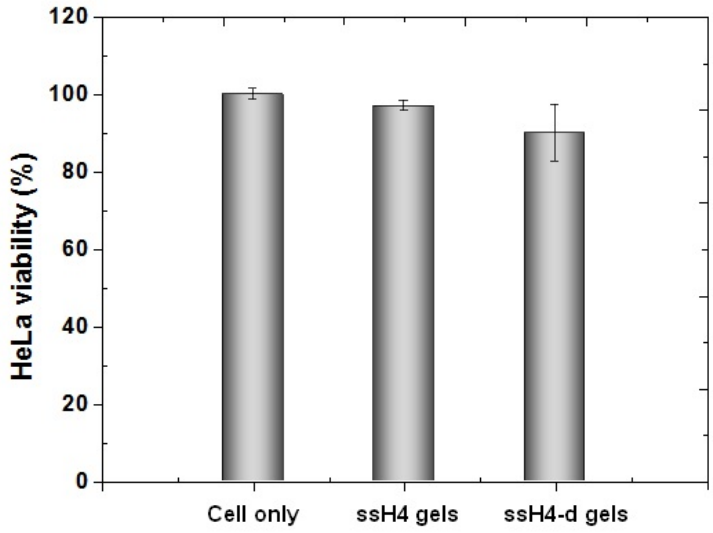

Figure C.6. Viability of HeLa cells cultured with ssH4 and ssH4-d gels for 48 h.

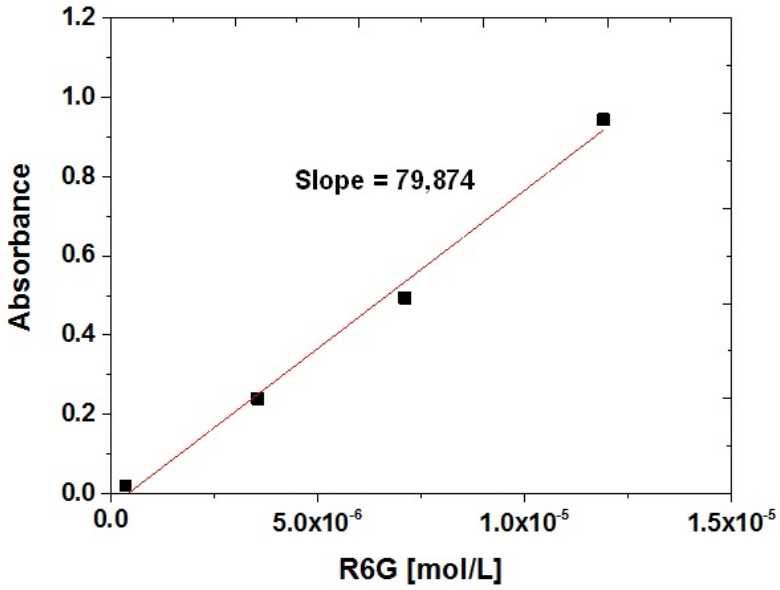

Figure C.7. Absorbance vs concentration of R6G to determined its extinction coefficient in aqueous buffer solution at pH = 8.0.

References

[1] D. F. Williams, *Biomaterials* **2009**, *30*, 5897.
[2] B. D. Ulery, L. S. Nair, C. T. Laurencin, *Journal of polymer science Part B: polymer physics* **2011**, *49*, 832.
[3] E. Cabane, X. Zhang, K. Langowska, C. G. Palivan, W. Meier, *Biointerphases* **2012**, *7*, 9.
[4] B. Jeong, A. Gutowska, *Trends in Biotechnology* **2002**, *20*, 305.
[5] I. Y. Galaev, B. Mattiasson, *Trends in Biotechnology* **1999**, *17*, 335.
[6] A. Kikuchi, T. Okano, *Progress in Polymer Science* **2002**, *27*, 1165.
[7] T.-B. Ren, Y. Feng, Z.-H. Zhang, L. Li, Y.-Y. Li, *Soft Matter* **2011**, *7*, 2329-2331.
[8] E. S. Lee, K. Na, Y. H. Bae, *Nano Letters* **2005**, *5*, 325-329.
[9] J.-M. Schumers, C.-A. Fustin, J.-F. Gohy, *Macromolecular Rapid Communications* **2010**, *31*, 1588-1607.
[10] C. Allen, D. Maysinger, A. Eisenberg, *Colloids and Surfaces B: Biointerfaces* **1999**, *16*, 3.
[11] S. Creutz, J. V. Stam, F. C. D. Schryver, R. Jerome, *Macromolecules* **1998**, *31*, 681.
[12] M. Yokoyama, S. Fukushima, R. Uehara, K. Okamoto, K. Kataoka, Y. Sakurai, T. Okano, *Journal of Controlled Release* **1998**, *50*, 79.
[13] R. Nagarajan, K. Ganesh, *Journal of Chemical Physics* **1989**, *90*, 5843.
[14] D. V. Devine, K. Wong, K. Serrano, A. Chonn, P. R. Cullis, *Biochimica et Biophysica Acta* **1994**, *1191*, 43-51.
[15] H. Harashima, K. Sakata, K. Funato, H. Kiwada, *Pharmacological Research* **1994**, *11*, 402-406.
[16] S. M. Moghimi, H. Hedeman, I. S. Muir, L. Illum, S. S. Davis, *Biochmicia et Biophysica Acta* **1993**, *1157*, 233-240.
[17] D. L. Elbert, J. A. Hubbell, *Annual Review of materials science* **1996**, *26*, 365-394.
[18] R. J. Hunter, *Foundations of colloid science, Vol. 1*, Oxford university press, New York, **1991**.
[19] R. Gref, A. Domb, P. Quellec, T. Blunk, R. H. Müller, J. M. Verbavatz, R. Langer, *Advanced Drug Delivery Reviews* **1995**, *16*, 215-233.
[20] R. Nagarajan, M. Barry, E. Ruckenstein, *Langmuir* **1986**, *2*, 210-215.
[21] J. Liu, F. Zeng, C. Allen, *Journal of Controlled release* **2005**, *103*, 481.
[22] A. S. Mikhail, C. Allen, *Journal of Controlled Release* **2009**, *138*, 214-223.
[23] T. Nakanishi, S. Fukushima, K. Okamoto, M. Suzuki, Y. Matsumura, M. Yokoyama, T. Okano, Y. Sakurai, K. Kataoka, *Journal of Controlled Release* **2001**, *74*, 295-302.
[24] G. S. Kwon, M. Naito, M. Yokoyama, T. Okano, Y. Sakurai, K. Kataoka, *Pharmacological Research* **1995**, *12*, 192-195.
[25] S. Jeon, J. H. Lee, J. D. Andrade, P. G. DeGennes, *Journal of Colloid interface science* **1991**, *142*, 149-158.
[26] F. Danhier, O. Feron, V. Preat, *Journal of Controlled Release* **2010**, *148*, 135-146.
[27] S. Taurin, H. Nehoff, K. Greish, *Journal of Controlled Release* **2012**, *164*, 265.
[28] H. Maeda, T. Sawa, T. Konno, *Journal of Controlled Release* **2001**, *74*, 47-61.
[29] Y. Matsumura, H. Maeda, *Cancer Research* **1986**, *46*, 6387-6392.
[30] R. K. Jain, *Journal of the National Cancer Institute* **1989**, *81*, 570-576.
[31] Y. Lu, P. S. Low, *Journal of Controlled Release* **2003**, *91*, 17.
[32] J. D. Byrne, T. Betancourt, L. Brannon-Peppas, *Advanced Drug Delivery Reviews* **2008**, *60*, 1615.

[33] Y. Jeong, S. Seo, I. Park, H. Lee, I. Kang, T. Akaike, C. Cho, *International journal of pharmaceutics* **2005**, *296*, 151.
[34] H. Lee, M. Hu, R. M. Reilly, C. Allen, *Molecular pharmaceutics* **2007**, *4*, 769.
[35] J. You, S. Li, F. D. Cui, Y. Du, H. Yuan, F. Q. Hu, *Nanotechnology* **2008**, *19*.
[36] T. Noh, Y. H. Kook, C. Park, H. Youn, H. Kim, E. T. Oh, E. K. Choi, H. J. Park, C. Kim, *Journal of Polymer Science Part A: Polymer Chemistry* **2008**, *46*, 7321.
[37] N. Nasongkla, X. Shuai, H. Ai, B. D. Weinberg, J. Pink, D. A. Boothman, J. Gao, *Angewandte Chemie: International Edition* **2004**, *43*, 6323.
[38] H. S. Yoo, T. G. Park, *Journal of Controlled Release* **2004**, *100*, 247.
[39] Y. Bae, N. Nishiyama, K. Kataoka, *Bioconjugate chemistry* **2007**, *18*, 1131.
[40] C. Mamot, D. C. Drummond, C. O. Noble, V. Kallab, Z. Guo, K. Hong, D. B. Kirpotin, J. W. Park, *Cancer Research* **2005**, *65*, 11631.
[41] Y. Yamamoto, Y. Nagasaki, Y. Kato, Y. Sugiyama, K. Kataoka, *Journal of Controlled Release* **2001**, *77*, 27.
[42] G. S. Kwon, M. Yokoyama, T. Okano, Y. Sakurai, K. Kataoka, *Pharmaceutical Research* **1993**, *10*, 970.
[43] E. V. Batrakova, S. Li, Y. Li, V. Y. Alakhov, W. F. Elmquist, A. V. Kabanov, *Journal of Controlled Release* **2004**, *100*, 389.
[44] L. W. Seymour, R. Duncan, J. Strohalm, J. Kopecek, *Journal of Biomedical Materials Research* **1987**, *21*, 1341.
[45] H. S. Choi, W. Liu, P. Mistra, E. Tanaka, J. P. Zimmer, B. I. Ipe, M. G. Bawendi, J. V. Frangioni, *Nature Biotechnology* **2007**, *25*, 1165.
[46] Y. Teng, M. E. Morrison, P. Munk, S. E. Webber, *Macromolecules* **1998**, *31*, 3578.
[47] M. Cavalier, J. P. Benoit, C. Thies, *Journal of pharmacy and pharmacology* **1986**, *38*, 249.
[48] M. A. Ward, T. K. Georgiou, *Polymers* **2011**, *3*, 1215-1242.
[49] M. Talleli, C. J. F. Rijcken, S. Oliveira, R. v. d. Meel, P. M. P. v. B. e. Henegouwen, T. Lammers, C. F. v. Nostrum, G. Storm, W. E. Hennink, *Journal of Controlled Release* **2011**, *153*, 93.
[50] R. K. O'Reilly, M. J. Joralemon, C. J. Hawker, K. L. Wooley, *New Journal of Chemistry* **2007**, *31*, 718.
[51] Q. Zhang, E. E. Remsen, K. L. Wooley, *Journal of the American Chemical Society* **2000**, *122*, 3642.
[52] H. Huang, E. E. Remsen, T. Kowalewski, K. L. Wooley, *Journal of American Chemical Society* **1999**, *121*, 3805.
[53] Q. Zhang, N. R. Ko, J. K. Oh, *Chemical Communications* **2012**, *48*, 7542-7552.
[54] B. Khorsand Sourkohi, A. Cunningham, Q. Zhang, J. K. Oh, *Biomacromolecules* **2011**, *12*, 3819-3825.
[55] G. Saito, J. A. Swanson, K.-D. Lee, *Advanced Drug Delivery Reviews* **2003**, *55*, 199-215.
[56] R. Franco, O. J. Schoneveld, A. Pappa, M. I. Panayiotidis, *Archives of Physiology and Biochemistry* **2007**, *113*, 234.
[57] F. Michelet, R. Gueguen, P. Leroy, M. Wellman, A. Nicolas, G. Siest, *Clinical chemistry* **1995**, *41*, 1509.
[58] A. Russo, W. DeGraff, N. Friedman, J. B. Mitchell, *Cancer Research* **1986**, *46*, 2845-2848.
[59] J. M. Estrela, A. Ortega, E. Obrador, *Critical Reviews in Clinical Laboratory Sciences* **2006**, *43*, 143-181.
[60] H. Wei, R.-X. Zhuo, X.-Z. Zhang, *Progress in Polymer Science* **2013**, *38*, 503-535.
[61] E. Fleige, M. A. Quadir, R. Haag, *Advanced Drug Delivery Reviews* **2012**, *64*, 866-884.
[62] H. Sun, B. Guo, R. Cheng, F. Meng, H. Liu, Z. Zhong, *Biomaterials* **2009**, *30*, 6358.

[63] Y. Sun, X. Yan, T. Yuan, J. Liang, Y. Fan, Z. Gu, X. Zhang, *Biomaterials* **2010**, *31*, 7124.
[64] J. Liu, Y. Pang, W. Huang, X. Huang, L. Meng, X. Zhu, Y. Zhou, D. Yan, *Biomacromolecules* **2011**, *12*, 1567.
[65] J. Liu, Y. Pang, W. Huang, Z. Zhu, X. Zhu, Y. Zhou, D. Yan, *Biomacromolecules* **2011**, *12*, 2407.
[66] Q. Zhang, S. Aleksanian, S. M. Noh, J. K. Oh, *Polymer Chemistry* **2013**, *4*, 351.
[67] D. Han, X. Tong, Y. Zhao, *Langmuir* **2012**, *28*, 2327.
[68] H. Fan, J. Huang, Y. Li, J. Yu, J. Chen, *Polymer* **2010**, *51*, 5107-5114.
[69] L. Zhang, T. Xu, Z. Lin, *Journal of membrane science* **2006**, *281*, 491.
[70] H. Wei, X.-Z. Zhang, Y. Zhou, S.-X. Cheng, R.-X. Zhuo, *Biomaterials* **2006**, *27*, 2028.
[71] S. V. Aathimanikandan, E. N. Savariar, S. Thayumanavan, *Journal of American Chemical Society* **2005**, *127*, 14922.
[72] Y. Li, S. Pan, W. Zhang, Z. Du, *Nanotechnology* **2009**, *20*, 065104.
[73] L. M. D., S. S. Pennadam, J. Ellis, C. Alexander, D. C. Gorecki, *The journal of gene medecine* **2007**, *9*, 44.
[74] Z. W. Mao, L. Ma, J. Yan, M. Yan, C. Y. Gao, J. C. Shen, *Biomaterials* **2007**, *28*, 4488.
[75] R. Chevre, O. L. Bihan, F. Beilvert, B. Chatin, B. Barteau, M. Mevel, O. Lambert, B. Pitard, *Nucleic Acids Research* **2011**, *39*, 1610.
[76] D. Cunliffe, C. D. Alarcon, V. Peters, J. R. Smith, C. Alexander, *Langmuir* **2003**, *19*, 2888.
[77] Y. Kumashiro, M. Yamato, T. Okano, *Annual Review of Biomedical Engineering* **2010**, *38*, 1977.
[78] V. M. Varghese, V. Raj, K. Sreenivasan, T. V. Kumary, *Journal of materials Science: Materials in medecine* **2010**, *21*, 1631.
[79] E. S. Gil, S. M. Hudson, *Progress in Polymer Science* **2004**, *29*, 1173-1222.
[80] M. Keerl, J. S. Pedersen, W. Richtering, *Journal of American Chemical Society* **2009**, *131*, 3093.
[81] M. Das, S. Mardyani, W. C. W. Chan, E. Kumacheva, *Advanced Materials* **2006**, *18*, 80.
[82] J. Kim, M. J. Serpe, L. A. Lyon, *Journal of American Chemical Society* **2004**, *126*, 9512.
[83] J. Kim, M. J. Serpe, L. A. Lyon, *Angewandte Chemie* **2005**, *117*, 1357.
[84] A. S. Hoffman, P. S. Stayton, V. Bulmus, G. Chen, J. Chen, C. Cheung, A. Chilkoti, Z. Ding, L. Dong, R. Fong, C. A. Lackey, C. J. Long, M. Miura, J. E. Morris, N. Murthy, Y. Nabeshima, T. G. Park, O. W. Press, T. Shimoboji, S. Shoemaker, H. J. Yang, N. Monji, R. C. Nowinski, C. A. Cole, J. H. Priest, J. M. Harris, K. Nakamae, T. Nishino, T. Miyata, *Journal of Biomedical Materials Research* **2000**, *52*, 577-586.
[85] J.-F. Lutz, K. Weichenhan, O. Akdemir, A. Hoth, *Macromolecules* **2007**, *40*, 2503.
[86] Y. Li, J. Yang, J. Li, Y. Liu, W. Liu, *RSC advances* **2012**, *2*, 2322.
[87] S. Yamamoto, J. Pietrasik, K. Matyjaszewski, *Macromolecules* **2007**, *40*, 9348.
[88] J.-F. Lutz, O. Akdemir, A. Hoth, *Journal of American Chemical Society* **2006**, *128*, 13046.
[89] K. E. Uhrich, S. M. Cannizzaro, R. S. Langer, K. M. Shakesheff, *Chemical Reviews* **1999**, *99*, 3181.
[90] L. Brannon-Peppas, *Journal of Controlled Release* **2000**, *66*, 321.
[91] J.-F. Lutz, *Advanced Materials* **2011**, *23*, 2237-2243.
[92] J.-F. Lutz, *Journal of Polymer Science Part A: Polymer Chemistry* **2008**, *46*, 3459.
[93] S. Sugihara, K. Hashimoto, S. Okabe, M. Shibayama, S. Kanaoka, S. Aoshima, *Macromolecules* **2004**, *37*, 336.
[94] H. G. Schild, *Progress in Polymer Science* **1992**, *17*, 163-249.
[95] J. K. Oh, R. Drumright, D. J. Siegwart, K. Matyjaszewski, *Progress in Polymer Science* **2008**, *33*, 448-477.

[96] R. Langer, J. P. Vacanti, *Science* **1993**, *260*, 920.
[97] N. A. Peppas, J. Z. Hilt, A. Khademhosseini, R. Langer, *Advanced Materials* **2006**, *18*, 1345-1360.
[98] B. V. Slaughter, S. S. Khurshid, O. Z. Fisher, A. Khademhosseini, N. A. Peppas, *Advanced Materials* **2009**, *21*, 3307-3329.
[99] A. Nelson-Mendez, S. Aleksanian, M. Oh, H.-S. Lim, J. K. Oh, *Soft Matter* **2011**, *7*, 7441.
[100] B. Neises, W. Steglich, *Angewandte Chemie International Edition English* **1978**, *17*, 522.
[101] D. M. Hunsicker, B. C. Dauphinais, S. P. Mc Ilrath, N. J. Robertson, *Macromolecular Rapid Communications* **2012**, *33*, 232-236.
[102] A. Muhlebach, S. G. Gaynor, K. Matyjaszewski, *Macromolecules* **1998**, *31*, 6046-6052.
[103] M. Kato, M. Kamigaito, M. Sawamoto, T. Higashimura, *Macromolecules* **1995**, *28*, 1721-1723.
[104] C. J. Hawker, A. W. Bosman, E. Harth, *Chemical Reviews* **2001**, *101*, 3661.
[105] T. Diaz, A. Fischer, A. Jonquieres, A. Brembilla, P. Lochon, *Macromolecules* **2003**, *36*, 2235.
[106] M. L. Becker, J. Liu, K. L. Wooley, *Biomacromolecules* **2005**, *6*, 220.
[107] R. E. Richard, M. Schwarz, S. Ranade, A. K. Chan, K. Matyjaszewski, B. Sumerlin, *ACS Symposium Series* **2006**, *944*, 234.
[108] X. Jiang, Z. Ge, J. Xu, H. Liu, S. Liu, *Biomacromolecules* **2007**, *8*, 3184.
[109] M. Licciardi, Y. Tang, N. C. Billingham, S. P. Armes, A. L. Lewis, *Biomacromolecules* **2005**, *6*, 1085.
[110] F. H. Schacher, P. A. Rupar, I. Manners, *Angewandte Chemie International Edition English* **2012**, *51*, 7898-7921.
[111] C. L. McCormick, B. S. Sumerlin, B. S. Lokitz, J. E. Stempka, *Soft Matter* **2008**, *4*, 1760.
[112] P. De, S. R. Gondi, D. Roy, B. S. Sumerlin, *Macromolecules* **2009**, *42*, 5614.
[113] M. Barz, F. K. Wolf, F. Canal, K. Koynov, M. J. Vicent, H. Frey, R. Zentel, *Macromolecular Rapid Communications* **2010**, *31*, 1492.
[114] K. Matyjaszewski, *Macromolecules* **2012**, *45*, 4015-4039.
[115] W. Jakubowski, K. Matyjaszewski, *Macromolecules* **2005**, *38*, 4139-4146.
[116] O. W. Webster, *Science* **1991**, *251*, 887-893.
[117] R. J. Young, P. A. Lovell, *Introduction to Polymers*, **2011**.
[118] K. Letchford, H. Burt, *European journal of pharmaceutics and biopharmaceutics* **2007**, *65*, 259.
[119] X. Cui, S. Mao, M. Liu, H. Yuan, Y. Du, *Langmuir* **2008**, *24*, 10771-10775.
[120] Kibron, **http://www.kibron.com/products/langmuir-tensiometers/deltapi, accessed on Sept 2013**.
[121] N. A. Clark, J. H. Lunacek, G. B. Benedek, *American journal of physics* **1970**, *38*, 575.
[122] S. Aleksanian, B. Khorsand, R. Schmidt, J. K. Oh, *Polymer Chemistry* **2012**, *3*, 2138.
[123] F. Ganji, S. Vasheghani-Farahani, E. Vasheghani-Farahani, *Iranian Polymer Journal* **2010**, *19*, 375-398.
[124] J. W. Goodwin, R. W. Hughes, *Rheology for Chemists: An Introduction*, 2nd Edition ed., RSC publishing, **2008**.
[125] K. S. Anseth, C. N. Bowman, L. Brannon-Peppas, *Biomaterials* **1996**, *17*, 1647-1657.
[126] X. B. Xiong, A. Falamarzian, S. M. Garg, A. Lavasanifar, *Journal of Controlled Release* **2011**, *155*, 248-261.
[127] A. Blanazs, S. P. Armes, A. J. Ryan, *Macromolecular Rapid Communications* **2009**, *30*, 267-277.
[128] A. Harada, K. Kataoka, *Progress in Polymer Science* **2006**, *31*, 949.

[129] N. Nishiyama, K. Kataoka, *Advances in polymer Science* **2006**, *193*, 67.
[130] A. Sharma, G. M. Soliman, N. Al-Hajaj, R. Sharma, D. Maysinger, A. Kakkar, *Biomacromolecules* **2012**, *13*, 239.
[131] N. Rapoport, *Progress in Polymer Science* **2007**, *32*, 962-990.
[132] O. J. Cayre, N. Chagneux, S. Biggs, *Soft Matter* **2011**, *7*, 2211.
[133] N. V. Tsarevsky, K. Matyjaszewski, *Macromolecules* **2002**, *35*, 9009.
[134] C. Li, J. Madsen, S. P. Armes, A. L. Lewis, *Angewandte Chemie International Edition English* **2006**, *45*, 3510.
[135] B. K. Sourkohi, R. Schmidt, J. K. Oh, *Macromolecular Rapid Communications* **2011**, *32*, 1652.
[136] L. Sun, W. Liu, C.-M. Dong, *Chemical communications* **2011**, *47*, 11282.
[137] A. Klaikherd, C. Nagamani, S. Thayumanavan, *Journal of American Chemical Society* **2009**, *131*, 4830.
[138] J. Dai, S. Lin, D. Cheng, S. Zou, X. Shuai, *Angewandte Chemie International Edition English* **2011**, *50*, 9404.
[139] E. Kim, D. Kim, H. Jung, J. Lee, S. Paul, N. Selvapalam, Y. Yang, N. Lim, C. G. Park, K. Kim, *Angewandte Chemie International Edition English* **2010**, *49*, 4405.
[140] J. Chen, C. Wu, D. Oupicky, *Biomacromolecules* **2009**, *10*, 2921.
[141] J. Chen, X. Qiu, J. Ouyang, J. Kong, W. Zhong, M. M. Q. Xing, *Biomacromolecules* **2011**, *12*, 3601.
[142] A. Nelson-Mendez, S. Aleksanian, M. Oh, H.-S. Lim, J. K. Oh, *Soft Matter* **2011**, *7*, 7441-7452.
[143] K. Matyjaszewski, T. P. Davis, John Wiley & Sons Inc., **2002**.
[144] P. Pinnel, A. Mendez-Nelson, S. M. Noh, J. H. Nam, K. O. Jung, *Macromolecular Chemistry and Physics* **2012**, *213*, 678.
[145] K. Loomis, K. McNeeley, R. V. Bellamkonda, *Soft Matter* **2011**, *7*, 839-856.
[146] J. K. Oh, K. Min, K. Matyjaszewski, *Macromolecules* **2006**, *39*, 3161-3167.
[147] A. Lavasanifar, J. Samuel, G. S. Kwon, *Journal of Controlled Release* **2001**, *77*, 155-160.
[148] L. Zhang, R. Guo, M. Yang, X. Jiang, B. Liu, *Advanced Materials* **2007**, *19*, 2988.
[149] V.-T. Huynh, P. d. Souza, M. H. Stenzel, *Macromolecules* **2011**, *44*, 7888.
[150] W. Chen, F. Meng, F. Li, S.-J. Ji, Z. Zhong, *Biomacromolecules* **2009**, *10*, 1727.
[151] C. M. Golini, B. W. Williams, J. B. Foresman, *Journal of Fluorescence* **1998**, *8*, 395.
[152] J. Jiang, X. Tong, D. Morris, Y. Zhao, *Macromolecules* **2006**, *39*, 4633.
[153] A. P. Goodwin, J. L. Mynar, Y. Ma, G. R. Fleming, J. M. J. Frechet, *Journal of American Chemical Society* **2005**, *127*, 9952.
[154] A. W. Jackson, D. A. Fulton, *macromolecules* **2012**, *45*, 2699.
[155] N. M. Green, *The Biochemical journal* **1963**, *89*, 585.
[156] K. Qi, Q. Ma, E. E. Remsen, C. G. Clark, K. L. Wooley, *Journal of American Chemical Society* **2004**, *126*, 6599.
[157] J. K. Oh, D. J. Siegwart, H.-i. Lee, G. Sherwood, L. Peteanu, J. O. Hollinger, K. Kataoka, K. Matyjaszewski, *Journal of American Chemical Society* **2007**, *129*, 5939.
[158] K. Na, T. B. Lee, K.-H. Park, E.-K. Shin, Y.-B. Lee, H.-K. Choi, *European journal of pharmaceutical science* **2003**, *18*, 165.
[159] S. Shinohara, T. Seki, T. Sakai, R. Yoshida, Y. Takeoka, *Angewandte Chemie International Edition English* **2008**, *47*, 9039-9043.
[160] Z. Ma, D. M. Nelson, Y. Hong, W. R. Wagner, *Biomacromolecules* **2010**, *11*, 1873.
[161] J. T. Keurentjes, M. F. Kemmere, H. Bruinewoud, M. A. Vertommen, S. A. Rovers, R. Hoogenboom, L. F. Stemkens, F. L. Peters, N. J. Tielen, D. T. van Asseldonk, A. F. Gabriel,

E. A. Joosten, M. A. Marcus, *Angewandte Chemie International Edition English* **2009**, *48*, 9867-9870.
[162] F. Cellesi, *Therapeutic delivery* **2012**, *3*, 1395.
[163] G. Ye, X. Li, X. Wang, *Chemical communications* **2010**, *46*, 3872.
[164] C. Wang, B. Yu, B. Knudsen, J. Harmon, F. Moussy, *Biomacromolecules* **2008**, *9*, 561.
[165] D. Arunbabu, A. Sannigrahi, T. Jana, *Soft Matter* **2011**, *7*, 2592.
[166] C. Gota, K. Okabe, T. Funatsu, Y. Harada, S. Uchiyama, *Journal of American Chemical Society* **2009**, *131*, 2766.
[167] S. Garty, N. Kimelman-Bleich, Z. Hayouka, D. Cohn, A. Friedler, G. Pelled, D. Gazit, *Biomacromolecules* **2010**, *11*, 1516.
[168] F. Fernandez-Trillo, J. C. M. v. Hest, J. C. Thies, T. Michon, R. Weberskirch, N. R. Cameron, *Advanced Materials* **2009**, *21*, 55.
[169] Y. Kaneko, S. Nakamura, K. Sakai, A. Kikuchi, T. Aoyagi, Y. Sakurai, T. Okano, *Journal of biomaterials science, polymer edition* **1999**, *10*, 1079.
[170] K. Okeyoshi, T. Abe, Y. Noguchi, H. Furukawa, R. Yoshida, *Macromolecular Rapid Communications* **2008**, *29*, 897-903.
[171] Y. Noguchi, K. Okeyoshi, R. Yoshida, *Macromolecular Rapid Communications* **2005**, *26*, 1913-1917.
[172] Y. Kaneko, S. Nakamura, K. Sakai, T. Aoyagi, A. Kikuchi, Y. Sakurai, T. Okano, *Macromolecules* **1998**, *31*, 6099.
[173] J. A. Yoon, T. Kowalewski, K. Matyjaszewski, *Macromolecules* **2011**, *44*, 2261-2268.
[174] G. David, B. C. Simionescu, A.-C. Albertsson, *Biomacromolecules* **2008**, *9*, 1678.
[175] J. Zhou, G. Wang, L. Zou, L. Tang, M. Marquez, Z. Hu, *Biomacromolecules* **2008**, *9*, 142.
[176] N. Morimoto, T. Ohki, K. Kurita, K. Akiyoshi, *Macromolecular Rapid Communications* **2008**, *29*, 672-676.
[177] E. C. Cho, J.-W. Kim, A. Fernandez-Nieves, D. A. Weitz, *Nano Letters* **2008**, *8*, 168.
[178] Y. Tan, K. Xu, P. Wang, W. Li, S. Sun, L. Dong, *Soft Matter* **2010**, *6*, 1467.
[179] R. Liu, J. M. Saunders, T. J. Freemont, B. R. Saunders, *Soft Matter* **2012**, *8*, 10932.
[180] Y. Wang, H. Xu, X. Zhang, *Advanced Materials* **2009**, *21*, 2849.
[181] N. V. Tsarevsky, K. Matyjaszewski, *Macromolecules* **2002**, *35*, 9009-9014.
[182] R. Cheng, F. Feng, F. Meng, C. Deng, J. Feijen, Z. Zhong, *Journal of Controlled Release* **2011**, *152*, 2.
[183] F. Meng, W. E. Hennink, Z. Zhong, *Biomaterials* **2009**, *30*, 2180.
[184] W. Li, J. A. Yoon, K. Matyjaszewski, *Journal of American Chemical Society* **2010**, *132*, 7823.
[185] K. Miyata, Y. Kakizawa, N. Nishiyama, A. Harada, Y. Yamasaki, H. Koyama, K. Kataoka, *Journal of American Chemical Society* **2004**, *126*, 2355.
[186] R. A. Petros, P. A. Ropp, J. M. DeSimone, *Journal of American Chemical Society* **2008**, *130*, 5008.
[187] W. Lv, S. Liu, W. Feng, J. Qi, G. Zhang, F. Zhang, X. Fan, *Macromolecular Rapid Communications* **2011**, *32*, 1101.
[188] H. A. Aliyar, P. D. Hamilton, N. Ravi, *Biomacromolecules* **2005**, *6*, 204-211.
[189] J. A. Yoon, S. A. Bencherif, B. Aksak, E. K. Kim, T. Kowalewski, J. K. Oh, K. Matyjaszewski, *Chemistry - an Asian Journal* **2011**, *6*, 128-136.
[190] D. Bontempo, L. H. Karina, A. F. Benjamin, D. M. Heather, *Journal of American Chemical Society* **2004**, *126*, 15372.
[191] C. Boyer, J. Liu, L. Wong, M. Tippett, V. Bulmus, T. P. Davis, *Journal of Polymer Science Part A: Polymer Chemistry* **2008**, *46*, 7207.

[192] C. Boyer, V. Bulmus, J. Liu, T. P. Davis, M. H. Stenzel, C. Barner-Kowollik, *Journal of American Chemical Society* **2007**, *129*, 7145.
[193] D. J. Phillips, M. I. Gibson, *Chemical communications* **2012**, *48*, 1054.
[194] K. Rahimian-Bajgiran, N. Chan, Q. Zhang, S. M. Noh, H.-I. Lee, J. K. Oh, *Chemical communications* **2013**, *49*, 807.
[195] W.-F. Dong, A. Kishimura, Y. Anraku, S. Chuanoi, K. Kataoka, *Journal of American Chemical Society* **2009**, *131*, 3804.
[196] J. A. Yoon, C. Gayathri, R. R. Gil, T. Kowalewski, K. Matyjaszewski, *Macromolecules* **2010**, *43*, 4791-4797.
[197] Q. Liu, P. Zhang, A. Qing, Y. Lan, M. Lu, *Polymer* **2006**, *47*, 2330-2336.
[198] N. V. Tsarevsky, T. Sarbu, B. Goebelt, K. Matyjaszewski, *Macromolecules* **2002**, *35*, 6142-6148.
[199] J. K. Oh, C. Tang, H. Gao, N. V. Tsarevsky, K. Matyjaszewski, *Journal of American Chemical Society* **2006**, 5578-5584.
[200] K. Min, H. Gao, K. Matyjaszewski, *Journal of American Chemical Society* **2005**, *127*, 3825.
[201] J. K. Oh, K. Matyjaszewski, *Journal of Polymer Science Part A: Polymer Chemistry* **2006**, *44*, 3787-3796.
[202] M. Cioffi, A. C. Hoffmann, L. P. B. M. Janssen, *Chemical Engineering Science* **2001**, *56*, 911.
[203] G. L. Ellman, *Archives of Biochemistry and Biophysics* **1959**, *82*, 70-77.

List of publications

S. Aleksanian; Y. Wen; N. Chan; Jung Kwon Oh* Tuning thermoresponsive kinetics of hydrogels with thiol-responsive degradation. *RSC Advances* **2014**, 4, 3713.

N. Chan; B. Khorsand; **S. Aleksanian**; Jung Kwon Oh* Dual location stimuli-responsive degradation strategy of block copolymer nanocarriers for accelerated release. *Chemical Communications* **2013**, 49, 7534.

Q. Zhang; **S. Aleksanian**; S. Man Noh; Jung Kwon Oh* Thiol-responsive block copolymer nanocarriers exhibiting tunable release with morphology changes*. Polymer Chemistry* **2013,** 4, 351.

S. Aleksanian; B. Khorsand; R. Schmidt; Jung Kwon Oh* Rapidly thiol-responsive degradable block copolymer nanocarriers with facile bioconjugation*. Polymer Chemistry* **2012,** *3*, 2138.

Q. Zhang; **S. Aleksanian**; A. Cunningham; J. K. Oh* New design of thiol-responsive degradable block copolymer micelles as controlled drug delivery vehicles, *ACS book entitled* "Progress in Controlled Radical Polymerization." *edited by K. Matyjaszewski, B. S. Sumerlin, and N. V. Tsarevsky* **2012**, *ACS*.

A. Nelson-Mendez; **S. Aleksanian**; M. Oh; H-S. Kim; J. K. Oh* Reductively-degradable polyester-based block copolymers prepared by facile polycondensation and ATRP: synthesis, degradation, and aqueous micellization. *Soft Matter* **2011**, *7*, 7441.